Nonlocal Theory of Relativistic Ponderomotive Force in High Intensity Lasers Based on the Phase Space Lagrangian and the Role in the Interaction with Various Mediums

Natsumi Iwata

Acknowledgements

First of all, I would like to express the deepest gratitude to my supervisor, Professor Yasuaki Kishimoto for his continuous encouragement and prospective guidance for my research for five years in Kyoto University. The present thesis would not have been achieved without his help. I am indebt to his generosity in having a wide viewpoint on nature, which has been a great help for me to keep faith in my research.

I would like to appreciate Professor Jiquan Li for his continuous support over five years. He has provided me helpful advices and encouragements. I am grateful to Doctor Kenji Imadera for his helpful advice and having deep discussions especially on the methodology used in my theoretical work. I sincerely appreciate the reviewers of this thesis, Profs. Yuji Nakamura, Shuji Sakabe and Kazunari Matsuda for a lot of important comments not only on the details of the contents of the thesis but also on the meanings, impacts and future prospectives of the study.

I would like to thank all the members of our laboratory, especially, Messrs. Ryutaro Matsui, Yuichi Sugiyama and Daiki Kawahito for their help and fruitful discusions on the numerical study of laser-cluster interaction.

I would like to acknowledge to Prof. Kunioki Mima in Osaka University and Dr. Sergei Bulanov in Japan Atomic Energy Agency (JAEA) for their encouragements and insightful comments to proceed my research. I am grateful to Dr. James Koga in JAEA for his continuous encouragement and fruitful discussions starting from the JAEA summer program in 2009, which initiated my research. I would like to appreciate Dr. Yuji Fukuda in JAEA for his valuable comments on the study of laser-cluster interaction from the viewpoint of a experimentalist. I would like to thank Profs. Yasuhiko Sentoku in Nevada University, Hideo Sugama in National Institute for Fusion Science (NIFS) and Toshihiro Taguchi in Setsunan University for valuable discussions and comments on the theoretical work and its applications. I would like to acknowledge to Dr. Tomohiro Masaki for his great help and support in developing the EPIC3D code.

I am grateful to my family, Masanori Iwata, Kayoko Iwata and my dear dog for all their support and encouragement in my life.

Abstract

Ponderomotive force, which corresponds to the pressure of electromagnetic fields, is a central concern in understanding a wide class of nonlinear plasma physics and in exploring many applications. An example is the force associated with high power lasers whose intensities lie in the relativistic regime for electrons, i.e. $10^{18-21}\mathrm{W/cm}^2$, which are realized by reducing the pulse width and spot size. By using the interaction between such high intensity lasers and matters, various applications have been opened up such as high intensity x-ray/neutron sources, compact accelerators and fast ignition-based laser fusion. In this regime, electrons are ejected easily from the interaction region due to the ponderomotive force. Therefore, designing laser field patterns and controlling the interaction are of special importance.

The ponderomotive force has been expressed as being proportional to the local gradient of the amplitude of electromagnetic field. This expression results from the first-order approximation with respect to the expansion parameter ϵ, i.e., the ratio between the excursion length of particles and the scale length of the field amplitude gradient. On the other hand, in recent years, more delicate control of laser field profiles in plasmas is anticipated. For instance, a flat top super Gaussian laser beam, in which the ponderomotive force is significantly weakened near the beam axis, is considered to be preferable in maintaining a long interaction between laser and particles, and in achieving efficient particle accelerations. In such flat-top field structures, the ponderomotive force estimated from the conventional first-order formula tends to be diminished near the beam axis, so that a residual higher-order force associated with nonlocal profile becomes important. However, there exists no formal theory to describe the higher-order force correctly except direct numerical integration which does not provide an adequate prospective guideline.

To circumvent the above difficulty, in Part I of this thesis, we explore a theory of ponderomotive force that includes nonlocal effects up to higher orders by using the noncanonical Lie perturbation method, which is based on the variational principle in noncanonical phase space coordinates incorporated with the Lie transformation. By properly choosing the gauge function and coordinate transformations, we successfully obtain a secular equation of motion describing the ponderomotive force up to the third order of ϵ. The higher-order terms are found to consist of the second and third spatial derivatives of the field amplitude, so that the ponderomotive force depends not only on the local field gradient,

but also on the field curvature and its variation. The formula is accessible to the regime in which laser fields exhibit characteristic structures such that higher derivatives of the field amplitude regulate the interaction. As an example, we have applied the obtained formula to study the particle motion in a flat-top super Gaussian and a concave hollow laser beam structures. In these profiles, since the local field gradient is diminished near the beam center, the higher-order terms dominate the dynamics. Comparison with the direct integration of the particle orbit demonstrates the validity of the formula derived here with a sufficient convergence of the expansion series up to $\mathscr{O}\left(\epsilon^3\right)$. We have also investigated the higher-order ponderomotive force by applying the averaging method to the equation of motion. It is found that the higher-order terms exhibit same parametric dependence as those derived by the Lie perturbation method, but the coefficients are different. As a result, the oscillation center trajectory derived by the averaging method does not agree with the direct integration of the particle orbit, which is considered to result from the lack of Hamiltonian structure in the averaging method.

In plasmas, laser field suffers from the reaction from plasma particle dynamics, so that the interaction has to be determined self-consistently. It is worthwhile to apply the idea of the nonlocal ponderomotive force to obtain the governing equation system that describes such a self-consistent interaction. To achieve it, further improvement of the present theory is necessary including the coordinate transformation in the Maxwell equations. However, we can readily see that the governing equation system exhibits higher order spatial derivatives than the existing equation. Consequently, qualitatively different dynamics and structure can be expected.

In order to examine the nonlocal ponderomotive theory, we carry out two-dimensional (2D) fully-relativistic electromagnetic particle-in-cell (PIC) simulations for the propagation of the fourth and sixth order super Gaussian laser beams in a plasma. It is found that the electron density exhibits a peaking near the axis as time goes on, while at the same time, the field amplitude changes the profile from the original flat top structure to that of a weak concave with a positive curvature. Such a structure modulation becomes more prominent in the case of flatter super Gaussian beam. Besides the beam axis, two points at which the field gradient and then the first order ponderomotive force vanish are found to appear. Namely, the higher order ponderomotive force plays an important role in regulating the interaction around these points. These structure and dynamics are considered to result from plural physical processes such as the higher order ponderomotive force near the axis, the resultant density modulation, generation of the Coulomb field, and change of linear and nonlinear susceptibilities.

In considering a fine scale control of high power laser-matter interaction, the state and structure of the target material are key ingredients to be

chosen properly according to the purpose. Besides solid and gas, cluster and cluster medium composed of multi clusters are interested, which exhibit prominent features essentially due to the existence of the surface of cluster. The cluster medium has a solid density locally, whereas in average, it can have an intermadiate density between solid and gas. Such a high degree of freedom of cluster medium is attributed to having many parameters that determine the internal structure of the medium, e.g., cluster size, packing fraction and spatial configuration of clusters. The above features of cluster medium can be utilized for various applications such as efficient ion acceleration and neutron generation by nuclear fusion.

In Part II of this thesis, we study the effect from internal structure of target mediums on the laser-matter interaction especially in the intensity regime of $10^{22-24}\mathrm{W/cm^2}$, where not only electrons but also ions can be accelerated to relativistic velocities. In such a regime, synergistic effects of radiation pressure acceleration and the cluster Coulomb explosion are expected, which will lead to a new dynamics with relativistically accelerated ions. Based on this idea, we perform PIC simulations for the interaction between high power laser and targets consisting of same mass but having different internal structures, i.e., cluster mediums with different cluster radii and solid thin film, in the intensity regime $10^{21-24}\mathrm{W/cm^2}$.

Comparison of interaction dynamics and ion energy distribution among different targets show the effects of the cluster Coulomb explosion inside of the medium. The results indicate that the internal structure, which corresponds to the free energy of the target medium, is important in determining the interaction dynamics and the resulting ion acceleration.

Contents

Chapter 1

Introduction

1.1 Development of high power lasers

With the advent of high power short pulse laser technologies in recent years, laser intensities have reached the range of 10^{22} W/cm^2 [1]. The electric and magnetic fields at these intensities are in the order of tela-volt per centimeter (10^{12} V/cm) and ten giga-gauss (10^{10} gauss), respectively. In such a strong laser electric field, quiver energy of electrons becomes more than 10 MeV. The light pressure of such intense laser field reaches to the order of tela-bar (10^{12} bar) that exceeds the pressure at the center of the sun, i.e., 2.4×10^{11} bar.

To realize such high intensity lasers, strong focusing of laser energy in space and time is a key issue. For instance, even when the source is a light energy of 1 joule, if it is confined in 10 femtoseconds ($= 10^{-14}$ s) in time, the power reaches to 10^{14} W which is larger than the energy that the whole human being is exhausting per unit time, i.e., about 10^{13} W. By focusing the laser power of 10^{14} W to near the optical limit, e.g., 5 μm radius spot which is the same order as the typical wavelength of the laser field 1 μm, the laser intensity reaches to the order of 10^{20} W/cm^2.

Figure 1.1 shows the development of laser intensity in time. Beginning with the first demonstration of the laser in 1960 [2], high power short pulse lasers whose pulse length ranging in micro (10^{-6}), pico (10^{-9}) and nano (10^{-12}) second had been realized with technological inventions such as Q-switching [3] and mode-locking [4]. However, due to the threshold for optical damages to laser amplifiers, the development of high power lasers had once been satulated around peak powers of giga-watt (10^9 W). The difficulty had been overcame by the innovation of chirped pulse amplification (CPA) in 1985 [5], which arrows a drastic improvement of laser intensity by more than five orders of magnitude [6]. In the following two decades, the intensity has been improved from the regime below 10^{16} W/cm^2, in which the laser electric field can be regarded as a perturbation to the Coulomb field in hydrogen atom, to the regime 10^{18-22} W/cm^2 where electrons irradiated by lasers are suddenly ionized by the strong laser electric field and accelerated to relativistic energies.

In the relativistic regime, laser-matter interaction is dominated by nonlinear and non-equilibrium processes. Besides the complexity, such a characteristic of interaction is rich in physics leading to various innovative applications, i.e., high intensity coherent light sources from Tela-heltz to X and gamma rays [7, 8], intense source of neutrons [9], compact particle accelerators [10] and fast ignition-based laser

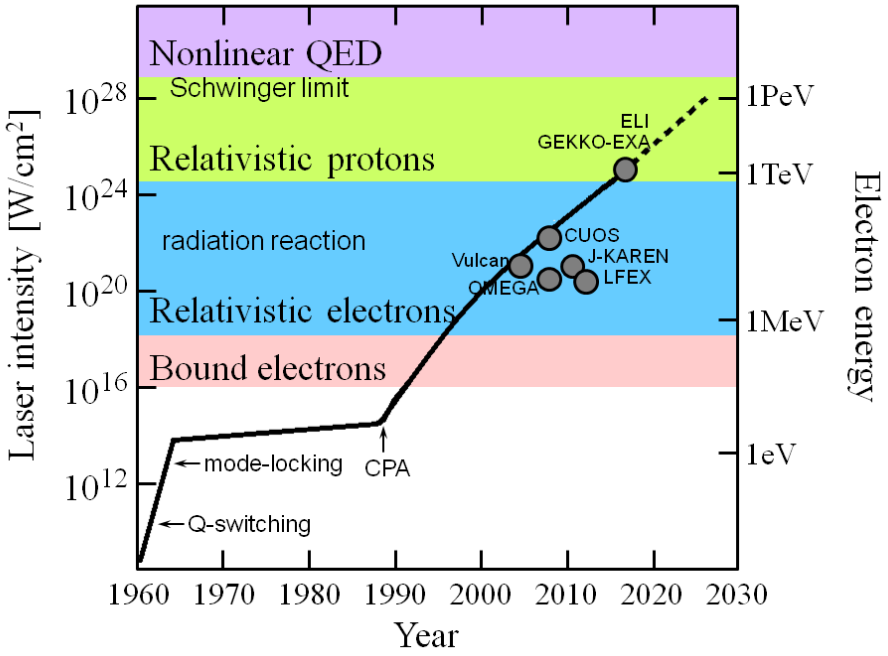

Figure 1.1: Development of high power lasers.

fusion [11].

Today, laser intensity has reached the order of 10^{22}W/cm^2. In this stage, damping of the electron energy due to the strong bremsstrahlung, referred to as radiation damping, cannot be neglected. Namely, more than 35% of the laser energy is found to be converted to radiation in the interaction between an overdense plasma slab and a laser pulse with a radiance of 10^{22}W/cm^2 [12]. In other words, it indicates that plasmas irradiated by lasers in the radiation dominant regime can be utilized as a source of intense high energy radiations such as a high-power gamma ray flash [8]. Moreover, higher intensities of 10^{23-26}W/cm^2 is expected to be achieved by further reducing the pulse width and spot size to the level of laser wavelength. In this regime, not only electrons but also ions become relativistic, so that a new dynamics, in which a rapid response of ions in the laser-plasma interaction is important, is expected. Higher intensities of 10^{26-28}W/cm^2 will bring electron-positron pair creation via three-body and/or Bethe-Heitler processes [13]. Then, electron-positron plasmas that emit high energy radiations are expected to be realized, which can demonstrate extreme plasmas in universe [14]. Furthermore, 10^{29}W/cm^2 will lead to vacuum breakdown which causes pair creations from the Schwinger field. By providing such a ultra high energy density state described by the nonlinear quantum electrodynamics (QED), high power lasers could enable to study collective interactions between intense field and matter in the QED stage.

1.2 Introduction to laser-matter interaction in the relativistic regime

1.2.1 Particle motion in laser fields

In the following, we introduce fundamentals of laser-matter interaction.

We start from motion of a charged particle in electromagnetic fields. A charged particle of mass m and charge q in electromagnetic fields suffers from the Lorentz force, which is described by the equation of motion as

$$\frac{d\mathbf{p}}{dt} = q\left(\mathbf{E} + \frac{\mathbf{v}}{c} \times \mathbf{B}\right). \tag{1.1}$$

Here, t is the time, $\mathbf{p}$ the mechanical momentum, $\mathbf{v}$ the velocity of the particle, c the speed of light, and $\mathbf{E}$ and $\mathbf{B}$ the electric and magnetic fields, respectively.

Non-relativistic case

In the nonrelativistic limit $v \ll c$, the second term on the right-hand side (RHS) of Eq. (1.1) is neglegible compared with the first term, and therefore, (1.1) is approximated to

$$\frac{d\mathbf{p}}{dt} = q\mathbf{E}. \tag{1.2}$$

Here, we consider a plane monochromatic electromagnetic (laser) field propagating in the z direction. Such a field can be given by $\mathbf{E} = \mathbf{E}_0 \cos(\omega t - kz)$, where ω and k are the frequency and wave number of the laser field, respectively. Note that in the non-relativistic case, the ratio between ωt and kz can be evaluated roughly as $kz/\omega t = z/ct \sim v_z/c \ll 1$. Therefore, the laser electric field can be written as $\mathbf{E} = \mathbf{E}_0 \cos\omega t$ in the non-relativistic regime. For laser fields with a spatially uniform amplitude $|\mathbf{E}_0| = E_0 = const.$, one can integrate Eq. (1.2) and obtain the particle motion that oscillates in the direction of the laser electric field as

$$\mathbf{p} = \int \mathbf{E}_0 \cos\omega t dt = \frac{|q|\,\mathbf{E}}{\omega} \sin\omega t \equiv p_{os.} \sin\omega t, \tag{1.3}$$

where $p_{\mathrm{os.}} = |q|\,E_0/\omega$ is the amplitude of the momentum of oscillatory motion due to the laser electric field.

Here, we introduce the normalized laser amplitude a_0, which is defined as $a_0 \equiv p_{\mathrm{os.}}/mc$. This parameter a_0 is related to the laser frequency ω and amplitudes of laser vector potential A_0 and electric field E_0 as

$$a_0 = \frac{p_{\mathrm{os.}}}{mc} = \frac{|q|\,A_0}{mc^2} = \frac{|q|\,E_0}{mc\omega}. \tag{1.4}$$

Note that the vector and scalar potentials, $\mathbf{A}$ and Φ, are related to the electric and magnetic fields as

$$\mathbf{E} = -\nabla\Phi - \frac{1}{c}\frac{\partial \mathbf{A}}{\partial t}, \tag{1.5}$$

$$\mathbf{B} = \nabla \times \mathbf{A} \tag{1.6}$$

In the last equality in Eq. (1.4), we used Eq. (1.5) with an assumption $\Phi = 0$. The parameter a_0 is commonly utilized to characterize the laser intensities.

The relativistic factor for the quiver motion averaged over the laser frequency, $\overline{p}_{\text{os.}} = \sqrt{\langle \mathbf{p}^2 \rangle} = p_{\text{os.}}/\sqrt{2}$, can be represented using a_0 as

$$\overline{\gamma}_{\text{os.}} = \sqrt{1 + \left\langle (a_0 \cos\omega t)^2 \right\rangle} = \sqrt{1 + \frac{a_0^2}{2}}. \tag{1.7}$$

Therefore, the particle motion is nonrelativistic $\gamma \sim 1$ for $a_0 \ll 1$ whereas relativistic $\gamma > 1$ for $a_0 > 1$.

Relativistic case

In the above, we showed that the motion of charged particle lies in the direction of the laser electric field as seen from Eq. (1.3) in the non-relativistic case. On the other hand, when the laser intensity becomes relativistic, a motion in the direction of laser propagation also appears. This is due to the fact that the second term on the RHS of Eq. (1.1), which includes the factor v/c, cannot be neglected in the relativistic case $v \sim c$.

In considering the relativistic motion, we use the following expression for the normalized vector potential of the laser field:

$$\mathbf{a} = a_0 \left(\sin(\omega t - kz)\, \delta_x \hat{\mathbf{e}}_x + \cos(\omega t - kz)\, \delta_y \hat{\mathbf{e}}_y \right), \tag{1.8}$$

where $\mathbf{e}_\perp = (\mathbf{e}_x, \mathbf{e}_y)$ is the unit vector in the perpendicular direction, and δ_x and δ_y are factors relating to the polarization of the laser field and satisfy the relation $\delta_x^2 + \delta_y^2 = 1$. For instance, $(\delta_x,\, \delta_y) = (1, 0)$ and $(0, 1)$ are given for linear polarization in the x and y directions, respectively, while $\delta_x = \delta_y = 1/\sqrt{2}$ for circular polarization.

In the relativistic regime, although the equation of motion becomes complicated due to the nonlinearity, one can obtain an exact analytical solution in the case of plane monochromatic field which has a constant amplitude. The derivation of the particle motion based on the equation of motion is shown in Sec. 3.1 as the zeroth order motion in a spatially non-uniform laser field. Instead, here we derive the particle motion in the uniform field by uding the momentum and energy conservation laws.

The motion of charged particle in the electromagnetic field $\mathbf{a}$ given by Eq. (1.8) can be derived from the conservation relation for the canonical momentum as follows. The relativistic Hamiltonian h for a charged particle in electromagnetic field is given by

$$h(t, z, \mathbf{p}_c) = \sqrt{m^2c^4 + c^2 \left(\mathbf{p}_c - mc\mathbf{a}(t, z)\right)^2}, \tag{1.9}$$

where $\mathbf{p}_c$ is the canonical momentum given by $\mathbf{p}_c = \mathbf{p} + mc\mathbf{a}$. Since we have assumed a uniform field with a constant amplitude $|\mathbf{a}| = a_0$, the Hamiltonian has no dependence on x and y, so that the corresponding canonical variable p_{cx} and p_{cy} are found to be constants of motion, i.e.,

$$\mathbf{p}_{c\perp} = \mathbf{p}_\perp - mc\mathbf{a} = const. \tag{1.10}$$

On the other hand, in the parallel z direction, one can find a conservation relation $p_z - \gamma mc = const.$ where γ is the relativistic factor of the particle. This relation can be obtained by the energy and momentum conservation laws as follows. We consider a system that includes a laser field having the energy $N_0\hbar\omega$ and momentum in the z direction $N_0\hbar\omega/c$, and a charged particle which initially has an energy of $\gamma_0 mc^2$ and a momentum p_{z0} in the z direction. When such a particle interacts with the laser field, the particle gains energy and momentum while the laser field loses the corresponding energy and momentum in the z direction, which can be represented by $(N_0 - N)\hbar\omega$ and $(N_0 - N)\hbar\omega/c$, respectively, where $N_0 - N$ is the absorpted photon numbers. The energy and the z-direction momentum conservations are given by

$$N\hbar\omega + \gamma mc^2 = N_0\hbar\omega + \gamma_0 mc^2, \tag{1.11}$$

$$\frac{N\hbar\omega}{c} + p_z = \frac{N_0\hbar\omega}{c} + p_{z0}. \tag{1.12}$$

Combining these relations, we find

$$p_z - \gamma mc = p_{z0} - \gamma_0 mc, \tag{1.13}$$

where the RHS is constant determined by the initial condition for the particle. Here, we introduce a variable p_η and a constant ζ_0 that are defined by

$$p_\eta \equiv p_z - \gamma mc, \tag{1.14}$$

$$-mc\zeta_0 \equiv p_{z0} - \gamma_0 mc. \tag{1.15}$$

In the present section, we consider a simple case $\zeta_0 = 1$, which corresponds to the initial condition of $\mathbf{p}_0 = \mathbf{0}$, i.e., the initial momentum of the particle is zero.

Using Eqs. (1.13) and (1.15) with $\zeta_0 = 1$, we obtain

$$\begin{aligned}(\gamma mc)^2 &= (p_z + mc)^2 \\ &= p_z^2 + 2mcp_z + m^2c^2.\end{aligned} \tag{1.16}$$

From this relation and the definition of the gamma factor, i.e., $mc\gamma = \left(m^2c^2 + \mathbf{p}^2\right)^{1/2}$,

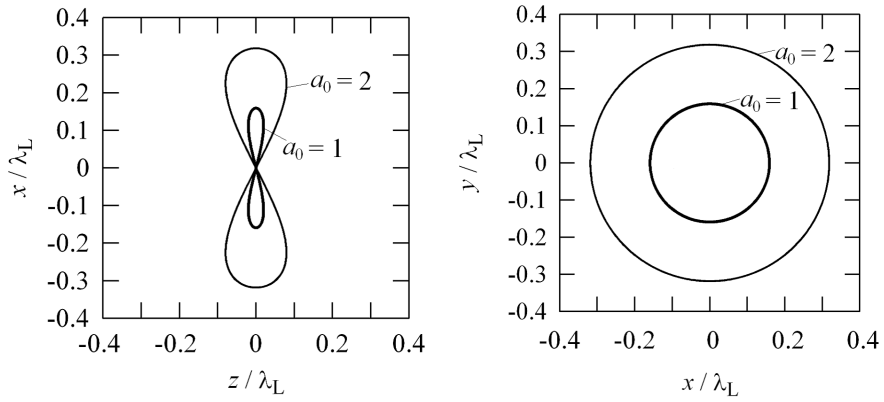

Figure 1.2: Figure-eight orbit in the uniform laser field with linear polarization (left) and circular orbit in the uniform laser field with circular polarization (right) for $a_0 = 1$ and 2 in the average rest frame. The initial condition for the particle is set to be $(\mathbf{x}, \mathbf{p}) = (\mathbf{0}, \mathbf{0})$.

the relation between transverse and longitudinal momenta is found to be

$$p_z = \frac{\mathbf{p}_\perp^2}{2mc}. \tag{1.17}$$

By substituting the solution for $\mathbf{p}_\perp$ which is obtained from Eq. (1.10), the motion in the longitudinal direction is derived as

$$p_z = \frac{mc\mathbf{a}^2}{2} = \frac{a_0^2}{2}\left(\delta_x^2 \sin^2(\omega t - kz) + \delta_y^2 \cos^2(\omega t - kz)\right). \tag{1.18}$$

Equations (1.10) and (1.18) denotes that, for the linearly polarized laser field with $(\delta_x, \delta_y) = (1, 0)$, the particle exhibits the figure-eight oscillation in the x-z plane drifting in the z direction, while, for the circular polarization where $\delta_x = \delta_y = 1/\sqrt{2}$, the particle exhibits a gyration motion in the x-y plane drifting in the z direction, respectively. In Fig. 1.2, we show the trajectories for both linear and circular polarizations with $a_0 = 1$ and 2 in the average rest frame that moves toward the z direction with the same velocity as the drift motion of the particle. The above particle motion in uniform laser field can also be derived from the Hamilton-Jacobi equation based on the canonical Hamiltonian theory [15].

The relativistic factor for these motions are given by using the notation p_η as

$$\gamma = -\frac{\omega}{mc^2}\frac{1}{2k_z p_\eta}\left(m^2c^2 + \mathbf{p}_\perp^2 + p_\eta^2\right). \tag{1.19}$$

In the case of $\zeta_0 = 1$, it leads to

$$\begin{aligned}\gamma &= \frac{\omega}{mc^2}\frac{1}{2k_z mc}\left(2m^2c^2 + (mca_0 \sin\eta)^2\right) \\ &= 1 + \frac{(a_0 \sin\eta)^2}{2} = 1 + \frac{\mathbf{a}^2}{2},\end{aligned} \tag{1.20}$$

for the linear polarization with $(\delta_x, \delta_y) = (1, 0)$, and

$$\begin{aligned}\gamma &= \frac{\omega}{mc^2}\frac{1}{2k_z mc}\left(2m^2c^2 + (mca_0\sin\eta)^2 + (mca_0\cos\eta)^2\right) \\ &= 1 + \frac{a_0^2\left(\sin^2\eta + \cos^2\eta\right)}{2} = 1 + \frac{a_0^2}{2},\end{aligned} \tag{1.21}$$

for the circular polarization with $\delta_x = \delta_y = 1/\sqrt{2}$. Hence, the averaged relativistic factor for the figure-eight motion in the linear polarized laser field is obtained as

$$\overline{\gamma} = 1 + \frac{a_0^2}{4}, \tag{1.22}$$

while for the gyration motion in the circular polarized laser field is as

$$\overline{\gamma} = 1 + \frac{a_0^2}{2}. \tag{1.23}$$

1.2.2 Classification of laser intensity regimes

Now, we consider several important thresholds of laser intensity that classify qualitatively different stages of laser-matter interaction. Here, the laser intensity is represented by the Poynting vector $\mathbf{S}$ and is related to the amplitude of the electric field E_0 as

$$I = \langle|\mathbf{S}|\rangle = \frac{c}{4\pi}\left\langle\mathbf{E}^2\right\rangle = \frac{c}{2}\epsilon_0 E_0^2, \tag{1.24}$$

in the MKS unit, where ϵ_0 is the dielectric constant in vacuum. Thus, laser electric field E_0 is related to the laser intensity I as

$$E_0\ [\mathrm{V/m}] = 2.744\times10^3\left(I\ [\mathrm{W/cm^2}]\right)^{1/2}. \tag{1.25}$$

The corresponding normalized amplitude a_0 is obtained as

$$a_0 = 8.55\times10^{-10}\lambda\ [\mu\mathrm{m}]\left(I\ [\mathrm{W/cm^2}]\right)^{1/2}, \tag{1.26}$$

for electrons.

The first threshold that separate the fundamental of high intensity laser-matter interaction is determined by the relation between laser electric field E_0 and the Coulomb field in the hydrogen atom E_{1s}. Namely, electrons behave as bounded particles for $E_0/E_{1s} \sim 1$, whereas as free electrons for $E_0/E_{1s} \gg 1$. The Coulomb

electric field at the 1s orbit is given by

$$E_{1s} = \frac{e}{4\pi\epsilon_0 a_{\rm bohr}^2} = 5.15 \times 10^{11}\ [\mathrm{V/m}], \tag{1.27}$$

where $a_{\rm bohr}$ is the Bohr radius. Together with Eq. (1.25), we obtain the relation

$$\frac{E_0}{E_{1s}} = 5.33 \times 10^{-9} \left(I\ [\mathrm{W/cm^2}]\right)^{1/2}. \tag{1.28}$$

Thus, laser intensity that satisfies $E_0/E_{1s} = 1$ is found to be $I = 3.52\times10^{16}$ [W/cm^2].

Here, ionization can also take place even when the laser intensity is below the threshold for $E_0/E_{1s} = 1$ by the multiphoton ionization. In the uncertainty principle, virtual state can be sustained during the time $\Delta t \sim \hbar/\Delta U$ where ΔU is energy of the state. This means that the ionization can take place if photons whose energy $\hbar\omega$ is smaller than the ionization energy ΔU interacts with the electron bounded in the atom. In the case of Hydrogen atom, ΔU is 13.6 eV. Considering the cross section $\pi a_{\rm bohr}^2$, we can evaluate the laser intensity needed to the multiphoton ionization as

$$I = \frac{\Delta U}{\pi a_{\rm bohr}^2 \Delta t} = 5.12 \times 10^{14}\ [\mathrm{W/cm^2}]. \tag{1.29}$$

The next threshold appears at the intensity where the electron motion becomes relativistic. As is explained above, $a_0 \geq 1$ is the condition for relativistic behavior, so that from Eq. (1.26), we have the threshold of the intensity

$$I \geq 1.368 \times 10^{18}\ [\mathrm{W/cm^2}] \equiv I_e, \tag{1.30}$$

above which electrons become relativistic. For protons having mass m_p, the intensity that corresponds to $a_0 = 1$ is obtained, by noting $a_0 \propto 1/m$, as

$$I_i = I_e \left(\frac{m_p}{m_e}\right)^2 = 4.61 \times 10^{24}\ [\mathrm{W/cm^2}]. \tag{1.31}$$

Therefore, above this intensity, not only electrons but also protons are accelerated directly by the laser light to the relativistic energy.

The third threshold is related to vacuum breakdown and is referred to as the Schwinger limit. This limit indicates the energy that is needed to create an electron-positron pair from vacuum as real particles. Namely, in order to realize the pair production, the energy equivalent to the total mass of single electron and positron, i.e. $\epsilon_{\rm pair} = 2m_e c^2 = 2 \times 0.511$[MeV], is necessary. Thus, the laser intensity that satisfies the Schwinger condition $I_{\rm Sch.}$ is given by

$$I_{\rm Sch.} \geq \frac{\epsilon_{\rm pair}}{\lambda_e^3} c = 8.53 \times 10^{28}\ [\mathrm{W/cm^2}]. \tag{1.32}$$

where λ_e is the Compton length for electron which is equivalent to multiply the light velocity c to the surviving time Δt determined by the uncertainty principle $\Delta E \Delta t \sim \hbar$.

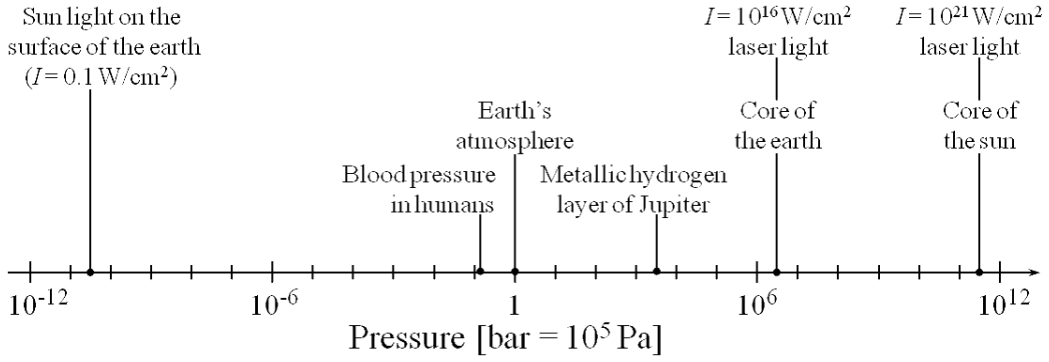

Figure 1.3: Various pressures in nature and laser fields.

1.3 Ponderomotive force and its role in laser plasma physics

1.3.1 The origin of ponderomotive force and the formulation

Ponderomotive force is the force that corresponds to the light pressure. It is found by James Clerk Maxwell that when a light of intensity I is irradiated normally to a surface of reflectivity R in vacuum, the light pressure

$$p_L = (1 + R)\frac{I}{c}, \tag{1.33}$$

is exerted [17]. Here, $R = 0$ and 1 are applied for the condition of complete absorption and reflection, respectively. In Fig. 1.3, we summarize various pressures in nature and laser fields. For instance, p_L from the sun light on the surface of the earth $I = 0.1$ W/cm^2 is $p_L = 30$ picobar, while that from the laser light with intensity of $I = 1 \times 10^{16}$ W/cm^2 is $p_L = 3$ megabar which is equivalent to the pressure at the core of the earth, i.e., 3.6 megabar. When the laser intensity reaches to $I = 1 \times 10^{21}$ W/cm^2, the light pressure becomes $p_L = 0.3$ terabar that corresponds to the pressure at the core of the sun, i.e., 0.25 terabar. This indicates that the nuclear fusion will take place at this order of intensity.

Charged particles irradiated by electromagnetic field suffer from the Lorentz force as in Eq. (1.1). As shown in the introduction Sec. 1.2, when the amplitude of the electromagnetic field is constant, the charged particle in laser electromagnetic field exhibits drift motion with a constant velocity in the propagation direction of the laser light in addition to the quiver motion. On the other hand, when the field amplitude has spatial or temporal dependences as in the case of focused laser beam or laser pulse, the charged particle suffers additionally from the secular light pressure force, i.e., the ponderomotive force. As shown in Fig. 1.4, when the laser field amplitude is spatially non-uniform in the direction of the linearly-polarized laser electric field for instance, the figure-eight orbit is not closed being pushed by the ponderomotive force $\mathbf{F}_p$, and the particle is gradually ejected from the laser field in the time scale that is slow in contrast to the laser frequency.

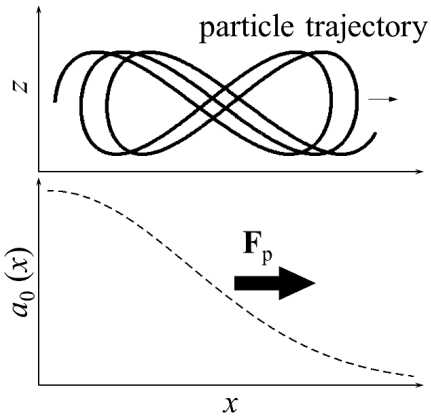

Figure 1.4: Ponderomotive force acting on a charged particle in laser field.

Here, we denote the motion is secular when the corresponding quantity has a finite value after averaging over the laser phase $\eta = \omega t - \mathbf{k} \cdot \mathbf{x}$:

$$\langle a(\eta) \rangle = \frac{1}{\eta_0} \int_{\eta}^{\eta+\eta_0} a(\eta') d\eta. \tag{1.34}$$

The phase interval η_0 is larger than the one cycle 2π of the fast variations and is small in comparison with the characterstic phase interval τ_s of variation of the slow variables. In the nonrelativistic case where $\eta \sim \omega t$ is satisfied, the phase averaging Eq. (1.34) can be written in terms of averaging over time t_0 that is large in comparison to the fast time scale ω^{-1}. We note here that spatial variations of all the quantities are assumed to be little compared with the excursion length of the quivering particle in the high frequency laser field. Such a situation can be represented by using the eikonal description where the slow and fast variations of the quantity are expressed by the amplitude and phase, respectively, as

$$a\,(t, \mathbf{x}) = a_0\,(t, \mathbf{x})\, e^{i\eta(t,\mathbf{x})}, \tag{1.35}$$

which we will introduce in deriving the laser beam proparation under the paraxial approximation in Sec. 1.3.2.

Standard derivation of the ponderomotive force

In physics, there often exists such a situation where dynamical system exhibits two or more typical time and/or spatial scales. In such a case, the averaging method is one of the useful ways to analyze the dynamics [18, 19]. In the averaging method, based on the scale separation used in Eq. (1.34), we split physical quantities into two as

$$f = \langle f \rangle + [f]_{os.} = f_s + f_f, \tag{1.36}$$

where $[\ ]_{os.}$ denotes taking fast oscillation part, and subscripts s and f represent

slowly and fastly varying parts, respectively. Namely, we have relations

$$\frac{1}{\eta_0}\int_{\eta}^{\eta+\eta_0} f_s \; d\eta \neq 0, \tag{1.37}$$

$$\frac{1}{\eta_0}\int_{\eta}^{\eta+\eta_0} f_f \; d\eta = 0. \tag{1.38}$$

Here, based on the averaging method, we derive the ponderomotive force that is expressed by the gradient of the field amplitude. We separate the equation of motion Eq. (1.1) using

$$\mathbf{E} = \mathbf{E}_f, \tag{1.39}$$

$$\mathbf{B} = \mathbf{B}_f, \tag{1.40}$$

$$\mathbf{p} = \mathbf{p}_f + \mathbf{p}_s, \tag{1.41}$$

$$\mathbf{v} = \mathbf{v}_f + \mathbf{v}_s, \tag{1.42}$$

together with the eikonal description for the field,

$$\mathbf{E} = \mathbf{E}_0\left(\eta, \mathbf{x}\right)\sin\eta. \tag{1.43}$$

Taking average over η, we obtain the slow scale equation,

$$\frac{\partial \mathbf{p}_s}{\partial t} + \mathbf{v}_s \cdot \nabla \mathbf{p}_s + \langle \mathbf{v}_f \cdot \nabla \mathbf{p}_f \rangle = q\left\langle \frac{\mathbf{v}_f}{c} \times \mathbf{B} \right\rangle. \tag{1.44}$$

Then, subtracting Eq. (1.44) from the original equation of motion, we obtain the fast scale equation

$$\frac{\partial \mathbf{p}_f}{\partial t} + \left[\mathbf{v}_f \cdot \nabla \mathbf{p}_f\right]_{os.} = q\left(\mathbf{E} + \frac{\mathbf{v}_s}{c} \times \mathbf{B} + \left[\frac{\mathbf{v}_f}{c} \times \mathbf{B}\right]_{os.}\right). \tag{1.45}$$

Here, we consider a perturbation expansion according to the expansion parameter ϵ defined as

$$l\, f_s^{-1} \nabla f_s\left(\mathbf{x}, \eta\right) \sim \epsilon \;\; \text{and} \;\; l\, f_f^{-1} \nabla f_f\left(\mathbf{x}, \eta\right) \sim \epsilon, \tag{1.46}$$

where l is the excursion length of the particle in the high frequency field. This relation indicates that both slow and fast components vary gently in space compared with l. Here, l is written in terms of the normalized laser vector potential a_0 as $l = a_0\lambda_L/2\pi$ for the initial condition $\mathbf{p}(\eta = 0) = \mathbf{0}$, i.e., the initial momentum of the particle is zero. The value of the excursion length l for the typical laser wavelength is obtained as $l\,[\mu\text{m}] = 0.131\, a_0$ for $\lambda_L = 0.82\,\mu$m and $l\,[\mu\text{m}] = 0.159\, a_0$ for $\lambda_L = 1\,\mu$m,

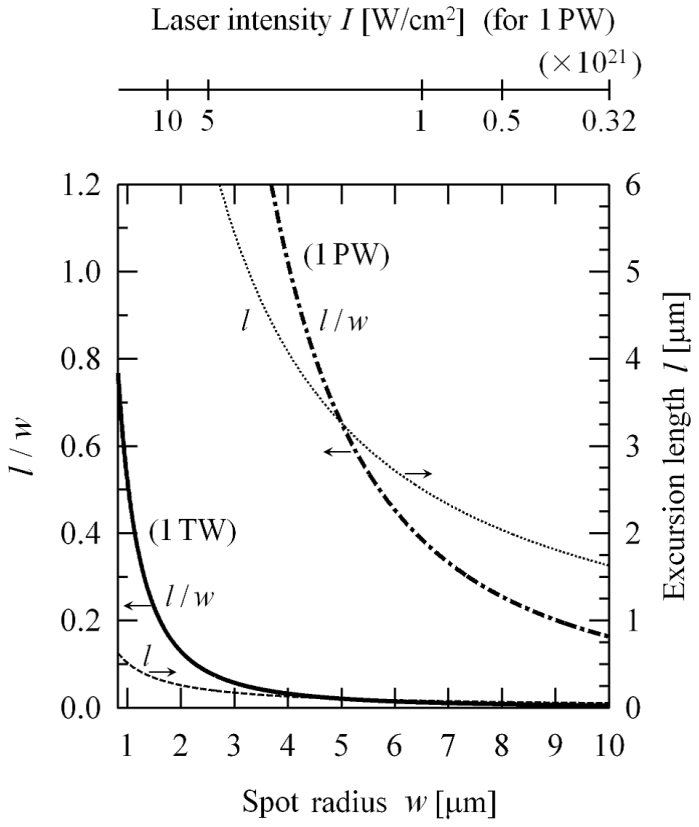

Figure 1.5: Excursion length l of an electron in a uniform laser field (dotted lines) and the ratio between l and the laser spot radius w (dash-dot line and solid line). The input laser power P is fixed to 1 TW $= 10^{12}$ W for two lines in the left side and 1 PW $= 10^{15}$ W for two lines in the right side, respectively. The laser wavelength is $\lambda_L = 0.82\,\mu$m and the initial condition of the particle is given by $\mathbf{p}(\eta = 0) = \mathbf{0}$. The upper scale shows the corresponding laser intensity evaluated by the relation $I = P/(\pi w^2)$ for the case with $P = 1$ PW.

respectively. We also order the temporal variation of the amplitude part of the eikonal field given in Eq. (1.43), i.e. $|\mathbf{E}| = E_0$, as

$$\frac{1}{E_0}\frac{\partial E_0}{\partial \eta} \sim \epsilon. \tag{1.47}$$

In Fig. 1.5, we evaluate the excursion length l and the ratio between l and the laser spot radius w, by which we can estimate the value of the expansion parameter ϵ, i.e., $l/w \sim \epsilon$. Here, we consider two cases where the input laser power P is fixed to $P = 1$ TW ($= 10^{12}$ W) and $P = 1$ PW ($= 10^{15}$ W), respectively. The laser wavelength is assumed to be $\lambda_L = 0.82\,\mu$m for both cases. Note that the laser intensity I is related to the laser power P and spot radius w as $I = P/(\pi w^2)$, which is shown in the upper scale in Fig. 1.5 for the case with $P = 1$ PW. Here, the dependences of l and l/w on the spot radius w are obtained as follows. The excursion length l, which is in proportion to the normalized amplitude a_0 and then

to the square root of intensity I, is found to be proportional to w^{-1}. The dotted lines in Fig. 1.5 show the dependence $l \propto w^{-1}$, while the dash-dot line and solid line exhibit $l/w \propto w^{-2}$. From this figure, we see that for $P = 1$ TW, l/w is smaller than unity down to the focusing limit $w \sim \lambda_L$, whereas for $P = 1$ PW, $l/w < 1$ is satisfied only when the spot radius is larger than 4 μm. These limitations denote the regime where the expansion Eq. (1.46) is valid.

Non-relativistic case

Firstly, we consider the non-relativistic limit $v/c \ll 1$, in which the slow and fast scale equations Eqs. (1.44) and (1.45) are reduced to

$$\frac{\partial \mathbf{v}_s}{\partial t} + \mathbf{v}_s \cdot \nabla \mathbf{v}_s + \langle \mathbf{v}_f \cdot \nabla \mathbf{v}_f \rangle = 0, \tag{1.48}$$

$$\frac{\partial \mathbf{v}_f}{\partial t} + [\mathbf{v}_f \cdot \nabla \mathbf{v}_f]_{os.} = \frac{q}{m}\mathbf{E}, \tag{1.49}$$

where the electric field is given by $\mathbf{E} = \mathbf{E}_0(t, \mathbf{x}) \sin \omega t$, and the ordering Eq. (1.47) is written as $\omega^{-1}\partial_t E_0 \sim \epsilon$. Neglecting the first order term with respect to ϵ in Eq. (1.49), we obtain the zeroth order equation of motion for the fast component,

$$\frac{\partial \mathbf{v}_f^{(0)}}{\partial t} = \frac{q}{m}\mathbf{E}, \tag{1.50}$$

By integrating Eq. (1.50), we obtain the zeroth order solution for $\mathbf{v}_f$ as

$$\mathbf{v}_f^{(0)} = \frac{q}{m}\mathbf{E}_0 \int \sin \omega t dt = -\frac{q}{m\omega}\mathbf{E}_0 \cos \omega t, \tag{1.51}$$

which denotes the fundamental oscillation by the laser electric field.

On the other hand, for the slow part, the second and third terms on the left-hand side (LHS) of Eq. (1.48) can be neglected in the zeroth order of ϵ, so that we obtain $\mathbf{v}_s^{(0)} = 0$. In the first order of ϵ, Eq. (1.48) becomes

$$\frac{\partial \mathbf{v}_s^{(1)}}{\partial t} = -\langle \mathbf{v}_f \cdot \nabla \mathbf{v}_f \rangle . \tag{1.52}$$

We here substitute the zeroth order solution for $\mathbf{v}_f^{(0)}$, which is given in Eq. (1.51), in the RHS of Eq. (1.52) that leads to

$$\frac{\partial \mathbf{v}_s^{(1)}}{\partial t} = -\frac{q^2}{m^2\omega^2}\mathbf{E}_0 \cdot \nabla \mathbf{E}_0 \left\langle \cos^2 \omega t \right\rangle = -\frac{q^2}{4m^2\omega^2}\nabla \mathbf{E}_0^2. \tag{1.53}$$

In the first order, we can use the relation $\partial_t = d/dt$, and therefore, we obtain the slow scale equation of motion up to the first order of ϵ as

$$m\frac{d\mathbf{v}_s}{dt} = -\frac{q^2}{4m\omega^2}\nabla \mathbf{E}_0^2. \tag{1.54}$$

The RHS is referred to as the ponderomotive force. From this discription, one can see that charged partcles are ejected inevitably from the regime where the field amplitude is large regardless of the sign of the charge. The ponderomotive force thus plays an important role in the interaction between plasmas and spatially localized laser fields, such as laser beam propagation in various mediums, laser wake field generation and the resultant particle acceleration.

Relativistic case

In the relativistic laser-plasma interaction in high intensity regime, the ponderomotive force dominates the interaction dynamics. This is because such a intense laser field is achieved by focusing the laser light to a small spot and/or reducing the pulse length, while the particle excursion length becomes larger as the field amplitude increases. The ponderomotive force, which is proportional to the laser field amplitude and its gradient as in Eq. (1.54), thus increases in such a high intensity situation.

In the relativistic case, the $\mathbf{v} \times \mathbf{B}$ terms in Eqs. (1.44) and (1.45) and the relativistic factor γ ($= \mathbf{p}/m\mathbf{v}$), which is approximated as $\gamma \sim 1$ in the non-relativistic limit, have to be taken into account. Here, it is useful to rewrite the equation of motion in terms of the normalized vector potential $\mathbf{a}$ as

$$\frac{d\mathbf{p}}{dt} = mc\left(-\frac{\partial \mathbf{a}}{\partial t} + \frac{\mathbf{p}}{\gamma m} \times (\nabla \times \mathbf{a})\right). \tag{1.55}$$

The scale separation leads to

$$\frac{\partial \mathbf{p}_s}{\partial t} + \mathbf{v}_s \cdot \nabla \mathbf{p}_s + \langle \mathbf{v}_f \cdot \nabla \mathbf{p}_f \rangle = c\left\langle \frac{\mathbf{p}_f}{\gamma} \times (\nabla \times \mathbf{a}) \right\rangle, \tag{1.56}$$

$$\frac{\partial \mathbf{p}_f}{\partial t} + [\mathbf{v}_f \cdot \nabla \mathbf{p}_f]_{os.} = -mc\frac{\partial \mathbf{a}}{\partial t} + c\left[\frac{\mathbf{p}}{\gamma} \times (\nabla \times \mathbf{a})\right]_{os.} \tag{1.57}$$

In the zeroth order of ϵ, we obtain the slow and fast scale equations as

$$\frac{\partial \mathbf{p}_s^{(0)}}{\partial t} = 0, \tag{1.58}$$

$$\frac{\partial}{\partial t}\left(\mathbf{p}_f^{(0)} + mc\mathbf{a}\right) = 0. \tag{1.59}$$

The fast equation Eq. (1.59) denotes the canonical momentum conservation in the uniform field, from which the solution for the fast component is obtained as $\mathbf{p}_f^{(0)} = -mc\mathbf{a}$. For the slow component, we have $\mathbf{p}_s^{(0)} = 0$. In the first order of ϵ, the slow scale equation is obtained as

$$\frac{\partial \mathbf{p}_s^{(1)}}{\partial t} = -\frac{1}{m}\left\langle \frac{\mathbf{p}_f}{\gamma} \cdot \nabla \mathbf{p}_f \right\rangle + c\left\langle \frac{\mathbf{p}_f}{\gamma} \times (\nabla \times \mathbf{a}) \right\rangle. \tag{1.60}$$

By substituting the zeroth order relation $\mathbf{a} = -\mathbf{p}_f/mc$ and using the vector formula

$$\mathbf{a} \times (\nabla \times \mathbf{a}) = \frac{1}{2}\nabla \mathbf{a}^2 - (\mathbf{a} \cdot \nabla)\, \mathbf{a}, \tag{1.61}$$

we obtain

$$\frac{d\mathbf{p}_s}{dt} = -\frac{mc^2}{2\overline{\gamma}}\nabla \overline{\mathbf{a}^2}, \tag{1.62}$$

where $\partial_t = d/dt$ which is satisfied in the first order approximation os utilized to the LHS. Equation (1.62) is the first-order slow scale equation of motion, and the RHS represents the relativistic ponderomotive force, which is derived on the basis of the first order approximation with respect to ϵ [20, 21, 22]. Therefore, the ponderomotive force is represented as being proportional to the laser field amplitude also in the relativistic regime.

1.3.2 Ponderomotive force and laser beam propagation in plasmas

Next, we consider the propagation of spatially localized laser electromagnetic field in plasmas. In this case, since the amplitude profile of the laser field in non-uniform, the ponderomotive force exists and plays a role in evacuating the peripheral plasmas. In such a case, the force balance between ponderomotive force and the electrostatic force originating from the charge separation of plasmas determines the interaction dynamics and structure such as plasma channeling formation and laser self-focusing.

To describe such a propagation dynamics, charge separation and Coulomb force, and resultant modulation to the laser field, have to be self-consistently determined. For this purpose, governing equations, such as the nonlinear Schrödinger (NS) equation, wave kinetic equation, etc., have been explored [23, 24].

In this section, in order to see the effect of ponderomotive force in determining the laser beam propagation, we derive the NS equation which describes the evolution of the envelope of a laser field in plasmas. The NS equation is obtained by coupling the field equations and the equation of motion for electrons, with an assumption that the ponderomotive force and the Coulomb force originated from the charge separation are balanced leading to a steady state in electron motion. The ponderomotive force is thus a key ingredient in describing the self-consistent laser plasma interactions. Note that in deriving the NS equation, the equation of motion for ions is not considered, because the time scale of ion motion is much slower than the laser period and also the secular response of electrons to the ponderomotive force and electrostatic charge separation force, due to the large mass ratio between electron and ion.

Field equations

We start from the Maxwell equations,

$$\nabla \cdot \mathbf{E} = 4\pi\rho, \tag{1.63}$$
$$\nabla \cdot \mathbf{B} = 0, \tag{1.64}$$
$$\nabla \times \mathbf{B} = \frac{1}{c}\frac{\partial \mathbf{E}}{\partial t} + \frac{4\pi}{c}\mathbf{J}, \tag{1.65}$$
$$\nabla \times \mathbf{E} = -\frac{1}{c}\frac{\partial \mathbf{B}}{\partial t}, \tag{1.66}$$

where ρ and $\mathbf{J}$ are the charge and current densities, respectively. Introducing the scalar and vector potentials defined by Eqs. (1.5) and (1.6), and normalizing them as

$$\mathbf{a} = \frac{e\mathbf{A}}{m_e c^2}, \tag{1.67}$$
$$\phi = \frac{e\Phi}{m_e c^2}, \tag{1.68}$$

where e and m_e are the charge and rest mass of electron, respectively, we rewrite the Maxwell equations Eqs. (1.65) and (1.66) in terms of $\mathbf{a}$ and ϕ as

$$\frac{1}{c^2}\frac{\partial^2 \mathbf{a}}{\partial t^2} - \nabla^2 \mathbf{a} + \nabla\left(\nabla \cdot \mathbf{a}\right) = \frac{1}{c^2}\left[-c\frac{\partial\left(\nabla\Phi\right)}{\partial t} + \frac{4\pi e}{m_e c}\mathbf{J}\right], \tag{1.69}$$
$$-\nabla^2\phi - \frac{1}{c}\frac{\partial\left(\nabla \cdot \mathbf{a}\right)}{\partial t} = \frac{4\pi e}{m_e c^2}\rho. \tag{1.70}$$

Here, we employ the Coulomb gauge given by

$$\nabla \cdot \mathbf{a} = 0. \tag{1.71}$$

Neglecting the longitudinal current component represented by the term $c\nabla(\partial_t\phi)$ on the RHS of Eq. (1.69), we obtain the wave equation for the vector potential,

$$\frac{1}{c^2}\frac{\partial^2 \mathbf{a}}{\partial t^2} - \nabla^2 \mathbf{a} = \frac{4\pi e}{m_e c}\mathbf{J}, \tag{1.72}$$

and the Poisson equation for the scalar potential,

$$-\nabla^2\phi = \frac{4\pi e}{m_e c^2}\rho. \tag{1.73}$$

Here, using an approximation $v_i \ll v_e$, we express $\mathbf{J}$ in terms of electron velocity $\mathbf{v}_e$ as

$$\mathbf{J} = -en_e\mathbf{v}_e + Zen_i\mathbf{v}_i \sim -en_e\mathbf{v}_e. \tag{1.74}$$

Then, Eq. (1.72) becomes

$$\frac{\partial^2\mathbf{a}}{\partial t^2} - c^2\nabla^2\mathbf{a} = -\omega_p^2\frac{n_e}{Zn}\frac{\mathbf{v}_e}{c}, \tag{1.75}$$

On the other hand, for the charge density ρ in the Poisson equation, we use the relation

$$\rho = -en_e + eZn_i = en\left(Z - \frac{n_e}{n}\right), \tag{1.76}$$

and obtain

$$c^2\nabla^2\phi = \omega_p^2\left(\frac{n_e}{Zn} - 1\right). \tag{1.77}$$

Equations (1.75) and (1.77) are the field equations which we will utilize in deriving the NS equation.

Equation of motion

The equation of motion for electron that suffers from the Lorentz force from the laser electromagnetic field and the Coulomb force from the static electric field due to charge separation is given by

$$\left(\frac{\partial}{\partial t} + \frac{\mathbf{p}}{\gamma_e m_e}\cdot\nabla\right)\mathbf{p} = m_e c\frac{\partial\mathbf{a}}{\partial t} + m_e c^2\nabla\phi - \frac{m_e c^2}{\gamma_e}\left(\frac{1}{2}\nabla\mathbf{a}^2 - (\mathbf{a}\cdot\nabla)\,\mathbf{a}\right). \tag{1.78}$$

We assume that the envelope of the field is x-dependent, i.e., $f = f(x)$, but approximately uniform satisfying Eq. (E.10). Then, the solution of Eq. (1.78) in the order of ϵ^0 is obtained as

$$\mathbf{p}_f = m_e c\mathbf{a} + \mathscr{O}(\epsilon), \tag{1.79}$$

where the subscript f denotes fast varying component oscillating in the laser phase $\eta = \omega t - kz$. Substituting the zeroth-order solution Eq. (1.79) to Eq. (1.78) and averaging it over η, one can obtain the slow component of the equation of motion as follows:

$$\left(\frac{\partial}{\partial t} + \frac{\overline{\mathbf{p}}}{\gamma_e m_e}\cdot\nabla\right)\mathbf{p}_s = m_e c^2\nabla\phi(x) - \frac{\overline{m_e c^2}}{2\gamma_e}\nabla\mathbf{a}^2(x) + \mathscr{O}\left(\epsilon^2\right), \tag{1.80}$$

where variable with subscript s corresponds to the slow component averaged over

the phase η and the overline denotes taking average in cycle η. The second term on the RHS of Eq. (1.80) is the first order ponderomotive force originating from terms $\mathbf{v} \times (\nabla \times \mathbf{a})$ and $(\mathbf{p}_f \cdot \nabla)\, \mathbf{p}_f$.

Here, we consider a steady state in the time scale of electron response that is assumed to be slow compared with the laser period. In such a condition, the LHS of Eq. (1.80) can be neglected and thus we have the following balance relation between the ponderomotive force and charge separation force:

$$m_e c^2 \nabla \phi\,(x) = \overline{\frac{m_e c^2}{2\gamma_e} \nabla \mathbf{a}^2\,(x)} + \mathscr{O}\left(\epsilon^2\right). \tag{1.81}$$

The scalar potential ϕ on the LHS of Eq. (1.81) can be expressed in terms of the electron density $n_e\,(x)$ with the help of the Poisson equation Eq. (1.77). Then, the slow response of the electron density to the field variation is found to be described as

$$\omega_p^2 \frac{n_e\,(x)}{Zn} = \omega_p^2 + \nabla \cdot \overline{\frac{c^2}{2\gamma_e} \nabla \mathbf{a}^2\,(x)} + \mathscr{O}\left(\epsilon^3\right). \tag{1.82}$$

The Nonlinear Schrödinger equation

Now, by using Eqs. (1.79) and (6.1), we express the electron density n_e and velocity $\mathbf{v}_e$ on the RHS of Eq. (1.75) in terms of the field $\mathbf{a}$ as

$$\frac{\partial^2 \mathbf{a}}{\partial t^2} - c^2 \nabla^2 \mathbf{a} = -\left[\omega_p^2 + \overline{\frac{m_e c^2}{2\gamma_e} \nabla \mathbf{a}^2\,(x)}\right] \frac{\mathbf{a}}{\gamma_e} + \mathscr{O}\left(\epsilon^3\right). \tag{1.83}$$

Here, we again employ the paraxial approximation where Eqs. (E.4) and (E.10) are satisfied, and introduce the eikonal description,

$$\mathbf{a}\,(\mathbf{x}_\perp, \eta) = \frac{1}{2}\left(a_0\,(\mathbf{x}_\perp, \eta)\, e^{i\eta} + c.c.\right) \hat{\mathbf{e}}_a, \tag{1.84}$$

where $\hat{\mathbf{e}}_a$ is the unit vector in the direction of $\mathbf{a}$. Note that the relation between $\mathbf{a}$ and the amplitude a_0 in Eq. (1.84) is written as

$$\left\langle \mathbf{a}^2 \right\rangle = \frac{a_0^2}{2}, \tag{1.85}$$

where the brackets indicates the average over the phase η.

Next, we transform the coordinate variables from (x, y, z, t) to $(x, y, z, \eta\,(t, z))$. In the new coordinates, the derivative operators on the LHS of Eq. (1.83) is written as

$$\frac{\partial^2}{\partial t^2} - c^2 \nabla^2 = \omega_p^2 \frac{\partial^2}{\partial \eta^2} - c^2 \left(\nabla_\perp^2 + \nabla_\parallel^2\right) + 2c^2 k \nabla_\parallel \frac{\partial}{\partial \eta}, \tag{1.86}$$

where $\nabla_\perp = (\partial_x, \partial_y)$ and $\nabla_\parallel = \partial_z$.

Employing the above descriptions Eqs. (E.11) and (1.84), we can rewrite the wave equation Eq. (1.83) as

$$\left(e^{i\eta} \left[\frac{\partial a_0}{\partial \eta} - \frac{i}{2}\frac{\partial^2 a_0}{\partial \eta^2} + \frac{ic^2}{2\omega_p^2}\left(\nabla_\perp^2 + \nabla_\parallel^2\right) a_0 + \frac{i}{2}\left(1 - \frac{1}{\gamma_e}\left[1 + \frac{1}{\omega_p^2}\nabla \cdot \overline{\frac{c^2}{4\gamma_e}\nabla a_0^2}\right]\right) a_0 \right] + c.c. \right) \hat{\mathbf{e}}_a + \mathscr{O}\left(\epsilon^3\right) = 0. \tag{1.87}$$

By assuming the paraxial approximation, $\partial_\eta^2 \ll \partial_\eta$ and $\nabla_\parallel^2 \ll k\nabla_\parallel$, and neglecting terms consist of ∂_η^2 and $\nabla_\parallel^2$, Eq. (1.87) leads to

$$\frac{\partial a_0}{\partial \eta} + \frac{ic^2}{2\omega_p^2}\nabla_\perp^2 a_0 + \frac{i}{2}\left(1 - \frac{1}{\gamma_e}\right) a_0 - \frac{i}{2}\frac{a_0}{k_p^2 \gamma_e}\nabla \cdot \left(\overline{\frac{a_0}{2\gamma_e}\nabla a_0}\right) + \mathscr{O}\left(\epsilon^3\right) = 0. \tag{1.88}$$

For simplicity, we here consider a circular polarized laser field in which γ_e has no oscillatory component and therefore Eq. (1.88) can be written as

$$\frac{\partial a_0}{\partial \eta} + \frac{ic^2}{2\omega_p^2}\nabla_\perp^2 a_0 + \frac{i}{2}\left(1 - \frac{1}{\overline{\gamma_e}}\right) a_0 - \frac{i}{2}\frac{a_0}{k_p^2 \overline{\gamma_e}}\nabla \cdot \left(\frac{a_0}{2\overline{\gamma_e}}\nabla a_0\right) + \mathscr{O}\left(\epsilon^3\right) = 0. \tag{1.89}$$

Weakly relativistic approximation

When we assume a weakly nonlinear regime where γ_e can be expanded as

$$\frac{1}{\overline{\gamma_e}} = \frac{1}{\sqrt{1 + \overline{a^2}}} \sim 1 - \frac{1}{2}\overline{a^2} = 1 - \frac{|a_0|^2}{4}, \tag{1.90}$$

Eq. (1.89) is approximated to

$$\frac{\partial a_0}{\partial \eta} + \frac{ic^2}{2\omega_p^2}\nabla_\perp^2 a_0 + \frac{i}{2}\left(1 - (1 - \frac{|a_0|^2}{4})\right) a_0 - \frac{i}{2}\frac{a_0}{k_p^2}(1 - \frac{|a_0|^2}{4})\nabla \cdot \left((1 - \frac{|a_0|^2}{4})\frac{a_0}{2}\nabla a_0\right) + \mathscr{O}\left(\epsilon^3\right) = 0, \tag{1.91}$$

which can be written as

$$\frac{\partial a_0}{\partial \eta} + \frac{ic^2}{2\omega_p^2}\nabla_\perp^2 a_0 + \frac{i}{2}\frac{|a_0|^2}{4} a_0 - \frac{i}{2}\frac{a_0}{k_p^2}\nabla \cdot \left(\frac{a_0}{2}\nabla a_0\right) + \mathscr{O}\left(a^5\right) + \mathscr{O}\left(\epsilon^3\right) = 0. \tag{1.92}$$

Then, by neglecting terms in the order of a_0^5 and ϵ^3 on the basis of the weak nonlinear and the paraxial approximations, we finally obtain the nonlinear Schrödinger (NS) equation given by

$$\frac{\partial a_0}{\partial \eta} + \frac{ic^2}{2\omega_p^2}\nabla_\perp^2 a_0 + \frac{i}{8}\left|a_0\right|^2 a_0 - \frac{i}{2}\frac{a_0}{k_p^2}\nabla^2\left|a_0\right|^2 = 0. \tag{1.93}$$

The NS equation is nonlinear having two terms that depend on a_0^3; one is the third term on the LHS of Eq. (1.93) which originates from the expansion of the relativistic factor, and another is the fourth term on the LHS of Eq. (1.93) which originates from the ponderomotive force term in the electron density shown in Eq. (6.1). We also note that the two second spatial derivative terms in the NS equation have different origins. Namely, the second term on the LHS of Eq. (1.93) is originated simply from the spatial derivative term in the wave equation, i.e., the second term on the LHS of Eq. (1.83), whereas, the last term on the LHS of Eq. (1.93) is originated from the ponderomotive force that is proportional to the gradient of the field amplitude a_0. Therefore, the ponderomotive force affects the order of nonlinearity and also the order of spatial derivative in the NS equation.

Solution for the Nonlinear Schrödinger equation

We consider obtaining the approxinated solution for the electron density response to the field variation described by Eq. (6.1), i.e.,

$$\omega_p^2\frac{n_e\left(x\right)}{Zn} = \omega_p^2 + \nabla\cdot\overline{\frac{c^2}{2\gamma_e}\nabla\mathbf{a}^2\left(x\right)} + \mathscr{O}\left(\epsilon^3\right). \tag{1.94}$$

using the expansion

$$n_e\left(x\right) = n_e^{(0)} + \epsilon n_e^{(1)}\left(x\right) + \epsilon^2 n_e^{(2)}\left(x\right) + \cdots. \tag{1.95}$$

Here, ϵ is the smallness parameter defined in Sec. 1.3.2 as $k^{-1}\nabla|\mathbf{a}\left(x\right)| \sim \epsilon \ll 1$. The zeroth order component of Eq. (1.94) is given by

$$\omega_p^2\frac{n_e^{(0)}}{Zn} = \omega_p^2, \tag{1.96}$$

which derives the zeroth order solution

$$n_e^{(0)} = Zn. \tag{1.97}$$

The first order component of Eq. (1.94) is given by

$$\omega_p^2\frac{n_e^{(1)}\left(x\right)}{Zn} = 0, \tag{1.98}$$

which leads to

$$n_e^{(1)} = 0. \tag{1.99}$$

The second order component of Eq. (1.94) is given by

$$\frac{n_e^{(2)}\left(x\right)}{Zn} = \frac{c^2}{\omega_p^2}\nabla\cdot\overline{\frac{1}{2\gamma_e}\nabla\mathbf{a}^2\left(x\right)}. \tag{1.100}$$

This equation denotes the electron density perturbation due to the ponderomotive force, which is balanced with the Coulomb force of the plasma charge separation.

1.4 Motivation and outline of the present study

I. Theoretical study on higher order nonlocal effects of relativistic ponderomotive force in high power lasers

As is described in Sec. 1.3, ponderomotive force, which corresponds to the pressure of electromagnetic fields, plays a dominant role in high intensity laser-matter interection. Moreover, in recent years, more delicate control of laser field profiles in plasmas for various applications is anticipated. For instance, a flat top super Gaussian beam, in which the ponderomotive force is significantly weakened near the axis, is considered to be preferable in maintaining long interaction between laser and particles, and also in achieving efficient particle acceleration via the laser piston and/or Coulomb explosion mechanism [25, 26].

In such a case, the force estimated from the conventional formula, i.e., the force proportional to the local field gradient, tends to be diminished, so that a residual higher order force associated with nonlocal profile will become important. Therefore, designing laser field patterns up to fine scales and controlling the interaction are key issues to lead experiments using such high power lasers to success. In order to realize them, it is important to take into account effects from the nonlocal particle motion in intense laser field on the ponderomotive force up to higher orders, which are not simply expressed by the local field gradient as the Fick's law [27].

Furthermore, the effect of plasmas, such as charge separation and Coulomb force, and resultant modulation to the laser field, has to be self-consistently determined in such a situation. However, there exists no formal theory to describe them correctly except direct numerical integration which cannot provide a prospective guideline.

To circumvent this difficulty, we herein explore a theory of relativistic ponderomotive force that includes nonlocal effects up to higher orders. One possible approach to this problem is to directly investigate the higher order terms based on the averaging method, which we showed in Sec. 1.3.1 up to the first order of ϵ. However, the result is not ensured up to higher orders since the method is not subject to the Hamiltonian structure which is essential in describing long time scale dynamics. Here, as a method keeping the Hamiltonian structure up to higher orders but avoiding the complication of canonical perturbation due to the usage of the limited class of canonical variables, we employ the variational principle in noncanonical phase space coordinates incorpolated with the Lie transformation which is referred to as the noncanonical Lie perturbation method [28].

By properly choosing the gauge function and coordinate transformations, we obtain a secular equation of motion describing the ponderomotive force including the nonlocal effect up to higher orders. The formula is accessible to the regime in which laser fields exhibit characteristic structures such that higher derivatives of the field amplitude regulate the interaction. As an example, we apply the obtained formula to study the particle motion in a flat-top super Gaussian and a concave hollow laser beam structures. In these profiles, since the local field gradient is diminished near the beam axis, the higher-order terms are expected to dominate the dynamics. In order to examine the nonlocal ponderomotive theory we propose here, we further study the propagation of super Gaussian laser beams in plasmas on the basis of the particle-in-cell (PIC) simulation. The self-consistent interaction are considered to

result from plual physical processes such as the higher order ponderomotive force near the beam axis, the resultant modulation of plasma density, generation of the Coulomb field, and change of linear and nonlinear susceptibilities, which could be described by generalizing the nonlinear Schrödinger equation system to include the higher order nonlocal effects.

Chapters for Part I are organized as follows: In Chap. 2, we introduce the noncaonical Lie perturbation method used in this study. In Chap. 3, we perform a noncanonical Lie perturbation analysis, and a new formula for the ponderomotive force that includes higher order nonlocal effects up to the third order of the expansion parameter ϵ is obtained. Based on the derived formula, we investigate its analytical solution in Chap. 4. Comparison with the solution for the conventional first order formula is discussed. In Chap. 5, we solve the third order formula numerically assuming a flat-top super Gaussian and a concave hollow laser beam profiles. Comparison with the direct integration of the particle orbit demonstrates the validity of the formula derived here with a sufficient convergence of the expansion series up to the third order of ϵ. In Chap. 6, we carry out a PIC simulation for the propagation of super Gaussian laser beams in plasmas. A prominent moduration of electron density and laser beam profiles is found to appear especially in the case of flatter super Gaussian beam. We discuss the role of the higher order nonlocal ponderomotive force in describing such a self-consistent interaction based on the nonlinear Schrödinger equation.

II. Numerical study on the interaction between high power laser and cluster medium

The interaction between high power laser and matter has opened up various kinds of application such as high energy particle acceleration, generation of intense radiations from tera-heltz to EUV and x-ray, and neutron production [6]. Here, the state of material is a key ingredient which determines the characteristics of the interaction, and has to be chosen properly according to the purpose. For instance, besides solid and gas, cluster is interested, which exhibit prominent features essentially due to the existence of surface, i.e., a large ratio of the surface to the volume. A cluster mode (slow mode) is one of the examples where the laser can propagate even when the average density of the medium is higher than the critical density, owing to the surface polarization of the cluster [29]. Neutron generation for nuclear fusion utilizing the Coulomb explosion of clusters has been intensively studied [9, 30]. Recently, high energy ion acceleration has been realized by the interaction between a high-contrast intense laser field and a medium composed of gas and clusters [31].

To control the laser-matter interaction in achieving such various applications, the internal structure of target mediums is considered to play an important role. The dependence of laser propagation and ion accerelation mechanisms on the state and structure of the target, e.g., the gas density, thickness of the solid film, cluster radius and packing fraction of cluster mediums, have been investigated assuming laser intensities up to 10^{20-21} W/cm^2, which are controlable in the current experiments.

In this study, we investigate the interaction between laser and cluster medium

extending the intensity higher than 10^{22} W/cm^2 up to 10^{24} W/cm^2, which is expected to be achieved in near future [32]. In this regime, not only electrons but also ions can be accelerated to relativistic velocities. One of new acceleration mechanisms achieved in this regime is the laser piston acceleration where a solid thin film is accelerated as a whole by the radiation pressure [25]. In such a regime, the ions in the cluster medium is expected to suffer from accelerations both by the direct radiation pressure and by the Coulomb explosion inside of the medium. In order to understand the synergistic effects of these acceleration mechanisms and their dependence on the internal structure of target mediums, we perform PIC simulations for the interaction between laser and cluster mediums consisting of the same total mass, i.e. same packing fraction, but having different cluster radius, using a fully-relativistic electromagnetic PIC code (EPIC3D) [33, 34].

Chapters for Part II are organized as follows: In Chap. 7, the background of the studies on laser-cluster interaction is described. Here, we introduce fundamentals of the Coulomb explosion of clusters and discuss the maximum ion energy that can be achieved by the single cluster Coulomb explosion. In Chap. 8, we carry out PIC simulations for the interaction of lasers in the intensity range of 10^{22-24} W/cm^2 with cluster mediums and also with a solid thin film. Comparisons of the interaction dynamics and achieved ion energies among cases of different targets are discussed in detail.

We summarize the studies presented in Parts I and II in Sec. 9. Derivation of the higher-order ponderomotive force using the averaging method is given in Appendix A. Appendix B shows a different choice of noncanonical coordinate that can also remove oscillations from the equation of motion in deriving the higher order ponderomotive force. In Appendix C, we assume an additional component of the laser vector potential, i.e., a small ϵ-order component in the direction of laser propagation, to satisfy the Maxwell equations in vacuum up to the first order. Lie perturbation analysis with such an additional component is performed, and its effect to the higher order ponderomotive force is discussed. In Appendix D, a calculation to verify the discussion on the possibility for expressing the higher order ponderomotive force by a potential form, which is given in Sec. 3.4.3, is performed. In Appendix E, we derive the Hermite-Gauss mode laser beam propagation in vacuum based on the paraxial approximation for the basic understanding of laser beam propagation discussed in Chap. 6. In Appendix F, convergence of the PIC simulation performed in Part II is checked by using different super particle numbers and mesh sizes.

Part I

Theoretical study on higher order nonlocal effects of relativistic ponderomotive force in high power lasers

Chapter 2

Methodology of Hamiltonian-based perturbation analysis

The ponderomotive force is derived generally by applying the averaging method to the equation of motion, and expressed as a force proportional to the local field gradient on the basis of the first order approximation with respect to the expansion parameter ϵ. However, in considering fine scale controll of the laser-matter interaction in high intensity regime, higher-order effects from the nonlocal particle motion will become important.

One approach to explore the higher-order nonlocal ponderomotive force is to simply extend the analysis based on the averaging method up to higher orders. However, the result is not ensured up to higher orders since the method is not subject to the Hamiltonian structure which is essential in describing long time scale dynamics.

Here, among various perturbation methods, we have reached an idea to employ the noncanonical Lie perturbation method [28]. This method is based on the phase space Lagrangian formalism which allows us to derive the perturbed motion rigoulously up to higher orders maintaining the Hamiltonian structure. Furthermore, incorpolating with the noncanonical Lie transformation, the methodology is perspective in spliting oscillatory and secular motions up to higher orders.

The noncanonical Lie perturbation method has been so far introduced to gyrokinetics for describing magnetically-confined fusion plasmas [36, 37]. The method is found to be efficient and powerful in describing the long time scale dynamics with rigolous energy conservation based on the gyro-center coordinate. The method is also introduced to beam orbit analyses in free-electron lasers (FEL) [38, 39]. These studies demonstrate that the methodology is superior in describing the relativistic particle motion in complicated electromagnetic fields.

In Sec. 2.1, we at first introduce the canonical and noncanonical Hamiltonian mechanics, and in Sec. 2.2, we describe the Lie perturbation theory together with determining the degrees of freedom of the gauge function and Lie generator for the near-identity transformation we employ in this study.

2.1 Hamiltonian mechanics

2.1.1 Canonical theory

The equation of motion is derived from applying the variational principle to the action S. The variational principle is the fundamental determination valid for all the mechanical system: The action S, a integrated quantity determined for the system, takes a minimum value for the actual motion of a particle. In other words, the variation of the action δS becomes zero. Since the physics unchanges under the Lorentz transformation, and so the equation of motion does, the action S must be a scalar. In this paper, we consider the system which includes electromagnetic fields and scalar particles. The action S for such a system is expressed as a sum of three parts, $S = S_m + S_{mf} + S_f$ where S_m, S_{mf} and S_f correspond to the action denoting the motion of free particles, interaction between particles and fields, and behavior of fields, respectively.

2.1.1.1 Action integral and variational principle

The action for a free scalar particle S_m is constracted from the quantities that characterize the particle in the system. A possible scalar integral is

$$-mc \int ds, \tag{2.1}$$

where m is the rest mass of the particle, c the light velocity and ds the world distance. The coefficient of the integral is determined so that S_m reduces to that of the nonrelativistic, $S_m^{(nr)}$, expressed as

$$S_m^{(nr)} = \int_{t_1}^{t_2} L_m^{(nr)} dt, \tag{2.2}$$

where $L_m^{(nr)}$ is the nonrelativistic Lagrangian defined by

$$L_m^{(nr)} = \frac{1}{2} m v^2. \tag{2.3}$$

Here, v is the velocity of the particle, and t_1 and t_2 are the time in which the particle arrives at the starting and ending points of the trajectory variation, respectively. Then, S_m is obtained as

$$S_m = -mc^2 \int \sqrt{1 - \frac{v^2}{c^2}} dt. \tag{2.4}$$

The action for the interacting part S_{mf} consists of the particle charge q, which is only the quantity denoting the response of particles to the fields, and the four vector for the field potential $A_\mu = (\phi, -\mathbf{A})$. Then, S_m is defined as

$$S_{mf} = -\frac{q}{c} \int A_\mu dx^\mu = \int \left(\frac{q}{c} \mathbf{A} \cdot \mathbf{v} - q\phi \right) dt. \tag{2.5}$$

where $x^\mu = (ct, \mathbf{x})$ and bold characters denote N dimensional vectors in the system

having N degrees of freedom. In this paper, we follow the Einstein summation convention: When an indexed variable appears twice in a single term, we take product in that term over all the index values.

From the sum of the actions $S = S_m + S_{mf}$, the relativistic Lagrangian describing the particle motion in electromagnetic fields is obtained as

$$L = -mc^2\sqrt{1 - \frac{v^2}{c^2}} + \frac{q}{c}\mathbf{A}\cdot\mathbf{v} - q\phi. \tag{2.6}$$

The Hamiltonian h, defined by the relation $h = \mathbf{p}_c \cdot \dot{\mathbf{q}} - L$, is written as

$$h = \sqrt{m^2c^4 + c^2\left(\mathbf{p}_c - q\mathbf{A}/c\right)^2} + q\phi, \tag{2.7}$$

where $\dot{\mathbf{q}} = \mathbf{v}$ and dot $\dot{}$ denotes total derivative by the independent variable t. Here, $\mathbf{p}_c$ is the canonical momentum corresponding to the coordinate $\mathbf{q}$ and has a relation between the mechanical momentum $\mathbf{p}$ as

$$\mathbf{p}_c = \mathbf{p} + \frac{q}{c}\mathbf{A} \tag{2.8}$$

2.1.1.2 Hamilton equation of motion

The action S is expressed in terms of the Hamiltonian h and the canonical phase space coordinate variables $\mathbf{q}, \mathbf{p}_c$ as

$$S = \int \left(\mathbf{p}_c \cdot \dot{\mathbf{q}} - h\right) dt = \int \left(-h dt + \mathbf{p}_c \cdot d\mathbf{q}\right). \tag{2.9}$$

The variation of the action Eq. (2.9) in the $2N$ dimensional phase space $(\mathbf{q}, \mathbf{p}_c)$ is carried out as

$$\delta S = \delta \int \left(\mathbf{p}_c \cdot \dot{\mathbf{q}} - h\right) dt = \int \left[\left(\dot{\mathbf{q}} - \frac{\partial h}{\partial \mathbf{p}_c}\right)\delta\mathbf{p}_c - \left(\dot{\mathbf{p}}_c + \frac{\partial h}{\partial \mathbf{q}}\right)\delta\mathbf{q}\right] dt. \tag{2.10}$$

Then, the variational principle $\delta S = 0$ leads to the Hamilton equation of motion in canonical coordinate,

$$\frac{d\mathbf{q}}{dt} = \frac{\partial h}{\partial \mathbf{p}_c}, \qquad \frac{d\mathbf{p}_c}{dt} = -\frac{\partial h}{\partial \mathbf{q}}. \tag{2.11}$$

Equation (2.11) can be also derived by using the notation of phase space Lagrangian $L\left(t; \mathbf{q}, \mathbf{p}_c\right)$ and taking its variation. In the phase space Lagrangian formalism, we describe the action integral as

$$S = \int \left(\mathbf{p}_c \cdot \frac{d\mathbf{q}}{dt} - h\left(t; \mathbf{q}, \mathbf{p}_c\right)\right) dt = \int L\left(t; \mathbf{q}, \mathbf{p}_c\right) dt. \tag{2.12}$$

Then, the variational priciple leads to the Eular-Lagrange equation which has the same form as the Hamilton equation Eq. (2.11).

2.1.1.3 Noether's theorem

One of the most important theorems incoorpolated with the Hamiltonian mechanics is the Noether's theorem. This theorem indicates the relation between conservation laws of various quantities and the corresponding symmetry of the system. Assume that the system has a translation symmetry so that Lagrangian has an invariance under the infinitesimal transformation,

$$q^j \mapsto q^{j\prime} = q^j + \delta q^j. \tag{2.13}$$

The change of Lagrangian must be zero, e.g. $\delta L = 0$, under the transformation Eq. (2.13), where δL is calculated as

$$\begin{aligned}
\delta L &= L\left(\mathbf{q}', \dot{\mathbf{q}}', t\right) - L\left(\mathbf{q}, \dot{\mathbf{q}}, t\right) \\
&= L\left(\mathbf{q}, \dot{\mathbf{q}}, t\right) + \frac{\partial L}{\partial q^j}\delta q^j + \frac{\partial L}{\partial \dot{q}^j}\delta \dot{q}^j - L\left(\mathbf{q}, \dot{\mathbf{q}}, t\right) \\
&= \frac{\partial L}{\partial q^j}\delta q^j + \frac{d}{dt}\left(\frac{\partial L}{\partial \dot{q}^j}\delta q^j\right) - \delta q^j \frac{d}{dt}\left(\frac{\partial L}{\partial \dot{q}^j}\right) \\
&= \left[\frac{\partial L}{\partial q^j} - \frac{d}{dt}\left(\frac{\partial L}{\partial \dot{q}^j}\right)\right]\delta q^j + \frac{d}{dt}\left(\frac{\partial L}{\partial \dot{q}^j}\delta q^j\right).
\end{aligned} \tag{2.14}$$

Comparing with the Eular-Lagrange equation,

$$\frac{\partial L}{\partial q^j} - \frac{d}{dt}\left(\frac{\partial L}{\partial \dot{q}^j}\right) = 0, \tag{2.15}$$

we see that the first term on the righthand side (RHS) of Eq. (2.14) is zero. Then, $\delta L = 0$ yields

$$\frac{d}{dt}\left(\frac{\partial L}{\partial \dot{q}^j}\delta q^j\right) = 0, \tag{2.16}$$

which leads to

$$\frac{\partial L}{\partial \dot{q}^j} = \text{const.} \tag{2.17}$$

By using the relation

$$\mathbf{p}_c = \frac{\partial L}{\partial \dot{\mathbf{q}}}, \tag{2.18}$$

we obtain the conservation law for the canonical momentum,

$$\mathbf{p}_c = \text{const.} \tag{2.19}$$

When the system is independent of one of the coordinate variables q^j, and therefore

the Hamiltonian does not consists of q^j, the equation of motion for the corresponding canonical variable becomes

$$\frac{dp_c^j}{dt} = 0, \tag{2.20}$$

which indicates that the quantity p_c^j is an invariant of the motion. The ignorable coordinate q^α is related to the symmetry of the system. This is so called the Noether's theorem: When the system has a symmetry, the corresponding invariant exists.

The Noether's theorem indicates that if we find an ignorable coordinate, then the number of the equations to be solved is reduced. In other words, the RHS of the Hamilton's equation Eq. (2.11) is zero for the partial derivative by the ignorable coordinate, and consequently, the corresponding coordinate variable is found to be constant. One of the merits to use the Hamiltonian formalism is that by transforming coordinate to that includes ignorable coordinates, we can significantly simplify the problem; namely, we can reduce the dimension to be solved. However, the coordinate transformation $(\mathbf{q}, \mathbf{p}_c) \mapsto (\mathbf{Q}, \mathbf{P}_c)$ in the canonical Hamilton theory is restricted to canonical transformations which require that, in the new coordinate $(\mathbf{Q}, \mathbf{P}_c)$, the Hamilton's equation with a scalar function K (new Hamiltonian),

$$\frac{d\mathbf{Q}}{dt} = \frac{\partial K}{\partial \mathbf{P}_c}, \qquad \frac{d\mathbf{P}_c}{dt} = -\frac{\partial K}{\partial \mathbf{Q}}, \tag{2.21}$$

is satisfied. This restriction sometimes makes it difficult to analyze the problem by using the canonical Hamilton theory. This is the reason why many problems still have been investigated on the basis of the equation of motion that employs noncanonical but physically understandable coordinates despite of the brilliant mathematical structure of the canonical theory.

2.1.2 Noncanonical theory

As mentioned in the previous section, coordinates available in the canonical theory is restricted to the canonical coordinates; such coordinates are not always appropriate to describe the motion in physically clear way. For this reason, here we consider extending the canonical Hamilton theory to that appricable to the noncanonical coordinate. This is realized by introducing a $2N + 1$ dimensional time and phase space vector

$$z^\mu = (t; \mathbf{q}, \mathbf{p}_c), \tag{2.22}$$

and the corresponding covariant vector

$$\gamma_\mu = (-h; \mathbf{p}_c, \mathbf{0}), \tag{2.23}$$

where the $\mu = 0$ components in z_c^μ and $\gamma_{c\mu}$ correspond to time and the minus sign of the Hamiltonian, respectively. By using these vectors, the integrant of the action integral is expressed as

$$\delta S = \delta \int \gamma_\mu dz^\mu = 0. \tag{2.24}$$

Here, Latin indices run from 1 to 6 whereas Greek from 0 to 6. The scalar $\gamma_\mu dz^\mu \equiv \hat{\gamma}$ is referred to as the fundamental one-form or phase space Lagrangian.

Here, one recongizes that, since the integrant is written in a scalar form, Eq. (2.24) is satisfied in an arbitrary coordinate not restricted to the canonical one. Then, we here consider a new arbitrary noncanonical coordinate Z^μ and derive the corresponding covartiant vector Γ_μ in the new coordinate. The relation between the old and new covariant vector is obtained from the scalar relationship

$$\gamma_\mu dz^\mu = \Gamma_\mu dZ^\mu, \tag{2.25}$$

as

$$\Gamma_\mu = \gamma_\nu \frac{\partial z^\nu}{\partial Z^\mu}. \tag{2.26}$$

This transformation is referred to as the noncanonical transformation since the coordinate Z^μ can be a noncanonical coordinate.

Writing the action integral in terms of the new 1-form as (2.26),

$$S = \int \Gamma_\mu dZ^\mu, \tag{2.27}$$

and then applying the variational principle to this action, the resulting equation of motion is that written in the noncanonical coordinate. Namely, by considering variation to (2.24) along the trajectory, we have

$$\delta S = \delta \int dz^0 \gamma_\mu \frac{dz^\mu}{dz^0} = \int dz^0 \left(\frac{\partial \gamma_\nu}{\partial z^\mu} - \frac{\partial \gamma_\mu}{\partial z^\nu} \right) \frac{dz^\nu}{dz^0} \delta z^\mu = 0, \tag{2.28}$$

Therefore, the Euler-Lagrange equation is derived as

$$\omega_{\mu\nu} \frac{dz^\nu}{dz^0} = 0, \tag{2.29}$$

where

$$\omega_{\mu\nu} \equiv \frac{\partial \gamma_\nu}{\partial z^\mu} - \frac{\partial \gamma_\mu}{\partial z^\nu}. \tag{2.30}$$

Here, the phase space component of $\omega_{\mu\nu}$, i.e., ω_{ij}, which is equivalent to the Lagrange bracket $[z^i, z^j]$, is referred to as Lagrange tensor. Note that in the canonical coordinate $z^\mu = (t; \mathbf{q}, \mathbf{p}_c)$, the Lagrange tensor becomes

$$\omega_{ij} = \begin{pmatrix} \mathbf{0} & -\mathbf{1} \\ \mathbf{1} & \mathbf{0} \end{pmatrix}, \tag{2.31}$$

where $\mathbf{0}$ and $\mathbf{1}$ denotes 3×3 zero matrix and identity matrix, respectively.

Equation (2.29) is separated into time and phase space components as

$$\omega_{ij}\frac{dz^j}{dz^0}+\left(\frac{\partial\gamma_0}{\partial z^i}-\frac{\partial\gamma_i}{\partial z^0}\right)=0, \tag{2.32}$$

$$\left(\frac{\partial\gamma_j}{\partial z^0}-\frac{\partial\gamma_0}{\partial z^j}\right)\frac{dz^j}{dz^0}=0. \tag{2.33}$$

However, the time component Eq. (2.33) can be also obtained from Eq. (2.32) utilizing the asymmetry of $\omega_{\mu\nu}$. Hence, only the phase space component in the Euler-Lagrange equation Eq. (2.29) are independent each other. Introducing the Poisson tensor J^{jk} defined as the inverse matrix of the Lagrange tensor, Eq. (2.32) is written as

$$\frac{dz^j}{dz^0}=J^{jk}\left(\frac{\partial\gamma_k}{\partial z^0}-\frac{\partial\gamma_0}{\partial z^k}\right). \tag{2.34}$$

This is the equation of motion in an arbitrary noncanonical coordinate. When we consider a canonical coordinate, the Poisson tensor becomes

$$J^{jk}=\begin{pmatrix}\mathbf{0} & \mathbf{1}\\ -\mathbf{1} & \mathbf{0}\end{pmatrix}. \tag{2.35}$$

Then, one can see that Eq. (2.34) is equivalent to the Hamilton equation

$$\frac{d\mathbf{q}}{dt}=\frac{\partial h}{\partial\mathbf{p}_c}, \tag{2.36}$$

$$\frac{d\mathbf{p}_c}{dt}=-\frac{\partial h}{\partial\mathbf{q}}. \tag{2.37}$$

Therefore, Eq. (2.34) is regarded as an extended Hamiltonian equation that is applicable in noncanonical coordinates.

2.2 Noncanonical Lie perturbation theory

The Lie transformation is a near identity transformation characterized by the generator g^μ as

$$z^\mu\mapsto z'^\mu=\exp\left(\mathscr{L}\right)z^\mu\equiv T^{-1}z^\mu, \tag{2.38}$$

where the operator $\mathscr{L}$ is defined as $\mathscr{L}f=g^\mu\partial_\mu f$ for scalar function f and $\mathscr{L}\xi_\mu=g^\nu\left(\partial_\nu\xi_\mu-\partial_\mu\xi_\nu\right)$ for 1-form $\hat{\xi}$. The corresponding covariant vector is transformed as

$$\gamma_\mu\mapsto\gamma'_\mu=T\gamma_\mu+\partial_\mu S, \tag{2.39}$$

where S is the gauge function. In the perturbation analysis, we repeat the Lie transformation as $T = \cdots T^{(3)}T^{(2)}T^{(1)}$ where $T^{(n)} = \exp\left(\epsilon^n \mathscr{L}^{(n)}\right)$.

In the Lie perturbation method, we can utilize $2N+2$ ($N = 3$) degrees of freedom determined by the $2N+1$ Lie generators and a gauge function S to make the 1-form suitable for the analysis. In the following, we derive the relation among generator, gauge function and the Lie-transformed 1-form used in this study.

We expand the 1-form by using the smallness parameter ϵ as

$$\hat{\gamma} = \hat{\gamma}^{(0)} + \epsilon\hat{\gamma}^{(1)} + \epsilon^2\hat{\gamma}^{(2)} + \cdots, \tag{2.40}$$

Under the coordinate transformation

$$z^\mu \to Z^\mu = \mathscr{Z}_{\rm f}^\mu(z) = \cdots T^{(1)-1}T^{(2)-1}T^{(3)-1}\mathscr{I}^\mu(z), \tag{2.41}$$

the 1-form is transformed as

$$\hat{\Gamma}(\cdot) = T\hat{\gamma}(\cdot) + dS(\cdot). \tag{2.42}$$

By expanding all the perturbed quantities, i.e. $\hat{\gamma}$, T and S, and collecting terms order-by-order, we obtain the following relations:

$$\hat{\Gamma}^{(0)}(\cdot) = \hat{\gamma}^{(0)}(\cdot), \tag{2.43}$$
$$\hat{\Gamma}^{(1)}(\cdot) = dS^{(1)}(\cdot) - L^{(1)}\hat{\gamma}^{(0)}(\cdot) + \hat{\gamma}^{(1)}(\cdot), \tag{2.44}$$
$$\hat{\Gamma}^{(2)}(\cdot) = dS^{(2)}(\cdot) - L^{(2)}\hat{\gamma}^{(0)}(\cdot) + \hat{\gamma}^{(2)}(\cdot) - L^{(1)}\hat{\gamma}^{(1)}(\cdot) + \frac{1}{2}L^{(1)2}\hat{\gamma}^{(0)}(\cdot), \tag{2.45}$$

which can be written in the general form

$$\hat{\Gamma}^{(n)}(\cdot) = dS^{(n)}(\cdot) - L^{(n)}\hat{\gamma}^{(0)}(\cdot) + C^{(n)}(\cdot). \tag{2.46}$$

Here, we note that in deriving the ponderomotive force on the basis of the perturbation method, spatial derivatives may be ordered as $\partial_i \sim \epsilon$. Therefore, we here separate the first and second terms on the RHS of Eq. (2.46) and rewrite the relation as

$$\Gamma_\mu^{(n)} = \left(\partial_\mu S^{(n)}\right)^{(n)} - \left(g^{\nu(n)}\left(\omega_{\nu\mu}^{(0)}\right)^{(0)}\right)^{(n)} + D_\mu^{(n)}, \tag{2.47}$$

where $D_\mu^{(n)}$ is defined by

$$D_\mu^{(n)} = \left(\partial_\mu S^{(n-1)}\right)^{(n)} - \left(g^{\nu(n-1)}\left(\omega_{\nu\mu}^{(0)}\right)^{(1)}\right)^{(n)} + C_\mu^{(n)}. \tag{2.48}$$

Note that $D_\mu^{(n)}$ can be obtained from the lower order calculations, i.e., $\geq \mathscr{O}\left(\epsilon^{n-1}\right)$.

We here introduce constraints for the Lie transformation as

$$g^{(n)0} = 0, \tag{2.49}$$

$$\Gamma_i^{(n)} = 0, \tag{2.50}$$

for $n \geq 1$. The first constraint Eq. (2.49) is equivalent to $Z^0 \left(= \mathscr{Z}_{\mathrm{f}}^0(z)\right) = z^0$. This denotes that we do not transform the zeroth component of the coordinates, which is time t in the basic canonical coordinates. The second $2N$ constraints Eq. (2.50) are introduced to make the perturbation analysis easy. Namely, under the condition Eq. (2.50), the phase space components of the new covariant vector in the Lie transformed coordinates have the same functional form as that in the zeroth order in the original coordinates as $\Gamma_i^{(n)}(\cdot) = \gamma_i^{(0)}(\cdot)$. Consequently, the Poisson tensor keeps its functional form as same as that in the zeroth order in the original coordinates. By substituting Eqs. (2.49) and (2.50) to Eq. (2.47), we have

$$\Gamma_0^{(n)} = \left(\partial_0 S^{(n)}\right)^{(n)} - g^{(n)j} \left(\omega_{j0}^{(0)}\right)^{(0)} + D_0^{(n)}, \tag{2.51}$$

$$0 = \left(\partial_i S^{(n)}\right)^{(n)} - g^{(n)j} \left(\omega_{ji}^{(0)}\right)^{(0)} + D_i^{(n)}, \tag{2.52}$$

for the zeroth and ith components, respectively. Oparating $\omega_{ji}^{(0)-1} = J^{(0)ij}$ to Eq. (2.52) from the right side, we obtain $g^{(n)j}$ as

$$g^{(n)j} = \left(\partial_i S^{(n)}\right)^{(n)} + D_i^{(n)} J^{(0)ij}. \tag{2.53}$$

Substituting Eq. (2.53) to the RHS of Eq. (2.51), we obtain the relation for $\Gamma_0^{(n)}$ as

$$\begin{aligned}\Gamma_0^{(n)} = &\left(\partial_0 S^{(n)}\right)^{(n)} + D_0^{(n)} \\ &- \left(\left(\partial_i S^{(n)}\right)^{(n)} + D_i^{(n)}\right) J^{(0)ij} \left(\omega_{j0}^{(0)}\right)^{(0)}.\end{aligned} \tag{2.54}$$

Here, we introduce the unperturbed flow vector $V^{(0)\mu}$ defined by $V^{(0)0} = 1$ and $V^{(0)i}(Z) = dZ^{(0)i}/dZ^0$. The latter can be rewritten as $J^{(0)ij} \left(\omega_{j0}^{(0)}\right)^{(0)} = -\left(V^{(0)i}\right)^{(0)}$. By using these relations on the RHS of Eq. (2.54), we obtain

$$\Gamma_0^{(n)} = \left(\left(\partial_\mu S^{(n)}\right)^{(n)} + D_\mu^{(n)}\right) \left(V^{(0)\mu}\right)^{(0)}. \tag{2.55}$$

Here, we assume the gauge function to satisfy the relation

$$\overline{\left(\partial_\mu S^{(n)}\right)^{(n)} \left(V^{(0)\mu}\right)^{(0)}} = 0, \tag{2.56}$$

Degree of freedom	Lie transformation		Lie generator, gauge function
1	$Z^0 = z^0$	$\rightarrow$	$g^{(n)0} = 0$
2N	$\Gamma_i^{(n)} = 0 \ (n \geq 1)$	$\rightarrow$	$g^{(n)j} = \left(\partial_i S^{(n)}\right)^{(n)} + D_i^{(n)} J^{(0)ij}$
1	$\Gamma_0^{(n)} = \overline{D_\mu^{(n)} \left(V^{(0)\mu}\right)^{(0)}}$	$\leftarrow$	$\overline{S^{(n)}} = 0$

Figure 2.1: Procedure of determining the degrees of freedom of Lie transformation.

which leads to

$$\overline{\Gamma_0^{(n)}} = \overline{D_\mu^{(n)} \left(V^{(0)\mu}\right)^{(0)}}. \tag{2.57}$$

For the oscillatory part, we can choose $\left[\Gamma_0^{(n)}\right]_{\text{os.}} = 0$. Here, the LHS in Eq. (2.56) is given by

$$\begin{aligned} \overline{\left(V^{(0)\mu}\right)^{(0)} \left(\partial_\mu S^{(n)}\right)^{(n)}} &= \overline{\frac{\partial S^{(n)}}{\partial \eta}} + \frac{dZ^i}{d\eta} \left(\frac{\partial S^{(n)}}{\partial Z^i}\right)^{(n)} \\ &= \frac{\partial S^{(n)}}{\partial \eta}, \end{aligned} \tag{2.58}$$

In the coordinates Z^μ. Using the relations $(dP_x/d\eta)^{(0)} = 0$, $dP_y/d\eta = 0$, $dp_\eta/d\eta = 0$, $\left(\partial_X S^{(n)}\right)^{(n)} = 0$, $\partial_Y S^{(n)} = 0$, $\partial_Z S^{(n)} = 0$ and $\left(\partial_\eta S^{(n-1)}\right)^{(n)} = 0$, Eq. (2.55) becomes

$$\overline{\frac{\partial S^{(n)}}{\partial \eta}} = 0 \Longrightarrow \overline{S^{(n)}} = 0. \tag{2.59}$$

Equation (2.59) denotes a restriction for obtaining the gauge function that has no secularity. Then, the gauge function is determined by Eq. (2.57) as

$$\frac{\partial S^{(n)}}{\partial \eta} = \left[D_\mu^{(n)} \left(V^{(0)\mu}\right)^{(0)}\right]_{\text{os.}}. \tag{2.60}$$

We summarize the process of determining the degrees of freedom of Lie transformation in Fig. 2.1.

Finally, we note on the meaning of *Avoiding Secularity* in determining the gauge function. We consider the gauge transformation

$$\gamma_\mu \mapsto \gamma'_\mu = \gamma_\mu + \partial_\mu S. \tag{2.61}$$

After the transformation, the action integral is given as

$$\int \gamma'_\mu dz^\mu = \int \gamma_\mu dz^\mu + \int \partial_\mu S dz^\mu = \int \gamma_\mu \frac{dz^\mu}{d\lambda} d\lambda + \int \frac{\partial S}{\partial z^\mu}\frac{dz^\mu}{d\lambda} d\lambda. \tag{2.62}$$

The first term on the RHS of Eq. (2.62) leads to the equations of motion obtained by non gauge-transformed 1-form. In order to confirm that the gauge transformation has no influence on the equations of motion, we investigate the second term on the RHS of Eq. (2.62). We consider the variation about the i component of trajectory, i.e., $z^i \to z^i + \delta z^i$ and $z^\mu \to z^\mu (\mu \neq i)$. Then, the variation of the second term on the RHS of Eq. (2.62) is

$$\begin{aligned}
\delta \int \frac{\partial S}{\partial z^\mu}\frac{dz^\mu}{d\lambda} d\lambda &= \int \left[\frac{\partial S(z^i + \delta z^i)}{\partial z^\mu} \frac{d}{d\lambda} \left(z^\mu + \delta z^\mu \right) - \frac{\partial S(z^i)}{\partial z^\mu}\frac{dz^\mu}{d\lambda} \right] d\lambda \\
&= \int \left[\left\{ \left(\frac{\partial S(z^i)}{\partial z^\mu} + \delta z^i \frac{\partial^2 S(z^i)}{\partial z^i z^\mu} + \cdots \right) \right\} \left\{ \frac{dz^\mu}{d\lambda} + \frac{d\delta z^\mu}{d\lambda} \right\} - \frac{\partial S(z^i)}{\partial z^\mu}\frac{dz^\mu}{d\lambda} \right] d\lambda \\
&= \int \left[\frac{\partial S(z^i)}{\partial z^i}\frac{d\delta z^i}{d\lambda} + \delta z^i \frac{\partial^2 S(z^i)}{\partial z^i z^\mu}\frac{dz^\mu}{d\lambda} + \cdots \right] d\lambda \\
&= \left[\frac{\partial S(z^i)}{\partial z^\mu} \delta z^\mu \right]_{\lambda_1}^{\lambda_2} - \int \delta z^i \frac{d}{d\lambda}\frac{\partial S(z^i)}{\partial z^i} d\lambda + \int \delta z^i \frac{d}{d\lambda}\frac{\partial S(z^i)}{\partial z^i} d\lambda + \mathcal{O}\left(\delta z^{i2} \right) \\
&= \left[\frac{\partial S(z^i)}{\partial z^\mu} \delta z^\mu \right]_{\lambda_1}^{\lambda_2} + \mathcal{O}\left(\delta z^{i2} \right).
\end{aligned} \tag{2.63}$$

In the derivation, we have used $\delta z^\mu = 0$ for $\mu \neq i$. The variation of δz at the ends of the trajectory are zero, i.e. $\delta z\left(\lambda_1\right) = \delta z\left(\lambda_2\right) = 0$, so that Eq. (2.62) is finally found to be

$$\int \gamma'_\mu dz^\mu = \int \gamma_\mu dz^\mu, \tag{2.64}$$

which indicates the invariance of the equations of motion under the gauge transformation. However, we must carefully note that if

$$\left.\frac{\partial S(z^i)}{\partial z^\mu}\right|_{\lambda_1} \text{ and/or } \left.\frac{\partial S(z^i)}{\partial z^\mu}\right|_{\lambda_2} \tag{2.65}$$

has a infinite value, then, we cannot make the first term on the RHS of Eq. (2.63) to zero. Thus, we conclude that only when Eq. (2.65) has a infinite value at any λ, the invariance of the equations of motion under the gauge transformation is valid.

In order to satisfy the condition for gauge invariance, S must not include terms that secularly increase with independent variable λ. In other words, S must be constructed by periodic or constant terms regarding to the independent variable. Otherwise, the value of Eq. (2.65) at $\lambda = \infty$ becomes infinity that cause secularity in gauge.

The motion in the original coordinate z^μ can be obtained by the backward transformation $z'^\mu \mapsto z^\mu$.

Chapter 3

Noncanonical Lie perturbation analysis of relativistic ponderomotive force

In this chapter, we perform the noncanonical Lie perturbation analysis to derive the relativistic ponderomotive force up to higher orders. The structure of this chapter is as follows.

In Sec. 3.1, we consider a proper set of coordinate variables to investigate the average force in laser fields in relativistic regime. In Sec. 3.1.1, the noncanonical transformation is performed, and the fundamental 1-form in the new coordinate suitable for the analysis is derived. By using the variational principle on the basis of the obtained 1-form, we derive the figure-eight motion in the uniform laser field, i.e. the zeroth order unperturbed motion, in Sec. 3.1.2, and by using the unperturbed solution, we further transform the coordinate to that of an oscillation center in Sec. 3.1.3. In Sec. 3.2, the expansion parameter ϵ for the perturbation is defined (Sec. 3.2.1), and then we perform the Lie perturbation analysis up to the third order of ϵ based on the oscillation center 1-form obtained in Sec. 3.1. In Sec. 3.4, discussions on the derived higher order 1-form and ponderomotive force are given.

3.1 Preparatory transformation

3.1.1 Proper noncanonical coordinates for relativistic particle motion in laser fields

Here, we study the relativistic motion of particle irradiated by high intensity laser light. For this purpose, we consider a system involves a charged particle q and electromagnetic fields represented by the scalar and vector potentials, Φ and $\mathbf{A}$, which are normalized as

$$(\phi, \mathbf{a}) \equiv \frac{|q|}{mc^2} (\Phi, \mathbf{A}) . \tag{3.1}$$

In such a system, the Hamiltonian is written as

$$h = \gamma mc^2 + \sigma mc^2\phi, \tag{3.2}$$

where σ is the sign of the charge, i.e., $\sigma = \pm 1$, and γ is the relativistic factor of particle given by

$$\gamma = \sqrt{m^2c^4 + c^2\left(\mathbf{p}_c - mc\mathbf{a}\right)^2}. \tag{3.3}$$

in the canonical coordinate Eq. (2.22) with $\mathbf{q} = \mathbf{x}$. Note that when an electromagnetic field exists, the canonical momentum is the summation of mechanical momentum $\mathbf{p}$ and the field part, i.e.,

$$\mathbf{p}_c = \mathbf{p} + mc\mathbf{a}. \tag{3.4}$$

Here, we assume a linearly polarized laser field propagating in the z-direction expressed by the vector potential $\mathbf{a} = (\mathbf{a}_\perp, a_z)$ where $\mathbf{a}_\perp = (a_x, a_y)$. Note that when one considers plasmas, a_z can represent a static perpendicular magnetic field in addition to the longitudinal component of the laser field, while Φ denotes a static electric field. Such static fields may given by the equilibrium of background plasma distribution.

In this section, we find a coordinate that leads to a perspective description of the relativistic particle motion in laser fields. First, we consider transformation of the independent variable t. In electromagnetic fields, charged particle basically exhibits a periodic motion in the period of laser phase $\eta = \omega t - \mathbf{k}\cdot\mathbf{x}$ rather than time t. The difference between η and t becomes significant in the relativistic regime where $d\eta/d(\omega t) \sim \gamma \gg 1$. Hence, we choose phase η as the new independent variable and execute the coordinate transformation $z_c^\mu \mapsto w^\mu$ where

$$z_c^\mu = \left(t; x, y, z, p_{cx}, p_{cy}, p_{cz}\right), \tag{3.5}$$
$$w^\mu = \left(\eta; x, y, z, p_{cx}, p_{cy}, p_{cz}\right). \tag{3.6}$$

Here, the covariant vector $\gamma_{c\mu}$ in the old coordinate z_c^μ is given by

$$\gamma_{c\mu} = \left(-mc^2\left(\gamma\left(\eta, \mathbf{p}_c, \mathbf{x}\right) + \sigma\phi\left(\mathbf{x}, t\right)\right); p_{cx}, p_{cy}, p_{cz}, 0, 0, 0\right), \tag{3.7}$$

where we explicitly write the variable dependence of γ and ϕ assuming that the fields $\mathbf{a}$ and ϕ depend on $\mathbf{x}$ and t. Note that the above transformation $t \mapsto \eta$ is necessary to move to an oscillation center coordinate that is shown later. To see the difference between coordinates z_c^μ and w^μ, we show in Fig. 3.1 a solution for coordinate variables z_c^i and w^i with respect to the independent variables t and η, respectively, assuming a uniform plane laser field $\mathbf{a} = a_0 \sin\left(\omega t - kz\right)\hat{\mathbf{e}}_x$ with $a_0 = 1$ and 2. The vertical axes are normalized by the laser wavelength $\lambda_L = 2\pi/k$ and the horizontal axes in Figs. 3.1 (a) and (b) are normalized by the laser period

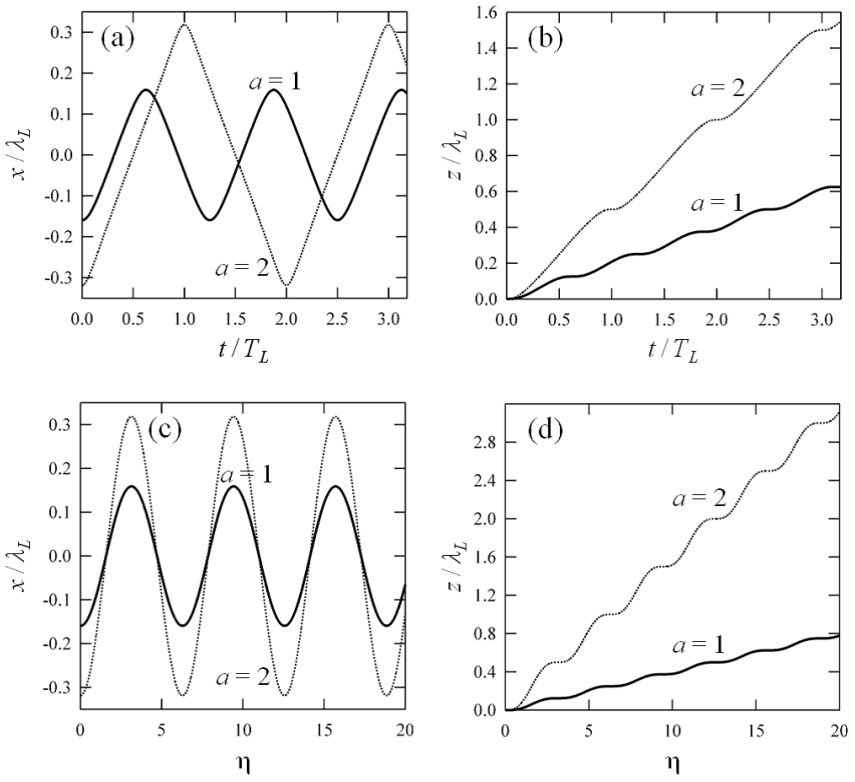

Figure 3.1: Solution for coordinate variables (a) and (b): z_c^i, (c) and (d): w^i $(i = 1, 3)$, in the case with a uniform plane laser field $\mathbf{a} = a_0 \sin\eta\ \hat{\mathbf{e}}_x$ where $a_0 = const$ and $\eta = \omega t - kz$. The vertical axes are normalized by the laser wavelength $\lambda_L = 2\pi/k$ and the horizontal axes in (a) and (b) are normalized by the laser period $T_L = 2\pi/\omega$.

$T_L = 2\pi/\omega$. Here, a vacuum with $\phi = 0$ is assumed, and the initial condition for the particle is set to be $(\mathbf{x}, \mathbf{p}_c) = (-l, 0, 0, 0, 0, 0)$ at $\eta = 0$ where l is the excursion length in the x direction. Comparing (a) and (c), or (b) and (d), we see a difference between particle orbits described by independent variables t and η, especially in the case of the larger field amplitude $a_0 = 2$. This is due to the relativistic effect discussed above, i.e., $d\eta/d(\omega t) \gg 1$ is satistied for intense fields with $a_0 \gg 1$. The shift of the oscillation frequency between $a_0 = 1$ and 2 in Fig. 3.1 (a) reflects the difference of the drift velocity in the z direction which affects the value of the phase $\eta = \omega t - kz$.

The covariant vector in the new coordinate w^μ is calculated using the transformation law Eq. (2.26) as

$$\psi_0 = \gamma_{c\mu}\frac{\partial z_c^\mu}{\partial w^0} = -\frac{h}{\omega} = -\frac{mc}{k}\left(\gamma + \sigma\phi\right), \tag{3.8}$$

$$\psi_i = \gamma_{c\mu}\frac{\partial z_c^\mu}{\partial w^i} = p_{ci} - \frac{h}{\omega}k_i = p_{ci} - mc\frac{k_i}{k}\left(\gamma + \sigma\phi\right) \quad (i = 1, 2, 3), \tag{3.9}$$

$$\psi_j = \gamma_{c\mu}\frac{\partial z_c^\mu}{\partial w^j} = 0 \quad (j = 4, 5, 6), \tag{3.10}$$

$$\tag{3.11}$$

Therefore, the 1-form in the new coordinate is given by

$$\hat{\psi} = -\frac{mc^2}{\omega}\left(\gamma + \sigma\phi\right) d\eta + \sum_{i=1}^{3}\left(p_{ci} - mc\frac{k_i}{k}\left(\gamma + \sigma\phi\right)\right) dx^i. \tag{3.12}$$

When we assume that the wave vector has only a component parallel to the propagation direction z, i.e., $\mathbf{k} = (0, 0, k_z)$, then Eq. (3.12) reduces to

$$\hat{\psi} = -\frac{mc^2}{\omega}\left(\gamma + \sigma\phi\right) d\eta + p_{cx}dx + p_{cy}dy + \left(p_{cz} - mc\left(\gamma + \sigma\phi\right)\right) dz. \tag{3.13}$$

The Lagrange tensor in this coordinate are

$$\omega_{ij} = \begin{pmatrix} \mathbf{\Omega}_1 & -\mathbf{\Omega}_2 \\ {}^t\mathbf{\Omega}_2 & \mathbf{0} \end{pmatrix}; \tag{3.14}$$

$$\mathbf{\Omega}_1 = mc\begin{pmatrix} 0 & 0 & -\partial_x\left(\gamma + \sigma\phi\right) \\ 0 & 0 & -\partial_y\left(\gamma + \sigma\phi\right) \\ \partial_x\left(\gamma + \sigma\phi\right) & \partial_y\left(\gamma + \sigma\phi\right) & 0 \end{pmatrix}, \tag{3.15}$$

$$\mathbf{\Omega}_2 = mc\begin{pmatrix} 1 & 0 & 0 \\ 0 & 1 & 0 \\ -\partial_{p_{cx}}\gamma & -\partial_{p_{cy}}\gamma & 1 - \partial_{p_{cz}}\gamma \end{pmatrix}, \tag{3.16}$$

Here, we see that Eq. (3.14) has complicated non-orthogonal components. Namely, even when spatially uniform field is assumed so that $\partial_i\phi = 0$ and $\partial_i\gamma = 0$ for $i = x, y, z$ are satisfied, the derivatives of relativistic factor γ appearing in Eq. (3.16) still exist. This complication is originated from ψ_1, ψ_2 and ψ_3 that include the relativistic factor γ explicitly. We found that this difficulty can be concoured by choosing

$$\mathbf{M}_c \equiv \mathbf{p}_c - \gamma mc\frac{\mathbf{k}}{k}, \tag{3.17}$$

as ones of coordinate variables. Note that when the condition $\mathbf{k} = (0, 0, k_z)$ is assumed, the above definition leads to

$$M_{cx} = p_{cx}, \tag{3.18}$$
$$M_{cx} = p_{cx}, \tag{3.19}$$
$$M_{cz} = p_{cz} - \gamma mc \equiv p_{c\eta}. \tag{3.20}$$

then, it is easy to see that $\mathbf{M}_c$ is constant of motion in a uniform laser field discussed in Sec. 1.2. Now, we transform coordinates from w^μ Eq. (3.6) to a new one defined

by

$$Z_c^\mu = (\eta; x, y, z, M_{cx}, M_{cy}, M_{cz})\,. \tag{3.21}$$

The covariant vector in the new coordinate is given as

$$\Gamma_{c0} = \psi_{c0}\frac{\partial w^0}{\partial Z_c^0} = -\frac{mc}{k}\left(\gamma + \sigma\phi\right), \tag{3.22}$$

$$\Gamma_{ci} = \psi_{ci}\frac{\partial w^i}{\partial Z_c^i} = M_{ci} - \sigma mc\frac{k_i}{k}\phi \quad (i = 1, 2, 3)\,, \tag{3.23}$$

$$\Gamma_{cj} = \psi_{cj}\frac{\partial w^j}{\partial Z_c^j} = 0 \quad (j = 4, 5, 6)\,. \tag{3.24}$$

Comparing Eqs. (3.9) and (3.23), we see that the relativistic factor γ no longer appears in the new covariant vector, which leads to a simpler Lagrange tensor with $\mathbf{\Omega}_2 = mc\ \mathbf{I}$.

Here, we note that the relativistic factor γ in the Hamiltonian component Γ_{c0} have to be expressed in term of the new coordinate variables. Since we are employing the canonical momentum, the Hamiltonian $-\Gamma_{c0}$ includes the vector potential $\mathbf{a}$ explicitly. Here, we notice that by introducing the mechanical momentum defined by $\mathbf{p} = \mathbf{p}_c - mc\mathbf{a}$, the Hamiltonian can be written in simpler form. Furthermore, the usage of mechanical momentum $\mathbf{p}$ as one of the coordinate variables instead of $\mathbf{p}_c$ has an advantage in deriving the *force* (acceleration) to the particle directly from the variational principle. Namely, when we employ the canonical momentum, the resulting Hamilton equation represents the variation of $\mathbf{p}_c$, which does not correspond to the particle equation of motion. In contrast, the set of mechanical coordinate variables $(\mathbf{x}, \mathbf{p})$ enables us to obtain the equation of motion and then the force directly from the variational principle.

From the above reasons, we define a new coordinate as

$$z^\mu = (\eta; x, y, z, M_x, M_y, M_z)\,, \tag{3.25}$$

where

$$\mathbf{M} = \mathbf{p} - \gamma mc\frac{\mathbf{k}}{k}. \tag{3.26}$$

For this purpose, one can use the definition of γ, i.e.,

$$(\gamma mc)^2 = m^2c^2 + \mathbf{p}^2, \tag{3.27}$$

and the relation

$$\mathbf{p}^2 = \mathbf{M}^2 + 2\mathbf{p}\left(\gamma mc + \sigma mc\phi\right)\cdot\frac{\mathbf{k}}{k} - \left(\gamma mc + \sigma mc\phi\right)^2. \tag{3.28}$$

Using Eq. (3.27), we have

$$\begin{aligned}(\gamma mc+\sigma mc\phi)^2 &= (\gamma mc)^2+2\gamma m^2c^2\sigma\phi+(\sigma mc\phi)^2\\ &= m^2c^2+\mathbf{M}^2+2\mathbf{p}\left(\gamma mc+\sigma mc\phi\right)\cdot\frac{\mathbf{k}}{k}-\left(\gamma mc+\sigma mc\phi\right)^2\\ &\quad+2\gamma m^2c^2\sigma\phi+\left(mc\phi\right)^2. \end{aligned} \tag{3.29}$$

By collecting terms proportional to $\gamma mc+\sigma mc\phi$, we rewrite Eq (3.29) as

$$2\left(\gamma mc+\sigma mc\phi\right)\left(\gamma mc+\sigma mc\phi-\mathbf{p}\cdot\frac{\mathbf{k}}{k}-\sigma mc\phi\right)=m^2c^2+\mathbf{M}^2-\left(mc\phi\right)^2. \tag{3.30}$$

Then, using the relation

$$\begin{aligned}\gamma mc+\sigma mc\phi-\mathbf{p}\cdot\frac{\mathbf{k}}{k}-\sigma mc\phi &= -\left[\mathbf{p}-\left(\gamma mc+\sigma mc\phi\right)\frac{\mathbf{k}}{k}\right]\cdot\frac{\mathbf{k}}{k}-\sigma mc\phi\\ &= -\mathbf{M}\cdot\frac{\mathbf{k}}{k}-\sigma mc\phi, \end{aligned} \tag{3.31}$$

we see that $\gamma mc+\sigma mc\phi$ is expressed in terms of new coordinate variables as

$$\gamma mc+\sigma mc\phi=-\frac{m^2c^2+\mathbf{M}^2-\left(mc\phi\right)^2}{2\left[\frac{\mathbf{k}}{k}\cdot\mathbf{M}+\sigma mc\phi\right]}. \tag{3.32}$$

Therefore, the new coordinate and the corresponding covariant vector are given as

$$z^\mu=\left(\eta;x,y,z,M_x,M_y,M_z\right), \tag{3.33}$$

$$\gamma_\mu=\left(-K;\mathbf{M}+\sigma mc\left(\mathbf{a}-\frac{\mathbf{k}}{k}\phi\right),\mathbf{0}\right), \tag{3.34}$$

where $\mathbf{a}=\mathbf{a}\left(\mathbf{x},\eta\right)$, $\phi=\phi\left(\mathbf{x},\eta\right)$, and

$$K=-\frac{m^2c^2+\mathbf{M}^2-\left(mc\phi\right)^2}{2k\left(\frac{\mathbf{k}}{k}\cdot\mathbf{M}+\sigma mc\phi\right)}. \tag{3.35}$$

Note that the new relativistic Hamiltonian K has no square root owing to choosing η and p_η as coordinate variables simultaneously. This is also an advantage of this coordinate, because one of the reasons for complication of relativistic analyses is the Hamiltonian that has a square root dependence. Actually, in many analyses in relativistic beam physics, the square root is eliminated using an approximation, which we does not introduced in the present study [38, 39].

The Lagrange and Poisson tensors in this mechanical coordinate are obtained as

$$\omega_{kj} = \begin{pmatrix} \mathbf{\Omega} & -\mathbf{1} \\ \mathbf{1} & \mathbf{0} \end{pmatrix}, \quad J^{jk} = \begin{pmatrix} \mathbf{0} & \mathbf{1} \\ -\mathbf{1} & \mathbf{\Omega} \end{pmatrix}, \tag{3.36}$$

where

$$\mathbf{\Omega} = \begin{pmatrix} 0 & -(\partial_x a_y - \partial_y a_x) & -(\partial_x a_z - \partial_z a_x) \\ \partial_x a_y - \partial_y a_x & 0 & -(\partial_y a_z - \partial_z a_y) \\ \partial_x a_z - \partial_z a_x & \partial_y a_z - \partial_z a_y & 0 \end{pmatrix}. \tag{3.37}$$

Note that in a uniform field, $\mathbf{\Omega} = \mathbf{0}$ is obtained, so that the Lagrange and Poisson tensors become the same as those in canonical coordinates.

When we assume the laser wave vector $\mathbf{k} = (0, 0, k_z)$, Eqs. (3.33)-(3.35) yield

$$z^\mu = (\eta;\ x, y, z, p_x, p_y, p_\eta), \tag{3.38}$$

$$\gamma_\mu = (-K;\ \mathbf{p}_\perp + mc\sigma\mathbf{a}_\perp, p_\eta + \sigma mc\,(a_z - \phi)\,, 0, 0, 0)\,, \tag{3.39}$$

$$K = -\frac{m^2c^2 + \mathbf{p}_\perp^2 + p_\eta^2 - (mc\phi)^2}{2k_z\,(p_\eta + \sigma mc\phi)}, \tag{3.40}$$

where $p_\eta \equiv p_z - \gamma mc$, which is equivarent to M_z with $\mathbf{k} = k_z\hat{\mathbf{e}}_z$.

Summary of the feature of each coordinate

We summarize the feature of each coordinate given in this section. Note that we herein consider the case where the laser wave vector is in the z-direction, i.e., $\mathbf{k} = (0, 0, k_z)$.

(1)

$$z_c^\mu = (t; x, y, z, p_{cx}, p_{cy}, p_{cz})\,, \tag{3.41}$$

$$\gamma_{c\mu} = (-h(t, \mathbf{p}_c, \mathbf{x}); p_{cx}, p_{cy}, p_{cz}, 0, 0, 0)\,, \tag{3.42}$$

$$h(t, \mathbf{p}_c, \mathbf{x}) = \sqrt{m^2c^2 + (\mathbf{p}_c - mc\mathbf{a})^2} + \sigma mc^2\phi, \tag{3.43}$$

where $\mathbf{a} = \mathbf{a}(t, \mathbf{x})$ and $\phi = \phi\,(t, \mathbf{x})$.

Merit Canonical relation leads to a simple Lagrange tensor.

Demerit The independent variable is time t, which is not suitable for describing the particle motion oscillating with the period of phase $\eta = \omega t - k_z z\,(t)$. Namely, we cannot remove the η-period oscillations, so that this coordinate cannot be a base for the oscillation center coordinate.

(2)

$$w^\mu = (\eta; x, y, z, p_{cx}, p_{cy}, p_{cz}) , \tag{3.44}$$

$$\psi_\mu = \left(-H(\eta, \mathbf{p}_c, \mathbf{x}); p_{cx}, p_{cy}, p_{cz} - k_z^2 H(\eta, \mathbf{p}_c, \mathbf{x}), 0, 0, 0\right) , \tag{3.45}$$

$$H(\eta, \mathbf{p}_c, \mathbf{x}) = \frac{1}{k_z}\left(\sqrt{m^2c^2 + (\mathbf{p}_c - mc\mathbf{a})^2} + \sigma mc\phi\right) , \tag{3.46}$$

where $\mathbf{a} = \mathbf{a}(\eta, \mathbf{x})$ and $\phi = \phi(\eta, \mathbf{x})$.

Merit The independent variable η enables to remove oscillations of period η using further coordinate transformation; therefore, this coordinate can be a base for the oscillation center coordinate.

Demerit The Lagrange tensor has complicated non-orthogonal components due to ψ_3 that depends on many coordinate variables.

(3)

$$Z_c^\mu = (\eta; x, y, z, p_{cx}, p_{cy}, p_{c\eta}) , \tag{3.47}$$

$$\Gamma_{c\mu} = (-K_c(\eta, \mathbf{p}_{c\perp}, p_{c\eta}, \mathbf{x}); p_{cx}, p_{cy}, p_{c\eta} - \sigma mc\phi, 0, 0, 0) , \tag{3.48}$$

$$K_c(\eta, \mathbf{p}_{c\perp}, p_{c\eta}, \mathbf{x}) = -\frac{m^2c^2 + (\mathbf{p}_{c\perp} - mc\mathbf{a}_\perp)^2 + (p_{c\eta} - mca_z)^2 - (mc\phi)^2}{2k_z\left(p_{c\eta} - mca_z + \sigma mc\phi\right)}, \tag{3.49}$$

where $\mathbf{a} = \mathbf{a}(\eta, \mathbf{x})$ and $\phi = \phi(\eta, \mathbf{x})$.

Merit Canonical relation leads to a simple Lagrange tensor even in the coordinate whose independent variable is η. The square root in the Hamiltonian is removed without any approximation.

Demerit The equation of motion derived from the 1-form is not for the mechanical momentum, but for the canonical one, from which a force to the particle is not obtained directly.

(4)

$$z^\mu = (\eta; x, y, z, p_x, p_y, p_\eta) , \tag{3.50}$$

$$\gamma_\mu = (-K(\eta, \mathbf{p}_{c\perp}, p_{c\eta}, \mathbf{x}); \mathbf{p}_\perp + \sigma mca_\perp, p_\eta + \sigma mc\left(a_z - \phi\right), 0, 0, 0) , \tag{3.51}$$

$$K(\eta, \mathbf{p}_\perp, p_\eta) = -\frac{m^2c^2 + \mathbf{p}_\perp^2 + p_\eta^2 - (mc\phi)^2}{2k_z\left(p_\eta + \sigma mc\phi\right)}. \tag{3.52}$$

where $\mathbf{a} = \mathbf{a}(\eta, \mathbf{x})$ and $\phi = \phi(\eta, \mathbf{x})$.

Merit A force to the particle can be obtained directly from the variational principle in this mechanical coordinate. Although the Lagrange tensor has non-orthogonal components, those in the uniform field are same as the simple canonical ones, i.e., the non-orthogonal components equal to zero; this means that the above coordinate is suitable to be used for the perturbation analysis, in which the perturbation is taken on the basis of the uniform field.

3.1.2 Particle motion in a uniform laser field

In the following analysis, we assume a laser field given by

$$\mathbf{a} = a_x(x)\sin\eta\ \hat{\mathbf{e}}_x. \tag{3.53}$$

where $\mathbf{k} = (0, 0, k_z)$ and then $\eta = \omega t - k_z z$. In this case, the noncanonical 1-form yields

$$z^\mu = (\eta; x, y, z, p_x, p_y, p_\eta) \tag{3.54}$$

$$\gamma_\mu = \left(\frac{1}{2p_\eta k_z}\left(m^2c^2 + p_x^2 + p_y^2 + p_\eta^2\right); p_x + mc\sigma a_x(x)\sin\eta, p_y, p_\eta - \sigma mc\phi, 0, 0, 0\right) \tag{3.55}$$

Firstly, before proceed to the perturbation analysis considering spatially nonuniform laser field, we derive the unperturbed motion of the particle on the basis of the 1-form given above. Here, we suppose a quasineutral plasma and assume the scalar potential ϕ to be a perturbation due to the charge separation. Hence, the *unperturbed* motion in our definition is the particle motion irradiated by the spatially uniform laser field with no background electrostatic potential.

In such a unperturbed situation, the unperturbed (zeroth order) 1-form is given by

$$z^\mu = (\eta; x, y, z, p_x, p_y, p_\eta) \tag{3.56}$$

$$\gamma_\mu^{(0)} = \left(\frac{1}{2p_\eta k_z}\left(m^2c^2 + p_x^2 + p_y^2 + p_\eta^2\right); p_x + mc\sigma a_x(X)\sin\eta, p_y, p_\eta, 0, 0, 0\right), \tag{3.57}$$

where we treat $a_x(X)$ as a constant assuming a spatially uniform laser field. The equations of motion are derived from the above 1-form as

$$\frac{dx}{d\eta} = J^{(0)14}\left(\frac{\partial\gamma_4^{(0)}}{\partial\eta} - \frac{\partial\gamma_0^{(0)}}{\partial p_x}\right) = -\frac{p_x}{p_\eta k_z} \tag{3.58}$$

$$\frac{dy}{d\eta} = J^{(0)25}\left(\frac{\partial\gamma_5^{(0)}}{\partial\eta} - \frac{\partial\gamma_0^{(0)}}{\partial p_y}\right) = -\frac{p_y}{p_\eta k_z} \tag{3.59}$$

$$\frac{dz}{d\eta} = J^{(0)36}\left(\frac{\partial\gamma_6^{(0)}}{\partial\eta} - \frac{\partial\gamma_0^{(0)}}{\partial p_\eta}\right) = \frac{1}{2p_\eta^2 k_z}\left(m^2c^2 + p_x^2 + p_y^2 - p_\eta^2\right) \tag{3.60}$$

$$\frac{dp_x}{d\eta} = J^{(0)41}\left(\frac{\partial\gamma_1^{(0)}}{\partial\eta} - \frac{\partial\gamma_0^{(0)}}{\partial x}\right) = -mc\sigma a_x(X)\cos\eta \tag{3.61}$$

$$\frac{dp_y}{d\eta} = J^{(0)52}\left(\frac{\partial\gamma_2^{(0)}}{\partial\eta} - \frac{\partial\gamma_0^{(0)}}{\partial y}\right) = 0 \tag{3.62}$$

$$\frac{dp_\eta}{d\eta} = J^{(0)63}\left(\frac{\partial\gamma_3^{(0)}}{\partial\eta} - \frac{\partial\gamma_0^{(0)}}{\partial z}\right) = 0, \tag{3.63}$$

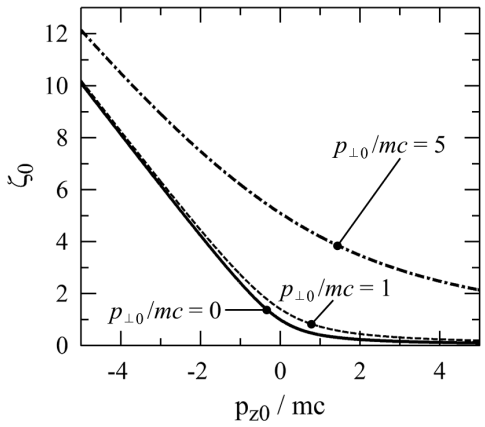

Figure 3.2: Plot of ζ_0 as a function of the initial parallel momentum p_{z0} for different initial transverse momenta $p_{\perp 0}$.

where the Poisson tensor obtained from Eqs. (3.56) and (3.57) is given by

$$\mathbf{J}^{(0)} = \begin{pmatrix} \mathbf{0} & \mathbf{1} \\ -\mathbf{1} & \mathbf{0} \end{pmatrix}. \tag{3.64}$$

These equations lead to the well-known figure-eight motion in the uniform linear polarized laser field,

$$x = \sigma l(X)\,(\cos\eta - 1) + x_0 \tag{3.65}$$
$$y = y_0 \tag{3.66}$$
$$z = \frac{1-\zeta_0^2}{2\zeta_0^2 k_z}\eta + \frac{k_z l^2(X)}{4}\left(\eta - \frac{1}{2}\sin 2\eta\right) \tag{3.67}$$
$$p_x = -mc\sigma a_x(X)\sin\eta \tag{3.68}$$
$$p_y = 0 \tag{3.69}$$
$$p_\eta = -mc\zeta_0, \tag{3.70}$$

where $l(X) \equiv a_x(X)/k_z\zeta_0$ is the excursion length, and ζ_0 is a constant depending on the initial condition defined by $\zeta_0 \equiv \gamma_0 - p_{z0}/mc$. We plot ζ_0 in Fig. 3.2 as a function of the initial parallel momentum p_{z0} for different three initial transverse momenta $p_{\perp 0}$. The figure-eight orbit described by Eqs. (3.65)-(3.67) is shown in Fig. 3.3 where η ranges from 0 to 20 in the normalized x-z plane. The left and right figures correspond to orbits in the laboratory frame and average rest frame, respectively, where the latter is an inertial frame that moves in the z direction with the same velocity as the drift motion of the particle. Here, we assume $a_0 = 1$ and 2 and initial condition for the particle $(\mathbf{x}, \mathbf{p}) = (\mathbf{0}, \mathbf{0})$ in the laboratory frame.

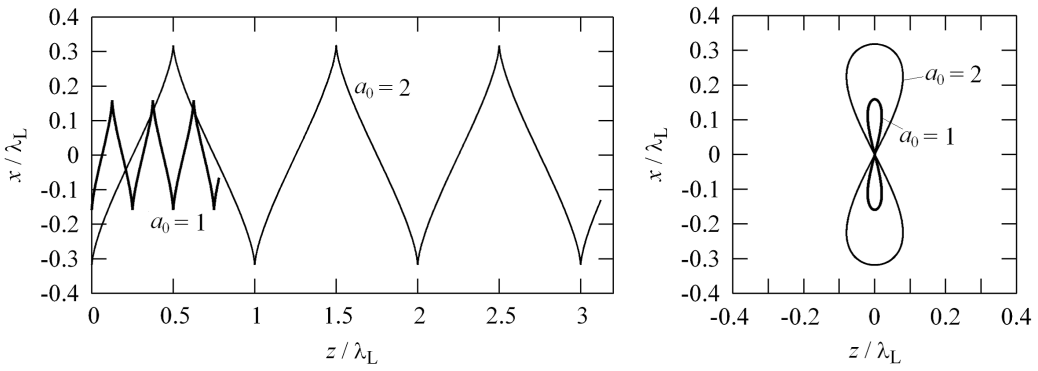

Figure 3.3: Figure-eight orbit in the uniform laser field with linear polarization for $a_0 = 1$ and 2 in the laboratory frame (left) and average rest frame (right). Here, η ranges from 0 to 20. The initial condition for the particle is set to be $(\mathbf{x}, \mathbf{p}) = (\mathbf{0}, \mathbf{0})$.

3.1.3 Transformation to the oscillation center coordinates

Now, based on the zeroth order figure-eight motion obtained above, we transform coordinates from Eq. (3.54) to those of an oscillation center,

$$Z^\mu = (\eta; X, Y, Z, P_x, P_y, p_\eta)\,. \tag{3.71}$$

The relation between the old and new coordinates is defined as

$$x\,(X,\eta) = X + \delta_x \tilde{x}^{(0)} = X + \delta_x \sigma l(X)\cos\eta, \tag{3.72}$$
$$y\,(Y) = Y, \tag{3.73}$$
$$z\,(Z,X,\eta) = Z + \delta_z \tilde{z}^{(0)} = Z - \delta_z \frac{k_z l^2(X)}{8}\sin 2\eta, \tag{3.74}$$
$$p_x\,(X,P_x,\eta) = P_x + \delta_x \tilde{p}_x^{(0)} = P_x - \delta_x \sigma m c a_x(X)\sin\eta, \tag{3.75}$$
$$p_y\,(P_y) = P_y, \tag{3.76}$$
$$p_\eta\,(p_\eta) = p_\eta, \tag{3.77}$$

Here, we mark the transformation using symbols δ_x and δ_z. We can take $\delta_x = \delta_z = 1$ for usual transformation to the oscillation center. The new covariant vector is obtained as

$$\begin{aligned}
\Gamma_0 &= \gamma_0 \frac{\partial z^0}{\partial Z^0} + \gamma_1 \frac{\partial z^1}{\partial Z^0} + \gamma_3 \frac{\partial z^3}{\partial Z^0} \\
&= \frac{m^2c^2 + P_x^2 + p_\eta^2}{2p_\eta k_z} - \delta_x\,(1+\alpha)\,P_x l(X)\sin\eta \\
&\quad - \delta_x \frac{mc}{2} l(X)\,(a_x(x) - \delta_x a_x(X))\,(1-\cos 2\eta) \\
&\quad + \delta_x^2\alpha^2 \frac{p_\eta k_z l^2(X)}{4} - \frac{p_\eta k_z l^2(X)}{4}\left(\delta_z + \delta_x^2\alpha^2\right)\cos 2\eta,
\end{aligned} \tag{3.78}$$

$$\begin{aligned}\Gamma_1 &= \gamma_1 \frac{\partial z^1}{\partial Z^1} + \gamma_3 \frac{\partial z^3}{\partial Z^1} \\ &= P_x + mc\sigma \left(a_x(x) - \delta_x a_x(X)\right) \sin\eta + \delta_x P_x \sigma \frac{\partial l}{\partial X} \cos\eta \\ &\quad + \delta_x \frac{mc}{2} \frac{\partial l}{\partial X} \left(a_x(x) - \delta_x a_x(X)\right) \sin 2\eta - \delta_z \frac{p_\eta k_z l(X)}{4} \frac{\partial l}{\partial X} \sin 2\eta, \end{aligned} \tag{3.79}$$

$$\Gamma_3 = \gamma_3 \frac{\partial z^3}{\partial Z^3} = p_\eta, \tag{3.80}$$

and $\Gamma_2 = P_y$ and $\Gamma_4 = \Gamma_5 = \Gamma_6 = 0$. Note that we hereafter express $a_x(X)$ and $l(X)$ without representing the variable dependence explicitly as a_x and l for simplicity.

3.2 Lie perturbation analysis

3.2.1 Definition of the expansion parameter

In this study, we expand $a_x(x)$ in Eq. (3.53) around the oscillation center $x = X$ as

$$a_x(x) = a_x(X)\left[1 + \epsilon\frac{(X-x)}{L} + \epsilon^2\frac{(X-x)^2}{2!R} + \epsilon^3\frac{(X-x)^3}{3!T} + \cdots\right], \tag{3.81}$$

where the expansion parameters are defined by

$$L^{-1} = L^{-1}(X) \equiv \frac{1}{a_x(X)}\frac{\partial a_x(X)}{\partial X}, \tag{3.82}$$

$$R^{-1} = R^{-1}(X) \equiv \frac{1}{a_x(X)}\frac{\partial^2 a_x(X)}{\partial X^2}, \tag{3.83}$$

$$T^{-1} = T^{-1}(X) \equiv \frac{1}{a_x(X)}\frac{\partial^3 a_x(X)}{\partial X^3}. \tag{3.84}$$

Therefore, L^{-1} and R^{-1} denote the gradient and curvature of the field amplitude, and T^{-1} the variation of curvature, respectively, that are evaluated at the oscillation center X. In the expansion Eq. (3.81), the orderings are defined as

$$\frac{l}{L} = \mathscr{O}(\epsilon), \frac{l^2}{R} = \mathscr{O}\left(\epsilon^2\right), \frac{l^3}{T} = \mathscr{O}\left(\epsilon^3\right). \tag{3.85}$$

Note that to satisfy the Maxwell equations, the electromagnetic field in vacuum with such a varying amplitude has a z component a_z and also the perpendicular component of the wave vector, $\mathbf{k}_\perp$; however, we neglect them in the present frame work for simplicity. In Appendix C, we consider the inclusion of a_z, which is found not to affect the nonlocal effect of the ponderomotive force derived in this study up to the third order of ϵ.

3.2.2 Zeroth order analysis

Here, we at first consider the oscillation center equations of motion that are derived from the zeroth order component of the covariant vector Γ_μ given by

$$\begin{aligned}\Gamma_\mu^{(0)} = \Bigg(&\frac{m^2c^2 + P_x^2 + p_\eta^2}{2p_\eta k_z} - \delta_x(1+\alpha)P_x l(X)\sigma\sin\eta + \delta_x^2\alpha^2\frac{p_\eta k_z l^2(X)}{4} \\ &- \frac{p_\eta k_z l^2(X)}{4}\left(\delta_z + \delta_x^2\alpha^2\right)\cos 2\eta - \alpha p_\eta\frac{k_z l^2}{2}(1-\delta_x)(1-\cos 2\eta) \\ &; P_x + \alpha p_\eta\sigma k_z l(1-\delta_x)\sin\eta, P_y, p_\eta, 0, 0, 0\Bigg).\end{aligned} \tag{3.86}$$

The equations of motion derived from the zeroth-order 1-form are obtained as

$$\frac{dX}{d\eta} = J^{14}\left(\frac{\partial\Gamma_4}{\partial\eta} - \frac{\partial\Gamma_0}{\partial P_x}\right) = -\frac{P_x}{p_\eta k_z} + \delta_x\sigma l\,(1+\alpha)\sin\eta, \tag{3.87}$$

$$\frac{dX}{d\eta} = J^{25}\left(\frac{\partial\Gamma_5}{\partial\eta} - \frac{\partial\Gamma_0}{\partial P_y}\right) = -\frac{P_y}{p_\eta k_z}, \tag{3.88}$$

$$\begin{aligned}\frac{dZ}{d\eta} &= J^{36}\left(\frac{\partial\Gamma_6}{\partial\eta} - \frac{\partial\Gamma_0}{\partial p_\eta}\right)\\ &= \frac{m^2c^2 + P_x^2 + P_y^2 - p_\eta^2}{2p_\eta^2 k_z} + \delta_x^2\frac{k_z l^2}{4}\alpha^2 - \delta_x\frac{P_x}{p_\eta}\sigma l\alpha\sin\eta\\ &\quad - \frac{k_z l^2}{4}\left(-\delta_z + \delta_x^2\alpha^2\right)\cos 2\eta,\end{aligned} \tag{3.89}$$

$$\begin{aligned}\frac{dP_x}{d\eta} &= J^{41}\left(\frac{\partial\Gamma_1}{\partial\eta} - \frac{\partial\Gamma_0}{\partial X}\right)\\ &= \epsilon\delta_x^2\alpha^2\frac{p_\eta k_z l}{2}\frac{l}{L} - \epsilon\delta_x P_x\sigma\frac{l}{L}(1+\alpha)\sin\eta\\ &\quad - \epsilon\frac{p_\eta k_z l}{2}\frac{l}{L}\left(\delta_z + \delta_x^2\alpha^2\right)\cos 2\eta\\ &\quad - \epsilon\alpha p_\eta k_z l\frac{l}{L}(1-\delta_x)(1-\cos 2\eta) - \alpha p_\eta k_z l\,(1-\delta_x)\cos\eta,\end{aligned} \tag{3.90}$$

$$\frac{dP_x}{d\eta} = J^{52}\left(\frac{\partial\Gamma_2}{\partial\eta} - \frac{\partial\Gamma_0}{\partial Y}\right) = 0, \tag{3.91}$$

$$\frac{dp_\eta}{d\eta} = J^{63}\left(\frac{\partial\Gamma_3}{\partial\eta} - \frac{\partial\Gamma_0}{\partial Z}\right) = 0. \tag{3.92}$$

As seen from Eq. (3.90), the zeroth order 1-form leads to the equation of motion not only in the order of ϵ^0 but also of ϵ^1. The latter results from the X derivative of the covariant vector, which appears in the RHS in the first line of Eq. (3.90). From this fact, the general relation can be obtained as follows: The nth order 1-form leads to the equation of motion in the order of ϵ^n and ϵ^{n+1}. The solution for Eq. (3.92) can be obtained as

$$p_\eta = -mc\zeta_0 \quad (\Leftrightarrow 1+\alpha = 0)\,. \tag{3.93}$$

By substituting the solution Eq. (3.117), we reduce the equations of motion as

$$\frac{dX}{d\eta} = \frac{P_x}{mc\zeta_0 k_z}, \tag{3.94}$$

$$\begin{aligned}\frac{dP_x}{d\eta} &= -\epsilon\frac{mca_x}{2}\frac{l}{L} + \epsilon\frac{mca_x}{2}\frac{l}{L}\left(\delta_z + \delta_x^2\alpha^2\right)\cos 2\eta\\ &\quad - \epsilon mc\zeta_0 k_z l\frac{l}{L}(1-\delta_x)(1-\cos 2\eta) - mc\sigma a_x\,(1-\delta_x)\cos\eta,\end{aligned} \tag{3.95}$$

$$\frac{dZ}{d\eta} = \frac{1-\zeta_0^2}{2\zeta_0^2 k_z} + \frac{k_z l^2}{4} + \frac{1}{2k_z}\left(\frac{P_x}{mc\zeta_0}\right)^2 - \delta_x\frac{P_x}{mc\zeta_0}\sigma l\sin\eta + \frac{k_z l^2}{4}(\delta_z - 1)\cos 2\eta. \tag{3.96}$$

Here, we notice that Eqs. (3.95) and (3.96) include oscillatory terms which is not suitable to describe the oscillation center motion. Especially, it is necessary to remove the oscillatory term appearing in Eq. (3.95) reminding that our purpose is to derive an equation system that describes the averaged motion in the x direction, i.e., the direction of the ponderomotive force.

One possible way is to utilize the degree of freedom of the noncanonical coordinate transformation. Namely, we can choose δ_x and δ_z to those remove oscillations. Firstly, we set $\delta_x = 1$ as usual oscillation center transformation so that the unnecessary oscillations in the X direction can be eliminated, and then Eqs. (3.94) and (3.95) yield to

$$\frac{dX}{d\eta} = \frac{P_x}{mc\zeta_0 k_z}, \tag{3.97}$$

$$\frac{dP_x}{d\eta} = -\epsilon\frac{mca_x}{2}\frac{l}{L} + \epsilon\frac{mca_x}{2}\frac{l}{L}\left(\delta_z + 1\right)\cos 2\eta. \tag{3.98}$$

The first term on the RHS of Eq. (3.98) corresponds to the first order transverse ponderomotive force. The remaining oscillation in Eq. (3.98) can also be removed in a similar way assuming $\delta_z = -1$. We note that in this case, the coordinate Z is not equivalent to the oscillation center variable. As an alternative, we found that a preparatory gauge transformation $\Gamma_\mu \mapsto \Gamma_\mu + \partial_\mu S$ can be utilized to remove the oscillation without changing the meaning of the oscillation center variables. Relation between the usage of $\delta_z = -1$ and the gauge transformation is discussed in Appendix B.

In the following analysis, we choose to utilize a preratatory gauge transformation assuming the oscillation center relation $\delta_z = 1$ in removing the oscillation appeared in Eq. (3.95).

3.2.3 Gauge transformation to remove oscillations

Here, we introduce a gauge function S for the removal of the oscillation as

$$S = p_\eta \frac{k_z l^2}{8}\left(1 + \alpha^2\right)\sin 2\eta. \tag{3.99}$$

Partial derivatives of S is calculated as

$$\partial_0 S = p_\eta \frac{k_z l^2}{4}\left(1 + \alpha^2\right)\cos 2\eta, \tag{3.100}$$

$$\partial_1 S = p_\eta \frac{k_z l}{4}\frac{l}{L}\left(1 + \alpha^2\right)\sin 2\eta, \tag{3.101}$$

$$\partial_6 S = p_\eta \frac{k_z l^2}{8}\left(1 - \alpha^2\right)\sin 2\eta, \tag{3.102}$$

and $\partial_2 S = \partial_3 S = \partial_4 S = 0$. Then, the covariant vector Γ_μ after the gauge transformation is given by

$$\Gamma_0 = \frac{m^2c^2 + P_x^2 + P_y^2 + p_\eta^2}{2p_\eta k_z} - (1+\alpha)\,\sigma P_x l(X)\sin\eta + \alpha^2\frac{p_\eta k_z l^2(X)}{4} - \frac{mc}{2}l(X)\left(a_x(x) - a_x(X)\right)(1-\cos 2\eta)\,, \tag{3.103}$$

$$\Gamma_1 = P_x + P_x\sigma\frac{l}{L}\bigg|_X\cos\eta + \frac{p_\eta k_z l(X)}{4}\frac{l}{L}\bigg|_X\alpha^2\sin 2\eta + mc\sigma\left(a_x(x) - a_x(X)\right)\sin\eta + \frac{mc}{2}\frac{l}{L}\bigg|_X\left(a_x(x) - a_x(X)\right)\sin 2\eta, \tag{3.104}$$

$$\left(\Gamma_2, \Gamma_3, \Gamma_4, \Gamma_5\right) = \left(P_y, p_\eta, 0, 0\right), \tag{3.105}$$

$$\Gamma_6 = \frac{k_z l^2}{8}\left(1-\alpha^2\right)\sin 2\eta. \tag{3.106}$$

In Eq. (3.103), one can see that the oscillatory term that causes a first order oscillation in Eq. (3.95) has now been removed. Therefore, we employ the 1-form given by the coordinates Eq. (3.71) and the covariant vector Eqs. (3.103)-(3.106) as the base for the Lie perturbation analysis in the following.

3.2.3.1 Fundamental one-form

The zeroth-order component of the covariant vector Γ_μ after the gauge transformation is given by

$$\Gamma_\mu^{(0)} = \Bigg(\frac{m^2c^2 + P_x^2 + p_\eta^2}{2p_\eta k_z} - (1+\alpha)\,P_x l(X)\sigma\sin\eta + \alpha^2\frac{p_\eta k_z l^2(X)}{4} ; P_x, P_y, p_\eta, 0, 0, \frac{k_z l^2}{8}\left(1-\alpha^2\right)\sin 2\eta\Bigg). \tag{3.107}$$

In this coordinate, because of the sixth component $\Gamma_6^{(0)}$ appears due to the gauge transformation procedure $\Gamma_6 \mapsto \Gamma_6 + \partial_6 S$, the Lagrange tensor calculated from the 0th-order 1-form now has a off-diagonal component

$$\omega_{61} = \frac{\Gamma_1}{Z^6} - \frac{\Gamma_6}{Z^1} = -\epsilon\frac{k_z l}{4}\frac{l}{L}\left(1-\alpha^2\right)\sin 2\eta. \tag{3.108}$$

Then, the Poisson tensor $\mathbf{J}$ calculated from the 0th-order 1-form is given by

$$\mathbf{J}^{(0)} = \begin{pmatrix} \mathbf{0} & \mathbf{\Omega} \\ -{}^t\mathbf{\Omega} & \mathbf{0} \end{pmatrix}; \quad \mathbf{\Omega} = \begin{pmatrix} 1 & 0 & 0 \\ 0 & 1 & 0 \\ -\omega_{61} & 0 & 1 \end{pmatrix}. \tag{3.109}$$

3.2.3.2 Equation of motion: The first order ponderomotive force

The equations of motion derived from the zeroth-order 1-form are obtained from

$$\frac{dX}{d\eta} = -\frac{\partial \Gamma_0}{\partial P_x}, \tag{3.110}$$

$$\frac{dY}{d\eta} = -\frac{\partial \Gamma_0}{\partial P_y}, \tag{3.111}$$

$$\frac{dZ}{d\eta} = \omega_{61}\frac{\partial \Gamma_0}{\partial P_x} + \left(\frac{\partial \Gamma_6}{\partial \eta} - \frac{\partial \Gamma_0}{\partial p_\eta}\right), \tag{3.112}$$

$$\frac{dP_x}{d\eta} = -\left(\frac{\partial \Gamma_1}{\partial \eta} - \frac{\partial \Gamma_0}{\partial X}\right), \tag{3.113}$$

$$\frac{dP_y}{d\eta} = 0, \tag{3.114}$$

$$\frac{dp_\eta}{d\eta} = 0, \tag{3.115}$$

From Eqs. (3.115) and (3.114), one can easily obtain the solution

$$P_y = 0, \tag{3.116}$$

$$p_\eta = -mc\zeta_0 \quad (\Leftrightarrow 1 + \alpha = 0)\,. \tag{3.117}$$

By substituting the solutions Eqs. (3.116) and (3.117), we have the reduced equations of motion,

$$\frac{dX}{d\eta} = \frac{P_x}{mc\zeta_0 k_z}, \tag{3.118}$$

$$\frac{dP_x}{d\eta} = -\epsilon\frac{mca_x}{2}\frac{l}{L}. \tag{3.119}$$

and $dY/d\eta = 0$ for the transverse directions and

$$\frac{dZ}{d\eta} = \frac{1-\zeta_0^2}{2\zeta_0^2 k_z} + \frac{k_z l^2}{4} + \frac{1}{2k_z}\left(\frac{P_x}{mc\zeta_0}\right)^2 - \frac{P_x}{mc\zeta_0}\sigma l \sin\eta, \tag{3.120}$$

for the Z direction, respectively. The RHS of Eq. (3.119) corresponds to the first order transverse ponderomotive force which is consistent with that obtained by the averaging method [21, 22, 40]. Note that the oscillatory term appeared in Eq. (3.95) is removed successfully owing to the gauge transformation. Combining Eqs. (3.118) and (3.119), we have

$$\frac{d^2X}{d\eta^2} = -\epsilon\frac{l}{2}\frac{l}{L}, \tag{3.121}$$

which we refer to as the first order ponderomotive formula derived by the Lie perturbation method. In the Z direction, secular terms in Eq. (3.120) correspond to the drift motion caused by the light momentum, or in other words, the averaged $\mathbf{v} \times \mathbf{B}$ motion.

3.2.4 First order analysis

3.2.4.1 Fundamental one-form

The first-order component of the covariant vector Γ_μ is given by

$$\Gamma_\mu^{(1)} = \Bigg(-\frac{p_\eta k_z l^2}{4}\alpha\sigma\frac{l}{L}\left(\cos\eta - \cos 3\eta\right); \\ \frac{p_\eta k_z l}{2}\frac{l}{L}\left(\alpha + \frac{\alpha^2}{2}\right)\sin 2\eta + P_x\sigma\frac{l}{L}\cos\eta, 0, 0, 0, 0, 0\Bigg) = C_\mu^{(1)}. \quad (3.122)$$

We execute the first order Lie transformation $Z^\mu \mapsto Z'^\mu = \exp\left(\epsilon\mathscr{L}^{(1)}\right) Z^\mu$. The covariant vector is transformed to Γ'_μ, where

$$\Gamma_0'^{(1)} = \overline{C_\mu^{(1)}\left(V^{(0)\mu}\right)^{(0)}} = 0, \quad (3.123)$$

and $\Gamma_i'^{(1)} = 0$ $(i = 1, 2, \cdots, 6)$. Therefore, 1-form up to the first order of ϵ, i.e., $\Gamma'_\mu dZ'^\mu$, has the same functional form as that of the zeroth order, $\Gamma_\mu^{(0)} dZ^\mu$.

3.2.4.2 Lie generator and gauge function

The first-order gauge function $S^{(1)}$ is given by the relation

$$\frac{\partial S^{(1)}}{\partial\eta} = -\left[C_\mu^{(1)}\left(V^{(0)\mu}\right)^{(0)}\right]_{\text{os.}}, \quad (3.124)$$

as

$$S^{(1)} = -\frac{p_\eta k_z l^2}{8}\sigma\frac{l}{L}\left(3\alpha^2 + \alpha^3\right)\left(\sin\eta - \frac{1}{3}\sin 3\eta\right) \\ + \frac{P_x l}{4}\left(1 - \frac{\alpha^2}{2}\right)\frac{l}{L}\cos 2\eta + \frac{P_x^2}{p_\eta k_z}\sigma\frac{l}{L}\sin\eta. \quad (3.125)$$

The generator of the 1st-order Lie transformation is obtained from the relations

$$g^{(1)1} = \left(\frac{\partial S^{(1)}}{\partial Z^4}\right)^{(1)} J^{(0)41} = -\left(\frac{\partial S^{(1)}}{\partial P_x}\right)^{(1)}, \quad (3.126)$$

$$g^{(1)3} = \left(\frac{\partial S^{(1)}}{\partial Z^6}\right)^{(1)} J^{(0)63} = -\left(\frac{\partial S^{(1)}}{\partial p_\eta}\right)^{(1)}, \quad (3.127)$$

$$g^{(1)4} = C_1^{(1)} J^{(0)14} = C_1^{(1)}, \quad (3.128)$$

$$g^{(1)2} = g^{(1)5} = g^{(1)6} = 0. \quad (3.129)$$

as follows:

$$g^{(1)1} = -\frac{1}{4}\left(1-\frac{\alpha^2}{2}\right) l\frac{l}{L}\cos 2\eta - \frac{2P_x}{p_\eta k_z}\sigma\frac{l}{L}\sin\eta, \tag{3.130}$$

$$g^{(1)3} = -\frac{k_z l^2}{8}\sigma\frac{l}{L}\alpha^2\left(3+2\alpha\right)\left(\sin\eta - \frac{1}{3}\sin 3\eta\right) + \frac{P_x^2}{p_\eta^2 k_z}\sigma\frac{l}{L}\sin\eta - \frac{P_x l}{4p_\eta}\frac{l}{L}\alpha^2\cos 2\eta, \tag{3.131}$$

$$g^{(1)4} = \frac{p_\eta k_z l}{2}\frac{l}{L}\left(\alpha+\frac{\alpha^2}{2}\right)\sin 2\eta + P_x\sigma\frac{l}{L}\cos\eta, \tag{3.132}$$

$$g^{(1)2} = g^{(1)5} = g^{(1)6} = 0. \tag{3.133}$$

From Eqs. (3.130)-(3.133), we see that the backward Lie transformation $\mathscr{G}_{\mathrm{b}}^{\mu}(\cdot) = \left(1-\epsilon L^{(1)}\right)\mathscr{I}^{\mu}(\cdot) = \mathscr{I}^{\mu}(\cdot) - \epsilon g^{(1)\mu}(\cdot)$ adds only oscillatory terms to the solution in the Lie transformed coordonate Z'^{μ}.

Here, we note that the terms added by the backward transformation correspond to increase/decrease of the figure-eight oscillation in the uniform field. Assuming that the field amplitude $a_x(x)$ and then the excursion length $l(x)$ have a linear dependence on x, i.e., $l(x) \propto a_x(x) \propto \pm a_0 x; a_0 = \text{const.}$, we obtain

$$g^{(1)1} \sim -\frac{1}{8}a_0^2 x\cos 2\eta. \tag{3.134}$$

By substituting the figure-eight oscillation $x = \sigma l\cos\eta$ in the RHS, we have the relation

$$g^{(1)1} \propto \mp\sigma l\cos\eta\cos 2\eta = \mp\frac{1}{2}\sigma l\left(\cos 3\eta + \cos\eta\right), \tag{3.135}$$

from which it is seen that the original figure-eight motion $x = \sigma l\cos\eta$ is increased/decreased depending on the sign of the field gradient.

3.2.5 Second order analysis

3.2.5.1 Fundamental one-form

The second-order component of the covariant vector Γ_μ is given by

$$\Gamma_\mu^{(2)} = \Bigg(-\frac{p_\eta}{16}k_z l^2\alpha\frac{l^2}{R}\left(1-\cos 4\eta\right) ; \frac{p_\eta k_z l}{8}\alpha\sigma\left(\frac{l^2}{R}+2\frac{l^2}{L^2}\right)\left(\sin 3\eta+\sin\eta\right), 0, 0, 0, 0, 0\Bigg). \tag{3.136}$$

Γ_0'' in the Lie-transformed coordinate is calculated from the relation

$$\Gamma_0^{\prime\prime(2)} = \overline{D_\mu^{(2)} \left(V^{(0)\mu}\right)^{(0)}}, \tag{3.137}$$

where

$$D_\mu^{(2)} = \Gamma_\mu^{(2)} - \left(L^{(1)}\Gamma_\mu^{(1)}\right)^{(2)} + \frac{1}{2}\left(L^{(1)2}\Gamma_\mu^{(0)}\right)^{(2)} - \left(L^{(1)}\Gamma_\mu^{(0)}\right)^{(2)} + \left(\partial_\mu S^{(1)}\right)^{(2)}. \tag{3.138}$$

After some algebra and averaging procedures, we finally obtain

$$\begin{aligned}\Gamma_0^{\prime\prime(2)} = -\frac{p_\eta'' k_z l^2}{16}\Bigg[&\alpha\frac{l^2}{R} + \left(\alpha + \frac{\alpha^2}{2} - \frac{\alpha^3}{2} - \frac{\alpha^4}{4}\right)\frac{l^2}{L^2} \\ &+ (1+\alpha)\left\{\left(\alpha^3 + 3\alpha^2 - \alpha\right)\frac{l^2}{R} + \left(2\alpha^3 + \frac{13}{2}\alpha^2 - \alpha\right)\frac{l^2}{L^2}\right\}\Bigg] \\ &+ \frac{P_x^{\prime\prime 2}}{2p_\eta'' k_z}\left[(1+\alpha)\frac{l^2}{R} - \left(2\alpha + \frac{1}{2}\right)\frac{l^2}{L^2}\right].\end{aligned} \tag{3.139}$$

Therefore, the 1-form up to the second-order in the Lie-transformed coordinate is found to be

$$Z^{\prime\prime\mu} = \left(\eta; X'', Y'', Z'', P_x'', P_y'', p_\eta''\right) \tag{3.140}$$

$$\begin{aligned}\Gamma_\mu'' = \Bigg(&\frac{m^2c^2 + P_x^{\prime\prime 2} + P_y^{\prime\prime 2} + p_\eta^{\prime\prime 2}}{2p_\eta'' k_z} - (1+\alpha)P_x''\sigma l\sin\eta + \frac{p_\eta'' k_z l^2}{4}\alpha^2 \\ &- \epsilon^2\frac{p_\eta'' k_z l^2}{16}\Bigg[\alpha\frac{l^2}{R} + \left(\alpha + \frac{\alpha^2}{2} - \frac{\alpha^3}{2} - \frac{\alpha^4}{4}\right)\frac{l^2}{L^2} \\ &+ (1+\alpha)\left\{\left(\alpha^3 + 3\alpha^2 - \alpha\right)\frac{l^2}{R} + \left(2\alpha^3 + \frac{13}{2}\alpha^2 - \alpha\right)\frac{l^2}{L^2}\right\}\Bigg] \\ &+ \epsilon^2\frac{P_x^{\prime\prime 2}}{2p_\eta'' k_z}\left[(1+\alpha)\frac{l^2}{R} - \left(2\alpha + \frac{1}{2}\right)\frac{l^2}{L^2}\right] \\ &; P_x'', P_y'', p_\eta'', 0, 0, \frac{k_z l^2}{8}\left(1-\alpha^2\right)\sin 2\eta\Bigg),\end{aligned} \tag{3.141}$$

3.2.5.2 Equation of motion: The third order ponderomotive force

The equation of motion for the 6th component is derived from the above 1-form as

$$\frac{dp_\eta''}{d\eta} = J^{63}\left(\frac{\partial\Gamma_3''}{\partial\eta} - \frac{\partial\Gamma_0''}{\partial Z''}\right) = 0. \tag{3.142}$$

Here, by using the solution $p_\eta'' = -mc\zeta_0 \Leftrightarrow 1+\alpha = 0$, we can reduce the covariant

vector Eq. (3.141) as

$$\Gamma''_{\mu}\Big|_{1+\alpha=0} = \left(\frac{m^2c^2 + P_x''^2 + P_y''^2 + p_\eta''^2}{2p''_\eta k_z} + \frac{p''_\eta k_z l^2}{4} + \epsilon^2 \frac{l}{16} p''_\eta k_z l \left(\frac{l^2}{R} + \frac{1}{4}\frac{l^2}{L^2} \right) + \epsilon^2 \frac{3}{4} \frac{P_x''^2}{p''_\eta k_z} \frac{l^2}{L^2}; P''_x, P''_y, p''_\eta, 0, 0, 0 \right). \tag{3.143}$$

This covariant vector leads to the reduced equations of motion in the X-direction given by

$$\frac{dX''}{d\eta} = \frac{P''_x}{mc\zeta_0 k_z} \left(1 + \epsilon^2 \frac{3}{2} \frac{l^2}{L^2} \right), \tag{3.144}$$

$$\frac{dP''_x}{d\eta} = -\epsilon \frac{mca_x}{2} \frac{l}{L} - \epsilon^3 \frac{mca_x}{16} \left(\frac{7}{2} \frac{l}{L} \frac{l^2}{R} + \frac{l^3}{T} + \frac{1}{2} \frac{l^3}{L^3} \right) - \epsilon^3 \frac{3}{2} \frac{P_x''^2}{mc\zeta_0 k_z l} \frac{l}{L} \frac{l^2}{R}. \tag{3.145}$$

The equation of motion for Z'' is obtained from (3.141) as

$$\frac{dZ''}{d\eta} = \frac{1-\zeta_0^2}{2\zeta_0^2 k_z} + \frac{k_z l^2}{4} + \frac{1}{2k_z} \left(\frac{P''_x}{mc\zeta_0} \right)^2 - \frac{P''_x}{mc\zeta_0} \sigma l \sin\eta + \epsilon^2 \frac{k_z l^2}{16} \left(3\frac{l^2}{R} + \frac{19}{4}\frac{l^2}{L^2} \right) - \epsilon^2 \frac{P_x''^2}{m^2c^2\zeta_0^2 k_z} \left(\frac{1}{2}\frac{l^2}{R} - \frac{7}{4}\frac{l^2}{L^2} \right). \tag{3.146}$$

where the solution $p''_\eta = -mc\zeta_0$ is utilized. Equations (3.144) and (3.145), which determine the transverse secular motion of the oscillation center up to $\mathscr{O}\left(\epsilon^3\right)$, are the central results in this study.

Combining Eqs. (3.144) and (3.145), we have

$$\frac{d^2X''}{d\eta^2} = -\frac{l}{2} \left[\epsilon \frac{l}{L} + \frac{\epsilon^3}{8} \left(\frac{7}{2} \frac{l}{L} \frac{l^2}{R} + \frac{l^3}{T} + \frac{25}{2} \frac{l^3}{L^3} \right) \right], \tag{3.147}$$

where we again neglect terms in the order of ϵ^5 using $P''_x \sim \mathscr{O}(\epsilon)$. The RHS of Eq. (3.147) corresponds to the relativistic ponderomotive force up to the third order of ϵ. As seen in Eq. (3.147), the ponderomotive force of the order following the first order is $\mathscr{O}\left(\epsilon^3\right)$, which consists of terms proportional to the second and third spatial derivatives of the field amplitude and also to the cube of the field gradient. Thus, the ponderomotive force depends not only on the local field gradient but also on the field curvature and its derivative (spatial variation of curvature), which correspond to the higher-order nonlocal structures not simply described by the local gradient.

In the Z'' direction, the zeroth-order translational motion proportional to $k_z l^2/4$ in the second term on the RHS of Eq. (3.146) is found to also be affected by the higher-order terms through the $\mathbf{v} \times \mathbf{B}$ force as seen in the fifth term on the RHS of Eq. (3.146).

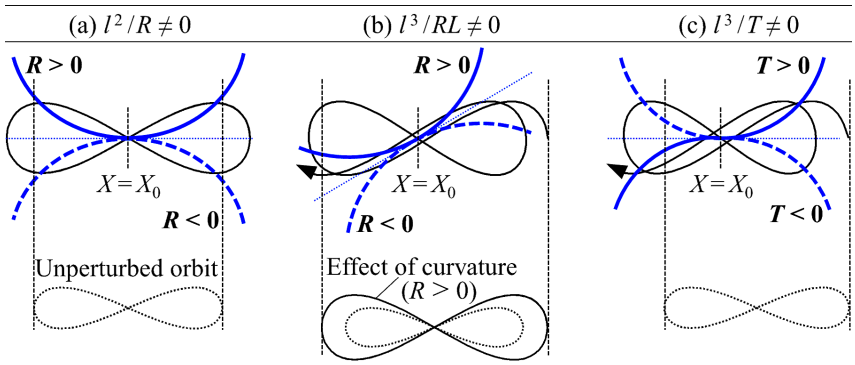

Figure 3.4: Effects of the curvature R^{-1} and third derivative T^{-1} of the field amplitude on the particle orbit. The field has (a) zero gradient and positive or negative curvature, (b) finite gradient and positive or negative curvature, and (c) zero gradient and positive or negative third derivative at $X = X_0$. The blue line denotes the field pattern and the black solid line represents the particle orbit in the x-z plane. In the lower part, the unperturbed orbits are shown for comparison.

3.3 Physical meaning of the nonlocal ponderomotive force

3.3.1 The higher order nonlocal effect described by the third order ponderomotive force

Here, we consider the physical meaning of the higher order ponderomotive force obtained in Sec. 3.2. The nonlocal effects represented by Eq. (3.147) can be explained using Fig. 3.4, which illustrates three typical laser field patterns as follows:

(a) A symmetrical concave (solid line) or convex (dashed line) structure where the gradient at the oscillation center $X = X_0$ is zero, so that $l/L = l^3/T = 0$ but $l^2/R \neq 0$.

(b) An asymmetric concave (solid line) or convex (dashed line) structure where the gradient is finite at $X = X_0$, so that $l/L \neq 0$ and $l^2/R \neq 0$ but $l^3/T = 0$.

(c) An asymmetric structure with curvature transition at $X = X_0$ where the gradient and curvature are both zero, so that $l/L = l^2/R = 0$ while $l^3/T \neq 0$.

The corresponding particle orbits around $X = X_0$ are shown in Fig. 3.4 (black solid lines) for cases $l^2/R > 0$ and $l^3/T > 0$.

In case (a), the excursion length increases (decreases) when the curvature is positive (negative) owing to the increase (decrease) of the η cycle-averaged field amplitude. However, since the change is symmetric for $X = X_0$, the nonlocal effect is canceled during one cycle of η. Therefore, case (a) does not produce ponderomotive force. This is the reason that the term $l^2/R \sim \mathscr{O}\left(\epsilon^2\right)$ does not appear independently in Eq. (3.147).

On the other hand, in case (b), the symmetry associated with the curvature l^2/R is broken by the coupling with the gradient $l/L > 0$. Consequently, an asymmetry is produced in the orbit, which leads to a ponderomotive force influenced by the curvature.

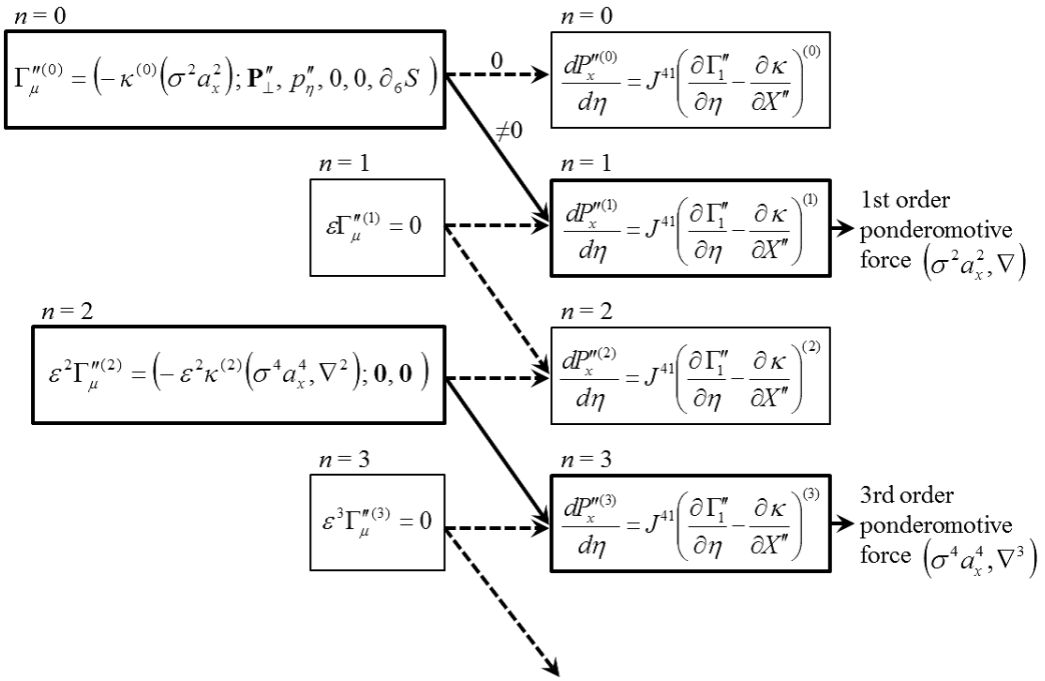

Figure 3.5: Overview of the derivation process from the fundamental one-form to the equation of motion. In the left side, κ denotes the Hamiltonian, and in the following brackets, the dependence of terms included in κ on the sign of particle charge σ, field amplitude a_x and spatial derivative ∇ is shown.

In case (c), the orbit also becomes asymmetric but in a different manner. Namely, although the field gradient is zero at the oscillation center, the nonlocal effect associated with the third derivative $l^3/T > 0$ yields a finite ponderomotive force.

These are the higher order nonlocal effects that cannot be simply represented by the local field gradient.

The general parity relation that all the even derivatives, i.e., $\partial^n a_x/\partial X^n$ $(n = 2, 4, 6, \cdots)$, do not appear alone in the equation of motion has been confirmed in orders higher than ϵ^3.

3.3.2 Symmetrical characteristic of the oscillation center one-form

In the above, we discussed the nonlocal effects relating to symmetry. Interestingly, the corresponding oscillation center 1-form is also found to exhibit a symmetrical aspect. To see it, we show an overview of the derivation process from the 1-form to the equation of motion in Fig. 3.5. Here, κ denotes the Hamiltonian, and in the following brackets, the dependence of terms included in κ on the sign of particle charge σ, field amplitude a_x and spatial derivative ∇ is shown.

As shown in the squares in the left side of Fig. 3.5, the Hamiltonian in odd orders $(n = 1, 3)$ is zero, while that in even orders $(n = 0, 2)$ is finite. Here, as discussed in Sec. 3.2.2, the nth order Hamiltonian leads to the force of $(n + 1)$th order, due to the X derivative of the Hamiltonian in formulating the equation of motion as seen in the squares in the right side in Fig. 3.5. Due to this relation, the obtained higher

order ponderomotive force has only the odd order, i.e., the first and third orders, whereas there appears no even-order force.

Here, it is worthwhile to consider the properties of terms whose orders are higher than $\mathscr{O}\left(\epsilon^3\right)$. Since the ponderomotive force is a pressure force associated with the electromagnetic field, it does not depend on the sign of the particle charge σ. From this requirement, only the terms proportional to σ^{2n} $(n = 1, 2, \cdots)$ can be retained in the secular 1-form, so that only the 1-form in $\mathscr{O}\left(\epsilon^{2n}\right)$ has a finite value and produces the ponderomotive force in the order of ϵ^{2n+1}. Therefore, the ponderomotive force next to the third order is expected to be $\mathscr{O}\left(\epsilon^5\right)$. We have confirmed that the third-order 1-form becomes zero, so that no fourth-order ponderomotive force appears.

3.4 Discussions

3.4.1 On the removal of the figure-eight oscillation

The gauge transformation performed in Sec. 3.2.3 removes a term that causes an oscillation in the x direction, but the zeroth-order 1-form itself still includes oscillatory terms as seen from Eq. (3.107). In other words, the oscillatory term is not removed completely but just moved from Γ_0 to Γ_6 which does not affect the equation of motion in the x direction.

This point is an essential difference from the noncanonical Lie perturbation analysis in gyrokinetics and also in studying the beam orbit in free-electron lasers (FEL).

In the present case, the zeroth-order fundamental orbit is the figure-eight motion which has in principle two frequencies, η and 2η. On the other hand, the gyration motion, which is the fundamental oscillation in the case of gyrokinetics, has only a single gyro frequency, $\omega_c = qB/mc$. For the beam trajectory in wiggler magnets in the FEL system, the fundamental oscillation is also described by a single wiggler frequency.

From the above reason, in the present system in which the fundamental particle orbit has more than one frequency, there exist no coordinates that remove the rapid oscillation complitely from the zeroth-order 1-form. In Appendix C, instead of the preparatory gauge transformation applied in this chapter, we perform a coordinate transformation that is different from the usual oscillation center transformation to remove oscillation from the x direction. We will see that, even in that case, the oscillation is not removed completely from the 1-form but moved from the x to z direction in the equations of motion.

The present analysis thus demonstrates that the degree of freedom of the gauge and coordinate transformations can be utilized to arrange the distribution of oscillatory terms in the phase space Lagrangian depending on the purpose.

3.4.2 Effect of non-uniformity of the laser field in the pulse direction

In the present study, we have assumed a laser field whose amplitude is nonuniform only in the transverse x direction. When the field amplitude has a non-uniformity also in the parallel z direction as $a_x = a_x(x, \eta)$, such as spatially and temporally

localized laser pulses, it is expected to affect not only in generating the ponderomotive force in the z direction, i.e., the pulse direction, but also as a modulation to the transverse ponderomotive force in higher orders.

From the odd-type structure of the ponderomotive force found in Sec. 3.3, the candidates for the transverse higher-order force associated with the non-uniformity in the pulse direction are considered to appear in the third order ϵ^3, being coupled with the non-uniformity in the transverse direction as

$$\epsilon^3 \frac{l}{L}\frac{1}{L_\eta^2}, \quad \epsilon^3 \frac{l}{L}\frac{1}{R_\eta}, \quad \epsilon^3 \frac{l^2}{L^2}\frac{1}{L_\eta}, \quad \epsilon^3 \frac{l^2}{R}\frac{1}{L_\eta}, \tag{3.148}$$

where we represent the gradienta and curvature by the phase η as $a_x^{-1}\partial a_x/\partial\eta = 1/L_\eta$, $a_x^{-1}\partial^2 a_x/\partial\eta^2 = 1/R_\eta$, respectively.

In Eq. (3.148), the first and second ones denote the modulation to the gradient l/L (odd-type structure) from the pulse non-uniformity $1/L_\eta^2$ and $1/R_\eta$ (even-type structures), whereas the third and fourth ones denote the modulation to the even-type structures l^2/R and l^2/L^2 from the pulse non-uniformity $1/L_\eta$ (odd-type structure). Among them, we can expect that only the first and second ones, i.e.,

$$\epsilon^3 \frac{l}{L}\frac{1}{L_\eta^2}, \quad \epsilon^3 \frac{l}{L}\frac{1}{R_\eta}, \tag{3.149}$$

can appear as the third order secular force in the transverse x direction for the same reason as the discussion for Fig. 3.4 (b) in Sec. 3.3.1. Namely, the curvature in the pulse direction $1/R_\eta$ increases/decreases the excursion length of the figure-eight motion due to the increase/decrease of the η cycle-averaged field amplitude. The couplings in Eqs. (3.149) break the symmetrical change in the figure-eight excursion by the pulse non-uniformity, and then yield a finite ponderomotive force.

3.4.3 Possibility for expressing the higher order ponderomotive force by a potential form

The ponderomotive force up to the first order of ϵ is expressed as a potential force. Here, we consider whether the higher order nonlocal ponderomotive force can be expressed as a potential force as

$$\frac{d^2 X''}{d\eta^2} = -\nabla\phi_p, \tag{3.150}$$

where ϕ_p is a scalar corresponding to the ponderomotive potential.

In the first order ϵ, one can easily see that the ponderomotive force can be written as

$$\frac{d^2 X}{d\eta^2} = -\frac{l}{2}\frac{l}{L} = -\frac{1}{4}\nabla l^2, \tag{3.151}$$

where $\nabla = \partial/\partial X''$. Hence, the ponderomotive potential up to the first order is

obtained as

$$\phi_p = \frac{l^2}{4}. \tag{3.152}$$

In contrast, we find that the ponderomotive force up to the third order cannot be expressed as a scalar potential form. The verification is given in Appendix D.

The above consideration, i.e., whether a description in the potential form is possible or not, is important because it is related to the generations of vortex in the particle motion and of the corresponding magnetic field. For instance, we assume the equation of motion $d\mathbf{p}/dt = -\nabla\phi + \mathbf{F}$ where the force $\mathbf{F}$ cannot be represented by the gradient of a scalar function as the scalar potential force $-\nabla\phi$ in the first term. By taking the curl of both sides of the equation of motion, the time evolution of the vorticity $\Omega = \nabla \times \mathbf{p}$ can be obtained as $d\Omega/dt = \nabla \times \mathbf{F}$. Here, notice that the scalar potential force term does not appear in the vorticity equation doe to the vector operation $\nabla \times (\nabla\phi) = 0$. Therefore, the nonpotential force $\mathbf{F}$ can be regarded as the source of vortices.

As a further extension of the present theory, it is worthwhile to explore the vector potential for the obtained higher order force [41]. Namely, when the higher order ponderomotive force has the corresponding vector potential, it may leads to a magnetic field generation through the particle motion suffered from the higher order nonlocal ponderomotive effects.

3.5 Conclusions

In this chapter, we explored a theory of ponderomotive force that includes nonlocal effects up to higher orders using the noncanonical Lie perturbation method.

By properly choosing the coordinate transformations and gauge functions, we successfully obtained a secular equation of motion describing the ponderomotive force up to the third order of ϵ. The higher-order terms consist of the second and third spatial derivatives of the field amplitude, so that the ponderomotive force depends not only on the local field gradient, but also on the field curvature and its variation. Such higher-order derivative terms originate from nonlocal particle motion not simply expressed by the local field gradient as Fick's law. The formula is then accessible to the regime in which laser fields exhibit characteristic transverse structures such that higher derivatives of the field amplitude regulate the interaction.

In the derivation process, it is noted that the oscillation cannot be removed completely from the fundamental 1-form due to the fact that the zeroth-order fundamental orbit in the present study has two frequencies, which is an essential difference from the noncanonical Lie perturbation analysis in previous studies such as gyrokinetics. Here, a proper gauge transformation successfully transfered the undesirable oscillation from the transverse to longitudinal direction.

The obtained higher order ponderomotive force are found to be subject to the symmetry of the field structure and also to a constraint that the ponderomotive force is a pressure force free from the sign of the particle charge.

Chapter 4

Analytical solution for the ponderomotive formula

In this chapter, we find an approximated solution for the first and third order ponderomotive formulae obtained in Chap. 3 assuming laser fields with the Gaussian and super Gaussian transverse structures. In the latter case, a qualitative difference between the first and third order formulae is obtained (Sec. 4.3). Parametric dependences of the oscillation center trajectories on the scale length of the field profile and also on the initial condition are discussed.

4.1 Taylor expansion of the ponderomotive terms

In Chap. 3, we derived the oscillation center equations of motion describing the ponderomotive force up to the first order ϵ, i.e.,

$$\frac{d^2X''}{d\eta^2} = -\epsilon\frac{l}{2}\frac{l}{L},$$

(Eq. (3.121)) and to the third order ϵ^3 (Eq. (3.147)), i.e.,

$$\frac{d^2X''}{d\eta^2} = -\frac{l}{2}\left[\epsilon\frac{l}{L} + \frac{\epsilon^3}{8}\left(\frac{7}{2}\frac{l}{L}\frac{l^2}{R} + \frac{l^3}{T} + \frac{25}{2}\frac{l^3}{L^3}\right)\right],$$

(Eq. (3.147)).

In this section, we consider the difference between the above first and third order ponderomotive formulae in detail by using the Taylor expansion for the field amplitude and its derivatives on the RHS of Eqs. (3.121) and (3.147) around a fixed position $X = X_0$. Here, the expansion parameter is defined by

$$\delta \equiv (X - X_0)\left.\frac{\partial(\ln a_x)}{\partial X}\right|_{X_0} = \frac{X - X_0}{L(X_0)}, \tag{4.1}$$

where X_0 is assumed to be the initial position of the oscillation center. The first order formula Eq. (3.121) is expanded to

$$\frac{d^2X}{d\eta^2} = A_0^{(1)} + \delta\,(X - X_0)\,A_1^{(1)} + \frac{\delta^2}{2!}\frac{(X - X_0)^2}{l(X_0)}A_2^{(1)} + \frac{\delta^3}{3!}\frac{(X - X_0)^3}{l^2(X_0)}A_3^{(1)} + \mathscr{O}\left(\delta^4\right), \tag{4.2}$$

while the third order formula Eq. (3.147) to

$$\frac{d^2X}{d\eta^2} = \left(A_0^{(1)} + A_0^{(3)}\right) + \delta\,(X - X_0)\left(A_1^{(1)} + A_1^{(3)}\right) + \frac{\delta^2}{2!}\frac{(X - X_0)^2}{l(X_0)}\left(A_2^{(1)} + A_2^{(3)}\right) + \frac{\delta^3}{3!}\frac{(X - X_0)^3}{l^2(X_0)}\left(A_3^{(1)} + A_3^{(3)}\right) + \mathscr{O}\left(\delta^4\right), \tag{4.3}$$

where

$$A_0^{(1)} = -\frac{\epsilon}{2} l \frac{l}{L}\bigg|_{X_0}, \tag{4.4}$$

$$A_0^{(3)} = -\frac{\epsilon^3}{16}\left[\frac{7}{2} l \frac{l}{L}\frac{l^2}{R}\bigg|_{X_0} + l\frac{l^3}{T}\bigg|_{X_0} + \frac{25}{2} l \frac{l^3}{L^3}\bigg|_{X_0}\right], \tag{4.5}$$

$$A_1^{(1)} = -\frac{\epsilon}{2}\left(\frac{l^2}{L^2}\bigg|_{X_0} + \frac{l^2}{R}\bigg|_{X_0}\right), \tag{4.6}$$

$$A_1^{(3)} = -\frac{\epsilon^3}{16}\left[\frac{89}{2}\frac{l^2}{L^2}\frac{l^2}{R}\bigg|_{X_0} + \frac{7}{2}\left(\frac{l^2}{R}\bigg|_{X_0}\right)^2 + \frac{13}{2}\frac{l}{L}\frac{l^3}{T}\bigg|_{X_0} + \frac{l^4}{Q}\bigg|_{X_0} + \frac{25}{2}\frac{l^4}{L^4}\bigg|_{X_0}\right], \tag{4.7}$$

$$A_2^{(1)} = -\frac{\epsilon}{2}\left(3\frac{l}{L}\frac{l^2}{R}\bigg|_{X_0} + \frac{l^3}{T}\bigg|_{X_0}\right), \tag{4.8}$$

$$A_2^{(3)} = -\frac{\epsilon^3}{16}\left[\frac{189}{2}\frac{l^3}{L^3}\frac{l^2}{R}\bigg|_{X_0} + 96\frac{l}{L}\left(\frac{l^2}{R}\bigg|_{X_0}\right)^2 + \frac{115}{2}\frac{l^2}{L^2}\frac{l^3}{T}\bigg|_{X_0} + \frac{27}{2}\frac{l^2}{R}\frac{l^3}{T}\bigg|_{X_0} + \frac{19}{2}\frac{l}{L}\frac{l^4}{Q}\bigg|_{X_0} + \frac{l^5}{F}\bigg|_{X_0}\right], \tag{4.9}$$

$$A_3^{(1)} = -\frac{\epsilon}{2}\left[3\left(\frac{l^2}{R}\bigg|_{X_0}\right)^2 + 4\frac{l}{L}\frac{l^3}{T}\bigg|_{X_0} + \frac{l^4}{Q}\bigg|_{X_0}\right], \tag{4.10}$$

$$A_3^{(3)} = -\frac{\epsilon^3}{16}\left[\frac{759}{2}\frac{l^2}{L^2}\left(\frac{l^2}{R}\right)^2\bigg|_{X_0} + 152\frac{l^3}{L^3}\frac{l^3}{T}\bigg|_{X_0} + 96\left(\frac{l^2}{R}\bigg|_{X_0}\right)^3 + 334\frac{l}{L}\frac{l^2}{R}\frac{l^3}{T}\bigg|_{X_0} + \frac{153}{2}\frac{l^2}{L^2}\frac{l^4}{Q}\bigg|_{X_0} + \frac{27}{2}\left(\frac{l^3}{T}\bigg|_{X_0}\right)^2 + 23\frac{l^2}{R}\frac{l^4}{Q}\bigg|_{X_0} + \frac{25}{2}\frac{l}{L}\frac{l^5}{F}\bigg|_{X_0} + \frac{l^6}{J}\bigg|_{X_0}\right]. \tag{4.11}$$

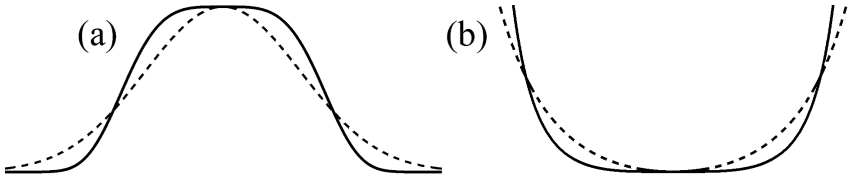

Figure 4.1: Transverse laser field profiles considered in Sec. 4.2 (a), i.e., Gaussian $\exp(-x^2/w^2)$ and super Gaussian $\exp(-x^4/w^4)$, and (b), i.e., $\exp(x^2/w^2)$ and $\exp(x^4/w^4)$ concave hollows.

Here, lQ^{-1}, lF^{-1} and lJ^{-1} correspond to the fourth, fifth and sixth deribatives of the field amplitude, respectively. The terms in the order ϵ^3, i.e. $A_0^{(3)}$, $A_1^{(3)}$, $A_2^{(3)}$ and $A_3^{(3)}$, originate from the third order term in the original equation Eq. (3.147).

Here, an important difference is found to appear when flat top/bottom field profiles are assumed.

4.2 Application to the flat-top super Gaussian-type transverse field structure

To see this, we assume a symmetrical concave/convex profile for the laser field amplitude in the transverse direction given by

$$a_x(x) = a_0 \exp\left[\pm\left(\frac{x}{w}\right)^s\right], \tag{4.12}$$

where w is a typical scale length of the field profile, i.e., the beam waist size for convex fields, while the hollow width for concave fields. Here, $s = 2$ corresponds to the Gaussian-type concave/convex profile, whereas $s = 4$ to that of the fourth order super Gaussian which exhibits flat top or flat bottom structure having more gentle amplitude gradient around the axis as shown in Fig. 4.1.

For $s = 2$, spatial deribatives up to the fourth order are calculated as

$$\frac{1}{L} = \frac{1}{l}\frac{\partial l}{\partial x} = \pm\frac{2}{w}\frac{x}{w}, \tag{4.13}$$

$$\frac{1}{R} = \frac{2}{w^2}\left(\pm 1 + 2\frac{x^2}{w^2}\right), \tag{4.14}$$

$$\frac{1}{T} = \frac{4}{w^3}\frac{x}{w}\left(3 \pm 2\frac{x^2}{w^2}\right), \tag{4.15}$$

$$\frac{1}{Q} = \frac{4}{w^4}\left(3 \pm 12\frac{x^2}{w^2} + 4\frac{x^4}{w^4}\right), \tag{4.16}$$

where signs are minus for convex field and plus for concave field, respectively. From Eqs. (4.13)-(4.16), we see that the odd-order derivatives Eqs. (4.13) and (4.15) vanish on the axis $x = 0$, while those of even-orders have finite values at $x = 0$.

On the other hand, for $s = 4$ super Gaussian, we have

$$\frac{1}{L} = \frac{1}{l}\frac{\partial l}{\partial x} = \pm\frac{4}{w}\frac{x^3}{w^3}, \tag{4.17}$$

$$\frac{1}{R} = \frac{4}{w^2}\frac{x^2}{w^2}\left(\pm 3 + 4\frac{x^4}{w^4}\right), \tag{4.18}$$

$$\frac{1}{T} = \frac{8}{w^3}\frac{x}{w}\left(\pm 3 + 18\frac{x^4}{w^4} \pm 8\frac{x^8}{w^8}\right), \tag{4.19}$$

$$\frac{1}{Q} = \frac{8}{w^4}\left(\pm 3 + 102\frac{x^4}{w^4} \pm 144\frac{x^8}{w^8} + 32\frac{x^{12}}{w^{12}}\right). \tag{4.20}$$

In this case, Eqs. (4.17)-(4.19) are found to be zero at $x = 0$. Therefore, different from the Gaussian case $s = 2$, derivatives that have finite values on the axis $x = 0$ are those of even orders larger than the third order, i.e., $\partial_x^{(n)} l$ $(n \geq 4)$. In other words, not only the gradient but also the curvature and its variation vanish on the axis $x = 0$. In Figs. 4.2 (a) and (b), we plot the first to fourth derivatives for $s = 2$ and $s = 4$ convex cases with minus sign in Eq. (4.12), which correspond to the Gaussian and fourth order super Gaussian beams, respectively. In the right side figures in (a) and (b), the derivatives in the peripheral of the beam axis $x = 0$ are shown, from which we see that the second and fourth derivatives are dominant near the axis in the cases of $s = 2$ and $s = 4$, respectively.

Now, we apply these field profiles to Eqs. (4.2) and (4.3) assuming that the oscillation center is initially on the axis, i.e., $X_0 = 0$. Here, we consider $s = 4$ with minus sign in Eq. (4.12). In this case, Eq. (4.2) derived from the first order ponderomotive formula yields to

$$\frac{d^2X}{d\eta^2} = -\frac{\delta^3\epsilon}{12}\frac{l^2}{Q}\left(X - X_0\right)^3 + \mathscr{O}\left(\delta^3\epsilon^3\right), \tag{4.21}$$

whereas, Eq. (4.3) from the third order formula becomes

$$\frac{d^2X}{d\eta^2} = -\frac{\delta\epsilon^3}{16}\frac{l^4}{Q}\left(X - X_0\right) - \frac{\delta^3\epsilon}{12}\frac{l^2}{Q}\left(X - X_0\right)^3 + \mathscr{O}\left(\delta^3\epsilon^3\right), \tag{4.22}$$

Here, we limit the situation such that the oscillation center is near the beam axis, i.e., $X \sim X_0$. In such a case, the second term on the RHS of Eq. (4.22) can be neglected compared with the first term, and then it leads to

$$\frac{d^2X}{d\eta^2} = -\frac{\delta\epsilon^3}{16}\frac{l^4}{Q}\left(X - X_0\right). \tag{4.23}$$

Comparing Eqs. (4.21) and (4.23), we find an essential difference, i.e., a linear term remains in Eq. (4.23) but not in Eq. (4.21). The remaining linear term in Eq. (4.23) corresponds to an ϵ^3 term in the coefficient (B) (Eq. (4.5)) that is derived from the term consisting of the third derivative lT^{-1} in the original third order ponderomotive formula Eq. (3.147) through the procedure of taking its first derivative in the Taylor expansion. Therefore, we conclude that in considering flat field structures

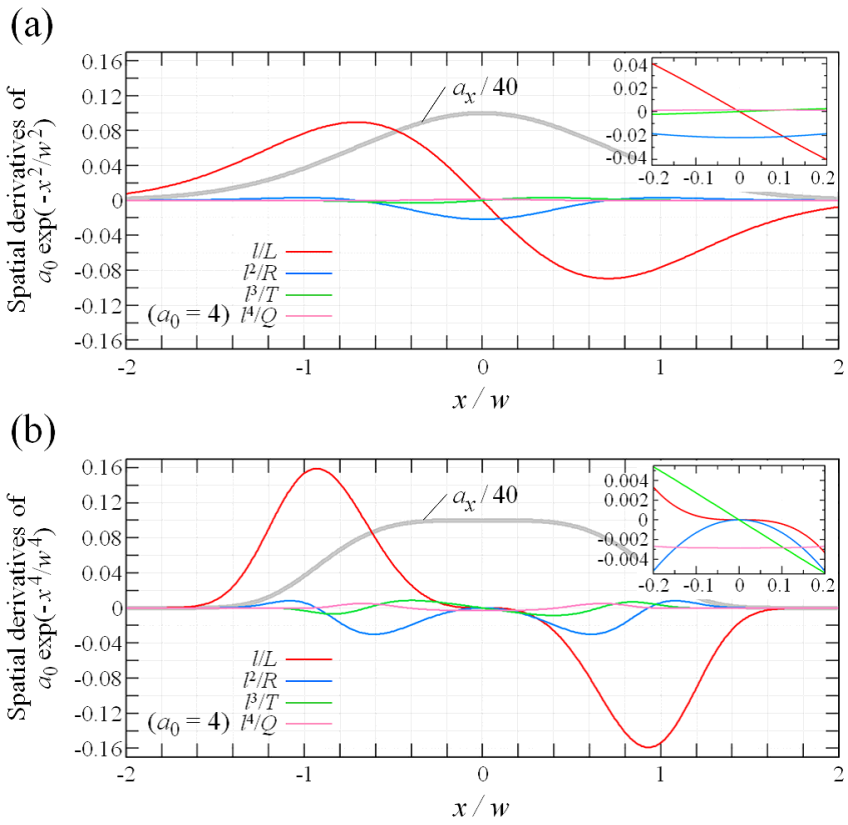

Figure 4.2: The first to fourth spatial derivatives normalized by the excursion length $l = a_0\lambda_L/2\pi\zeta_0$ where $a_0 = 4$, $\lambda_L = 820$ nm and $\zeta_0 = 1$ for (a) $s = 2$ convex Gaussian and (b) $s = 4$ convex super Gaussian laser fields.

such as $s = 4$ super Gaussian, the oscillation center equation of motion exhibits a qualitative difference depending on whether the higher order nonlocal effect of the field amplitude is taken into account or not.

4.3 Elliptic- and exponential-type trajectories of the oscillation center

Next, we consider the analytical solutions for Eqs. (4.21) and (4.23). Firstly, the solution for (4.21) is given using the Jacobi function sn as

$$\frac{X}{\lambda} = -\frac{(-1)^{1/4}}{2\pi}\sqrt{\frac{a_0}{\zeta_0}}\sqrt{\frac{P_{x0}}{mc\zeta_0}}\frac{w}{l}\mathrm{sn}\left(\Theta_s\eta, -2\right), \tag{4.24}$$

where

$$\Theta_s = \frac{(-1)^{3/4}}{\sqrt{a_0/\zeta_0}}\sqrt{\frac{P_{x0}}{mc\zeta_0}}\left(\frac{w}{l}\right)^{-1}. \tag{4.25}$$

The above solution can be expanded in the form

$$X \sim D_1\eta + D_5\eta^5; \tag{4.26}$$

$$D_1 = \frac{1}{2\pi}\frac{P_{x0}}{mc\zeta_0}, \tag{4.27}$$

$$D_5 = D_1\frac{1}{10}\frac{1}{4\pi^2}\left(\frac{P_{x0}}{mc\zeta_0}\right)^2\frac{1}{(w/\lambda)^2}\left(\frac{w}{l}\right)^{-2}. \tag{4.28}$$

Here, D_1 is a coefficient corresponding to the ballistic motion of the particle determined by the initial momentum P_{x0}, while D_5 is that to the acceleration due to the ponderomotive force.

On the other hand, the solution for Eq. (4.23) is found to have an exponential dependence on η as

$$\frac{X}{\lambda} = \frac{1}{2\pi\sqrt{6}}\frac{P_{x0}}{mc\zeta_0}\left(\frac{w}{l}\right)^2\left(\mathrm{e}^{\theta\eta} - \mathrm{e}^{-\theta\eta}\right), \tag{4.29}$$

where

$$\theta = \sqrt{\frac{3}{2}}\frac{1}{2\pi}\frac{a_0}{\zeta_0}\left(\frac{w}{l}\right)^{-2}. \tag{4.30}$$

The above solution can be expanded in the form

$$X \sim C_1\eta + C_3\eta^3; \tag{4.31}$$

$$C_1 = \frac{1}{2\pi}\frac{P_{x0}}{mc\zeta_0}, \tag{4.32}$$

$$C_3 = C_1\frac{1}{4}\left(\frac{w}{l}\right)^{-4}. \tag{4.33}$$

Similar as D_1 and D_5, the coefficient C_1 corresponds to the ballistic motion of the particle determined by the initial momentum P_{x0}, while C_3 to acceleration due to the ponderomotive force. Note that without neglecting X^3 term in Eq. (4.22), the solution is given by the Jacobi function cn as

$$\frac{X}{\lambda} = \frac{\sqrt{3}}{4\pi}\frac{a_0}{\zeta_0}\left[\left(1 + \frac{128}{3}\frac{\zeta_0^2}{a_0^2}\left(\frac{P_{x0}}{mc\zeta_0}\right)^2\frac{w^4}{l^4}\right)^{1/2} - 1\right]^{1/2} \times \mathrm{cn}\left(\Theta_c\eta, k\right), \tag{4.34}$$

where

$$\Theta_c = \sqrt{1 - \frac{1}{24}\frac{\zeta_0^2}{a_0^2}\frac{1}{(w/l)^4}\left(\frac{P_{x0}}{mc\zeta_0}\right)^2}, \tag{4.35}$$

and

$$k = 1 - \frac{\left(\frac{P_{x0}}{mc\zeta_0}\right)^2}{2\left(\frac{P_{x0}}{mc\zeta_0}\right)^2 - \frac{3}{64}\frac{a_0^2}{\zeta_0^2}\frac{l^4}{w^4}\left[\sqrt{1+\frac{128}{3}\frac{\zeta_0^2}{a_0^2}\frac{l^4}{w^4}\left(\frac{P_{x0}}{mc\zeta_0}\right)^2}-1\right]}, \tag{4.36}$$

which satisties $k = 1/2$ when the linear term becomes zero.

4.4 Discussions

4.4.1 Qualitative difference of the two types of solution

As discussed in Sec. 4.3, terms relating to the ponderomotive acceleration is $D_5\eta^5$ in Eq. (4.26) and $C_3\eta^3$ in Eq. (4.31), respectively. Therefore, it is worthwhile to investigate the parametric dependence of C_3 and D_5.

The coefficient C_3 is originated from the curvature variation $1/T$ in Eq. (3.145), and is proportional to $P_{x0}\,(l/w)^4$. On the other hand, D_5 originated from the first order ponderomotive force in Eq. (3.145) is proportional to $P_{x0}^3\,(l/w)^2$. Both C_3 and D_5 thus consist of the product of P_{x0} and l/w where P_{x0} is related to the initial ejection without which the oscillation center located at $X = 0$ does not move, and l/w to the ponderomotive force acceleration due to the nonlocality. Here, it is found that the dependence on l/w is stronger in C_3 than D_5, whereas that on P_{x0} is stronger in D_5 than C_3. These dependences suggest that the effect of the nonlocal particle motion is more pronounced in the third order ponderomotive formula than that of the first order as one can expect. The trajectories depart from the linear dependence, i.e. $X \sim \eta$, when terms $C_3\eta^3$ and $D_5\eta^5$ become effective in Eqs. (4.31) and (4.26), respectively. The ratio is given by

$$\frac{D_5}{C_3} = \frac{2}{5a_0^2}\left(\frac{P_{x0}}{mc}\right)^2, \tag{4.37}$$

and therefore, when the initial momentum P_{x0} is small satisfying $P_{x0}/mc \ll a_0$, the trajectory described by the third order formula is found to escape faster than that by the first order.

4.4.2 Extension to general field profiles

Note that in this section, we have assumed a laser field profile given by Eq. (4.12) with even numbers for the polynomial s. We can consider more general expression for the transversely non-uniform field profile given by

$$a_x\,(x) = a_0\sum_{s=1}^{\infty} f_s \exp\left[-\left(\frac{x}{w_s}\right)^s\right], \tag{4.38}$$

where f_s is a weighting function and w_s the specific scale length of the field amplitude variation corresponding to each polynomial s. Such an expression can represents complicated transverse field structures including asymmetry, which may be obtained

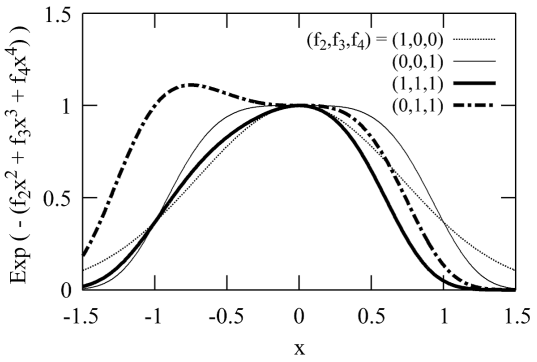

Figure 4.3: Examples of field structure represented by Eq. (4.38).

in experiments. Here, we note that in Sec. 4.2, it is found that the third order ponderomotive force plays an important role in determining the particle motion in the field profile $s = 4$, while the first order force can basically represent the motion when we assume $s = 2$. Similarly, a general relation can be obtained as follows: The nth order ponderomotive force becomes important in considering the field profile with $s = n + 1$. In Fig. 4.3, several examples for structures that can be represented by Eq. (4.38) using $s \leq 4$ are shown. Exploration of cases including asymmetry is interesting work to be devoted to future study.

4.5 Conclusions

In this chapter, we studied analytical solutions for the first and third order ponderomotive formulae obtained in Chap. 3 assuming laser field with the Gaussian and fourth order super Gaussian transverse structures. In the latter case, a qualitative difference between the first and third order formulae is obtained, which is found to be resulted from the fact that the first to third spatial derivatives of the field amplitude are diminished at the beam axis in the super Gaussian field profile. An oscillation center motion that exhibits exponential ejection from the beam center is derived as an approximated solution for the third order ponderomotive formula, whereas a solution represented by the Jacobi elliptic function is obtained for the first order formula.

By investigating the parametric dependences of the oscillation center trajectories on the scale length of the field profile and also on the initial condition of the particle, we found that the effect of the nonlocal particle motion, which is represented by the the ratio between the excursion length and beam radius, is more pronounced in the third order ponderomotive formula than that of the first order.

These results suggest that the first order formula underestimates the ponderomotive force at the peripheral of the beam axis in flat-top field structures.

Chapter 5

Numerical calculation for single particle motion in laser beams with flat transverse profiles

In the previous chapter, we find solutions for the oscillation center orbit analytically. The analytical solution is obtained based on an approximation that the oscillation center does not travel far from its initial position. Generally, the equation of motion cannot be solved analytically without such an approximation because the equation includes an arbitrary function of x, i.e., $a_x(x)$ and $l(x)$. Instead, we here perform a numerical integration to solve the oscillation center equation of motion and obtain the oscillation trajectory. In this chapter, we consider two types of transverse laser field amplitude profile; one is convex structure which simply eject the particle (Secs. 5.1 and 5.2), and the other is that of concave in which the particle is expected to exhibit the betatron oscillation in a slow period compared with that of the laser (Sec. 5.3).

We will show a comparison among the trajectories obtained by the first and third order ponderomotive formulae and also the trajectory calculated directly from the equation of motion for the particle. By these comparisons, we investigate the effect of the higher order nonlocal ponderomotoive force on the oscillation center dynamics.

5.1 Particle trajectories in super Gaussian laser beams

First, we consider the trajectory of the oscillation center of the particle in the laser field with fourth order super Gaussian beam profile, which is given by Eq. (4.12) in Sec. 4.2 with the minus sign and $s = 4$.

Here, we show numerical trajectories obtained by

(I) the first order ponderomotive formula,

$$\frac{dX'}{d\eta} = \frac{P'_x}{mc\zeta_0 k_z}, \tag{5.1}$$

$$\frac{dP'_x}{d\eta} = -\frac{mc\zeta_0 k_z l}{2}\epsilon \frac{l}{L}\bigg|_{X'}. \tag{5.2}$$

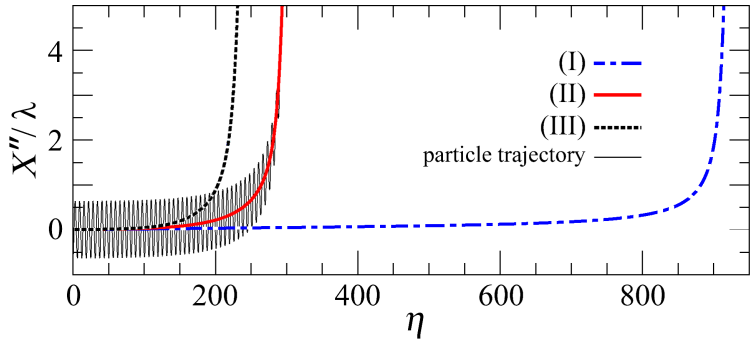

Figure 5.1: Comparison between the numerical trajectories for the oscillation center of a charged particle obtained from the Lie perturbation method up to (I) the first and (II) third orders, and (III) the averaging method up to the third order with respect to ϵ. The particle is irradiated by the laser beam with a transverse envelope $a_x = a_0 \exp\left(-x^4/w^4\right)$, where $a_0 = 4$ and $w = 5\mu m$. The black solid line shows the particle trajectory calculated by the full-order equation of motion.

(II) the third order ponderomotive formula derived by the Lie perturbation method,

$$\frac{dX''}{d\eta} = \frac{P_x''}{mc\zeta_0 k_z}\left(1 + \epsilon^2 \frac{3}{2}\frac{l^2}{L^2}\bigg|_{X''}\right), \tag{5.3}$$

$$\frac{dP_x''}{d\eta} = -\frac{mc\zeta_0 k_z}{2} l \left[\epsilon \frac{l}{L}\bigg|_{X''} + \frac{\epsilon^3}{8}\left(\frac{7}{2}\frac{l}{L}\frac{l^2}{R}\bigg|_{X''} + \frac{l^3}{T}\bigg|_{X''} + \frac{1}{2}\frac{l^3}{L^3}\bigg|_{X''}\right)\right]. \tag{5.4}$$

(III) the third order ponderomotive formula derived by the averaging method to the equation of motion given by Eqs. (A.84) and (A.85) in Appendix A, i.e.,

$$\frac{d\mathbf{x}_{s\perp}}{d\eta} = \frac{\mathbf{p}_{s\perp}}{m\omega\zeta_0},$$

$$\left(\frac{\partial}{\partial\eta} + \frac{\mathbf{p}_s\cdot\nabla}{m\omega\zeta_0}\right)\mathbf{p}_{s\perp} = -\frac{mca_x}{2}\left[\epsilon\frac{l}{L} + \frac{\epsilon^3}{8}\left(\frac{37}{2}\frac{l}{L}\frac{l^2}{R} + 2\frac{l^3}{T} + 10\frac{l^3}{L^3}\right)\right]\hat{\mathbf{e}}_x, \tag{5.5}$$

and

(IV) direct integration of the particle equation of motion,

$$\frac{d\mathbf{x}}{d\eta} = \frac{\mathbf{p}}{m\omega\zeta_0}, \tag{5.6}$$

$$\frac{d\mathbf{p}}{d\eta} = q\left(\mathbf{E} + \frac{\mathbf{v}}{c}\times\mathbf{B}\right)\frac{\omega\zeta_0}{\gamma}. \tag{5.7}$$

For the numerical integration, we use the fourth order Runge-Kutta method.

The numerical solutions obtained for cases (I)-(IV) are shown in Fig. 5.1. In this calculation, the normalized amplitude, beam radius and wavelength are assumed to be $a_0 = 4$, $w = 5\mu$m and $\lambda = 1\mu m$, and the initial condition for the oscillation center of the particle is $(X'', P_x'') = (0, 0.001mc)$. Note that the equation of motion in case (III) is expressed in the coordinate without the Lie transformation, whereas in cases

(I) and (II), the equations are given in the different coordinate Z''^{μ}. Thus, one needs to be careful about the initial condition for each coordinate. Here, we confirmed that the change of the initial condition resulting from the Lie transformation does not substantially affect the result; therefore, we used the same initial condition for all the cases.

We see that the trajectory for case (II) (the third-order formula) shows an almost exact agreement with that of the direct numerical calculation (IV), while the trajectories for case (I) (the first-order formula) and case (III) (averaging method up to $\mathscr{O}\left(\epsilon^3\right)$) exhibit significant differences in the ejection time (the time at which the oscillation center reaches to the laser beam radius, $X'' = w$). The trajectory in case (III) exhibits an ejection time that is a factor of 1.3 times shorter than that obtained by direct integration of the particle trajectory. This suggests that the result derived by the averaging method is not credible compared with that obtained by the Lie perturbation method, which preserves the Hamiltonian structure up to higher orders. In other words, this is considered to be a direct consequence of the lack of Hamiltonian structure in the averaging method while it is kept rigorously in the present approach.

Next, we compare cases (I) and (II). By using the relation $d\eta/dt = \omega\zeta_0/\gamma$, the ejection times for cases (I) and (II) are t =1460 fs and 480 fs, respectively. The physics leading to such a difference is explained as follows: The conventional first-order formula encompasses only at a narrow region through the local gradient, which is very weak in the present super Gaussian case. In contrast, the new formula, which incorporates terms up to the third order, can account for the global extent of the profile up to around the beam radius $X \sim w$. The new formula then can capture the rapid change of the field amplitude near the beam radius even when the oscillation center is located near the beam center. The new formula represents such nonlocal effects as a residual ponderomotive force, which enhances the ejection. For this reason, the first-order formula used in case (I) significantly overestimates the interaction time as seen from Fig. 5.1.

5.2 Condition for long time scale interaction in super Gaussian laser beam

Based on the above results, we further investigate the transverse initial condition allowed to keep the interaction without suffering ejection over a given phase advance $\Delta\eta$. Here, we impose the condition $w = 5$ μm, $a_0 = 4$ and $\Delta\eta = 300$ which corresponds to 1 psec time duration.

In Fig. 5.2 (a), the result is plotted in the normalized phase space for initial condition, $(X_0''/\lambda, P_{x0}''/mc)$. Here, blue circles and red squares show the results numerically obtained by using the first (case (I)) and third (case (II)) order ponderomotive formulae, respectively. The hatched area corresponds to that allowed for the long interaction. Namely, only the particles with initial conditions in the hatched area can keep the interaction during 1 psec. We see that the area of the hatched region is about 16 times larger in case (I) compared with that in case (II), which suggests that the higher order terms are effective in determining the particle dynamics near the beam axis.

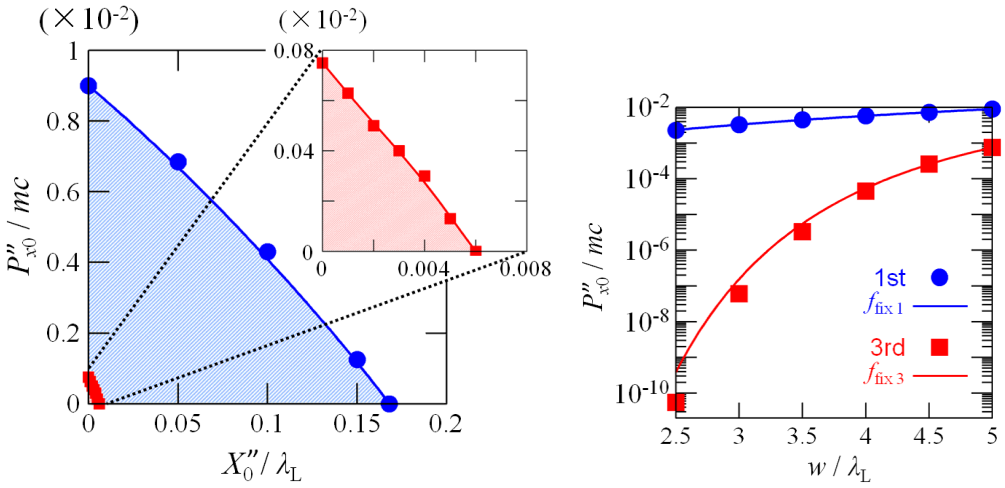

Figure 5.2: (a) The allowed area for the initial position and momentum in the perpendicular direction to maintain the interaction keeping $X'' < w = 5$ μm during $\Delta\eta = 300$ evaluated by the first (case(I), blue circle) and third (case(II), red square) order formulae. (b) The initial momentum P''_{x0} which leads to $X'' = w$ at $\eta = 300$ for each w in case (I) (blue circle) and (II) (red square). Here, $a_x = a_0 \exp\left(-x^4/w^4\right)$, $a_0 = 4$ and $\lambda = 1$ μm are assumed.

We also investigate the maximum initial momentum P''_{x0} for keeping the interaction during $\Delta\eta = 300$ with various beam radius w for both cases (I) and (II). The numerical result for each case is shown in Fig. 5.2 (b) by blue and red points. Here, the initial position is set to be $X'' = 0$. It is found that P''_{x0} decreases exponentially as $P''_{x0} \sim 1/\exp\left(\lambda^2/w^2\right)$ for case (II) as shown by the red line, while exhibits more gentle dependence $P''_{x0} \sim (w/\lambda)^{5/3}$ for case (I) as the blue line. These results suggest that the new particle motion associated with the third order terms predominantly and sensitively regulates the dynamics.

5.3 Betatron oscillation in concave hollow laser beam profiles

As another example, we consider confinement of a charged particle by the ponderomotive force. Here, the transverse profile of the laser field is assumed to be concave as shown on the right side of Fig. 4.1. In such a field, the particle exhibits a betatron oscillation around the bottom of the hollow structure owing to the ponderomotive force.

Figure 5.3 shows the numerical trajectory of the oscillation center in the hollow laser field with transverse envelopes (a) $a_x(x) = a_0 \exp\left(x^2/w^2\right)$ and (b) $a_x(x) = a_0 \exp\left(x^4/w^4\right)$, where $a_0 = 4$ and $w = 5$ μm. Note that in these cases the spatial derivatives at the center $x = 0$ are (a) $L^{-1} = T^{-1} = 0$ and $R^{-1} > 0$ and (b) $L^{-1} = R^{-1} = T^{-1} = 0$, while the fourth derivatives are positive in both cases. Blue and red lines correspond to the oscillation center trajectories for case (I) (first-order formula) and case (II) (third-order formula), respectively. In both Figs. 5.3 (a) and (b), the frequency of the betatron oscillation is downshifted in case (I) compared

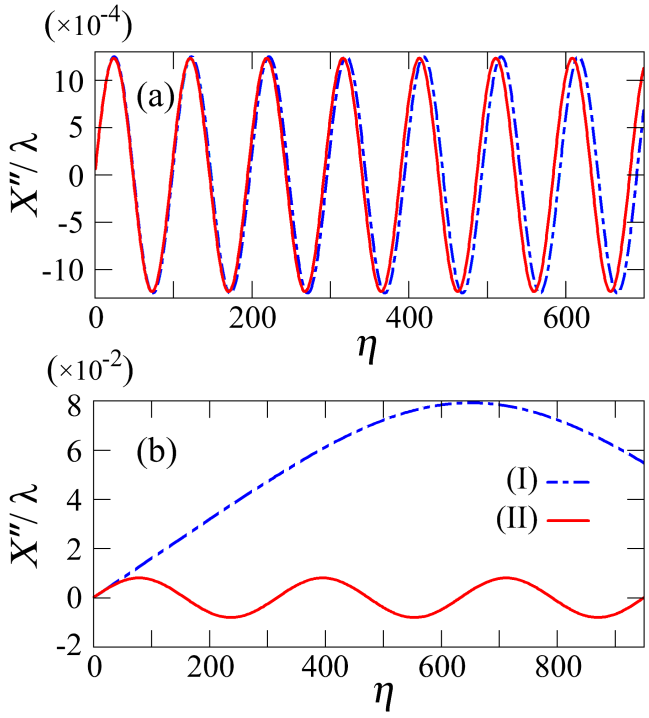

Figure 5.3: Numerical trajectories for the oscillation center of a charged particle irradiated by the laser field with transverse envelopes (a) $a_0 \exp\left(x^2/w^2\right)$ and (b) $a_0 \exp\left(x^4/w^4\right)$, where $a_0 = 4$ and $w = 5$ μm. Blue and red lines show the oscillation center trajectories obtained by the ponderomotive formulae up to the first and third orders, respectively.

with case (II). This is the effect from the third-order terms, which have finite values around $x = 0$. Comparing Figs. 5.3 (a) and (b), one can see that the difference in frequency is larger in (b). The result reflects the difference of field profiles: In case (a), the finite curvature at the center can represents the global structure of the field profile, whereas, in case (b), such a nonlocal structure is represented dominantly by derivatives higher than the second order around the beam axis.

5.4 Conclusions

In this section, we studied the particle motion in flat-top super Gaussian and concave hollow laser beam structures by using the Runge-Kutta numerical integration on the basis of the new formula for the ponderomotive force derived in Chap. 3.

Comparison between the oscillation center trajectory obtained by the third order formula and that obtained by a direct integration of the equation of motion for particle demonstrates the validity of the ponderomotive formula derived in this study with a sufficient convergence of the expansion series up to $\mathscr{O}\left(\epsilon^3\right)$.

We also compared the oscillation center trajectory with that obtained by the averaging method up to the third order. It is found that the trajectory derived by the averaging method does not agree with the direct integration of the particle,

which is considered to result from the lack of Hamiltonian structure in the averaging method.

Based on the above results, we investigated the transverse initial condition allowed to keep the interaction over a given phase advance in the super Gaussian laser beam. The allowed area in phase space for initial condition and its dependence on the beam radius suggest that the higher order nonlocal effect regulates the dynamics predominantly and sensitively.

Finally, we considered hollow concave transverse field profiles in which the oscillation center exhibit a slow time scale betatron oscillation. In this case, the difference between the first and third order formulae is found to appear as a betatron frequency shift.

These numerical results demonstrate the importance of the higher order nonlocal effect of relativistic ponderomotive force in pursuing long time scale particle dynamics in high power lasers with complex field patterns and also in considering delicate control of laser-matter interaction by designing the field profiles.

Chapter 6

Interaction between super Gaussian laser beams and plasmas

In Chap. 3, we have established a theory for the nonlocal ponderomotive force on the basis of the single particle model which assumes a charged particle in vacuum irradiated by lasers. In Chaps. 4 and 5, we have discussed the particle orbit in a fixed laser field profile and shown that the nonlocal theory of the ponderomotive force is important in understanding the delicate interaction between laser and plasma particles, especially in the case where the ponderomotive force estimated from the conventional formula tends to be diminished, so that a residual higher order force associated with nonlocal profile becomes important such as flat-top super Gaussian laser beams.

Based on these understandings for the single particle dynamics, the next concern worthwhile to be considered is the effect of the higher order ponderomotive force in laser-plasma interaction. In plasmas, the laser field suffers from the reaction from plasma particle dynamics, so that the interaction has to be determined self-consistently. In this chapter, in order to examine the importance of the nonlocal ponderomotive theory in laser-plasma interaction, we study the propagation of super Gaussian laser beams in plasmas based on the particle-in-cell (PIC) simulation.

6.1 Simulation setup

To investigate the interaction between laser beams and plasmas, here we carry out two-dimensional (2D) fully-relativistic electromagnetic PIC simulations.

We assume a laser field whose initial profile is given by $a_x(x) = a_0 \exp(-x^s/w^s)$ with the wavelength $\lambda_L = 0.82\,\mu$m, where a_0 is the amplitude at the beam axis and w the beam radius, which is assumed to be $w = 5\,\mu$m in the simulation. Here, we consider the case of $s = 2$, a Gaussian beam, and also $s = 4$ and 6, super Gaussian beams. We employ periodic and outgoing boundary conditions in x and z directions with the size of $L_x = 40\,\mu$m and $L_z = 80\,\mu$m. The mesh number in x and z directions are $N_x = 512$ and $N_z = 2048$, respectively. The laser whose electric field $\mathbf{E}$ is in the x direction is emitted by the antenna at $z = 0.16\,\mu$m with a Gaussian time profile which reaches the maximum value a_0 at t =40 fsec and then keeps the constant

value. Here, the normalized amplitude is assumed to be a_0 =4.41, 4 and 3.84 for s =2, 4 and 6, respectively, which keep the integrated value of $\mathbf{E}^2$ over x the same for each polynomial s.

6.2 Laser beam propagation in vacuum

First of all, we consider the laser beam propagation in vacuum. In Fig. 6.1, we show the propagation of (a) $s = 2$ Gaussian and (b) $s = 4$, (c) $s = 6$ super Gaussian laser beams. The upper figures in Figs. 6.1 (a)-(c) show the time evolution of the amplitude of laser electric field that are averaged over 5 μm along the moving frame with a constant velocity $v_z = c$ in the z direction, and the lower figures show the amplitude of the laser magnetic field B_z in the x-z plane.

Here, the laser beam propagation in vacuum is determined by the Maxwell equations, and the general solution under the geometrical approximation can be obtained as the superposition of the Hermite-Gaussian modes, which is shown in Appendix E. The $s = 2$ Gaussian profile is one of the solution, and is referred to as the fundamental Hermite-Gaussian mode with $m = n = 0$ in the Hermite polynomial (See Eq. (E.37)). Therefore, as shown in Fig. 6.1 (a), the laser beam with $s = 2$ Gaussian profile can propagate without changing its transverse structure. Namely, although the laser field expands in the scale of the Rayleigh length z_R, which is evaluated as $z_R = 96$ μm in this case, the transverse structure maintains the Gaussian shape at any position in the propagation direction z.

In contrast, $s = 4$ and 6 super Gaussian profiles are not maintained during the propagation as can be seen in Figs. 6.1 (b) and (c). This is due to the fact that these profiles are not the solution for the Maxwell equations in vacuum. Namely, the super Gaussian profile can be constructed by a superposition of the Hermite-Gaussian modes at a given position z at initial time; however, as the laser propagates, the superposition begins to be disintegrated since each Hermite polynomial develops in the transverse x direction differently depending on the position z. Consequently, the initial flat-top profiles in Figs. 6.1 (b) and especially (c) change at first to concave hollow structures and subsequently begin to exhibit a peaking at the beam axis with many points of curvature transition at the peripheral.

We here note that in the numerical calculations for a single particle orbit performed in Chap. 5, we fixed the laser field profile during the interaction. On the contrary, simulation results in Fig. 6.1 indicate that the laser field propagating in vacuum changes its shape in the time scale shorter than the ejection time obtained in Sec. 5.1. Such a propagation property may be different in the presence of plasmas, suffering from the self-consistent interaction such as laser self focusing.

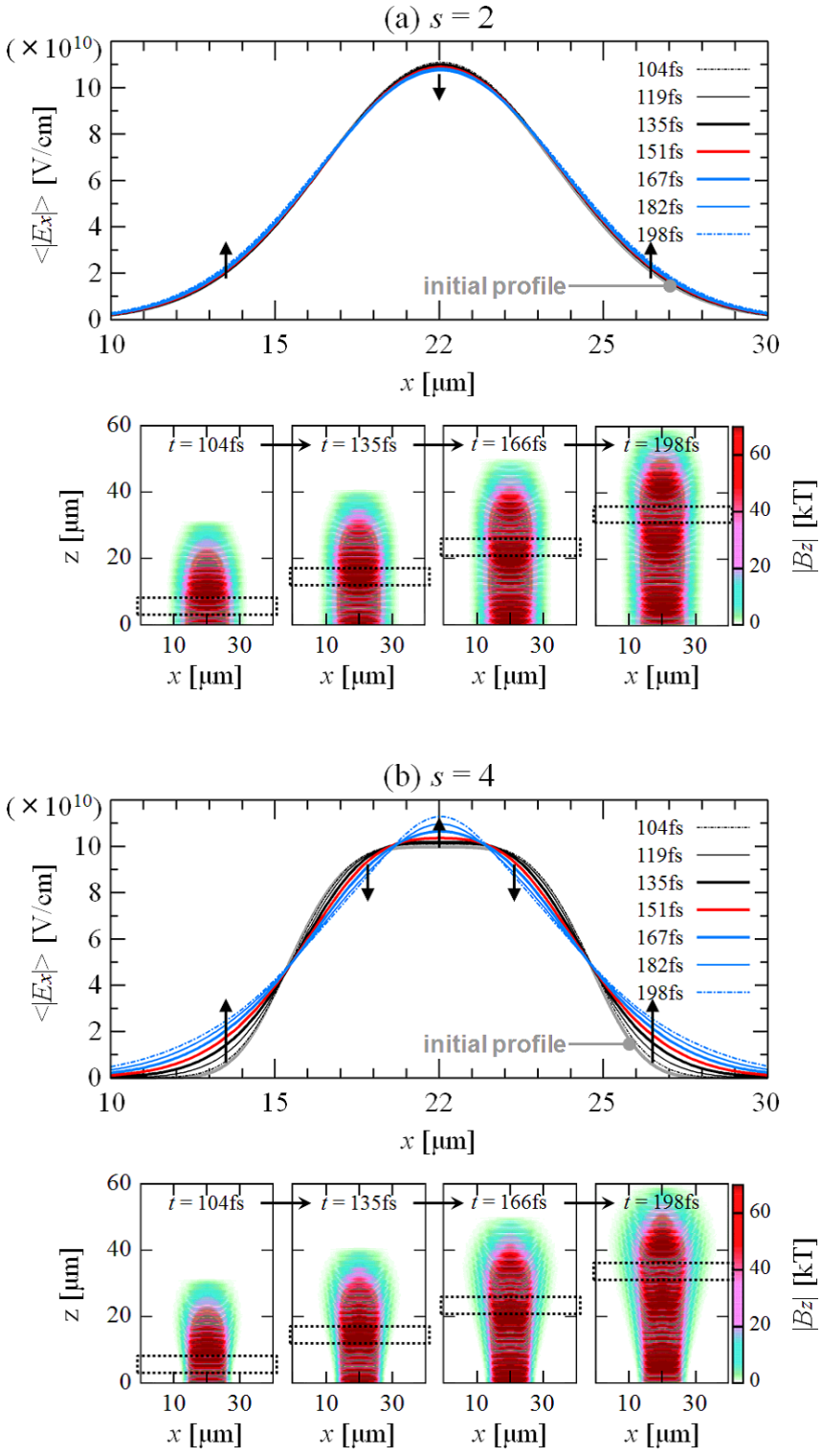
(a) s = 2
(×10^10)
<|Ex|> [V/cm]
104fs
119fs
135fs
151fs
167fs
182fs
198fs
initial profile
x [μm]
t = 104fs
t = 135fs
t = 166fs
t = 198fs
z [μm]
|Bz| [kT]
(b) s = 4
(×10^10)
<|Ex|> [V/cm]
104fs
119fs
135fs
151fs
167fs
182fs
198fs
initial profile
x [μm]
t = 104fs
t = 135fs
t = 166fs
t = 198fs
z [μm]
|Bz| [kT]

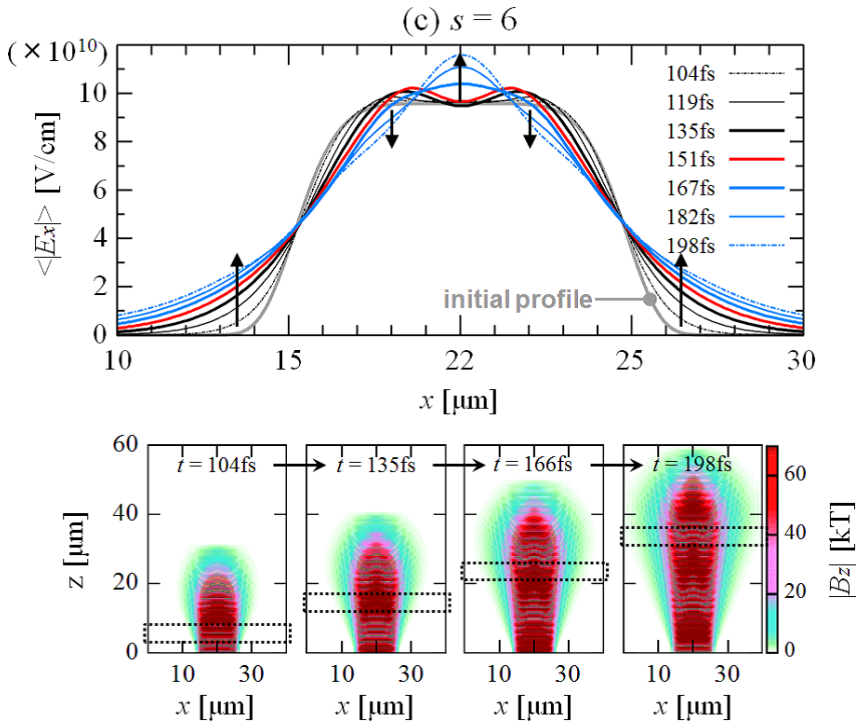

Figure 6.1: Propagation of laser beam with (a) $s = 2$ Gaussian and (b) $s = 4$, (c) $s = 6$ super Gaussian transverse beam profiles in vacuum. The upper and lower figures show the time evolutions of the laser electric field profile in the x direction and of the laser magnetic field amplitude in the x-z plane, respectively.

6.3 Laser beam propagation in plasmas

6.3.1 Equation system describing the laser-plasma interaction

Based on the above discussions, we herein study the effect of the higher order non-local ponderomotive force in the interaction between laser beams and plasmas. In such a situation, the effect of plasmas, such as charge separation and Coulomb force, and the resultant modulation to the laser field, have to be determined self-consistently. An example of the governing equation for such a situation is the non-linear Schrödinger (NS) equation which we derived in Sec. 1.3.2 in the introduction.

The NS equation determines the envelope of laser fields in plasmas assuming a balance relation between the ponderomotive force $\mathbf{F}_p$ and Coulomb force $-\nabla\phi$ in the electron momentum equation, which leads to

$$\omega_p^2 \frac{\delta n_e}{Z n_0} = \frac{1}{m_e} \nabla \cdot \mathbf{F}_p. \tag{6.1}$$

Here, ω_p is the plasma frequency, δn_e the electron density modulation from the background plasma density n_0, and Z the ion charge state. For the ponderomotive force $\mathbf{F}_p$, the first order formula proportional to the local field gradient is generally utilized.

Now, the idea of the nonlocal ponderomotive force proposed in this study can be applied to generalize the NS equation. In this case, three procedures are necessary, i.e., one is deriving the corresponding equations of motion keeping the electrostatic potential in Eqs. (3.144) and (3.145), equivalently in Eqs. (3.33)-(3.35), and the other two are deriving the wave equation and Poisson equation whose coordinates are transformed to those in the present noncanonical Lie perturbation analysis. The inertia term in the equation of motion can be neglected, which leads to a balance relation between ponderomotive force and Coulomb force. Then, the resultant three equations form a generalized NS equation system.

Although derivation of the equation system is a future work, we can readily see that the equation system exhibits higher order spatial derivatives, i.e., the fourth order spatial derivatives, while the second order in the conventional NS equation. Therefore, we can expect that the generalized NS equation system describes the propagation of laser fields with delicate field patterns such that the first order field gradient vanishes.

6.3.2 PIC simulation for laser beam propagation in plasmas

Plasma channel formation by the super Gaussian laser beam

Now, we consider the interaction between a laser beam and underdense plasma. Here, we assume a hydrogen plasma that is fully ionized at initial time. The plasma is distributed in the region $2.5 \leq z \leq 80\,\mu$m with a linear slope in $2.5 \leq z \leq 10\,\mu$m. The electron density in $z > 10\,\mu$m is $n_e = 0.02 n_c$ where n_c is the cutoff density.

In Fig. 6.2 (a), we show the electron density distribution n_e in the x-z plane in the case of $s = 4$, a super Gaussian case, at t =135, 151 and 167 fsec, respectively.

As the laser propagates, the electrons are evacuated from the central region due to the transverse ponderomotive force leading to a channel formation with a density wall at the peripherals of the laser beam. However, it is interesting to note that a density hump localized near the beam axis can be seen. This is due to the fact that the ponderomotive force is significantly reduced near the beam axis ascribed to the flat-top nature of the $s = 4$ super Gaussian beam.

Self-consistent correlation between electron density and field profiles

The electron density profiles near the axis for $s = 4$ are shown in Fig. 6.2 (b1) at three times that are same as those in Fig. 6.2 (a). Note here that the profiles are averaged over 5μm along the moving frame in the z direction shown by the squares in Fig. 6.2 (a). The velocity of the moving frame is taken to be $v_z = c(1 - 1/\gamma) \sim 0.8c$, which corresponds to the drift velocity of the particle irradiated by the uniform laser field of $a_0 = 4$. Therefore, the density profiles at the three times correspond to those of Lagrangian density which consists of almost same particles traveling with the moving frame. The detailed structures of the density and field are shown in Figs. 6.2 (c2) and (d2), respectively, where a limited region in Fig. 6.2 (b2) is enlarged. It is found that the density near the axis exhibits a peaking as time goes on while the laser field amplitude changes the profile from the flat top structure of $s = 4$ to that of a weak concave with a positive curvature.

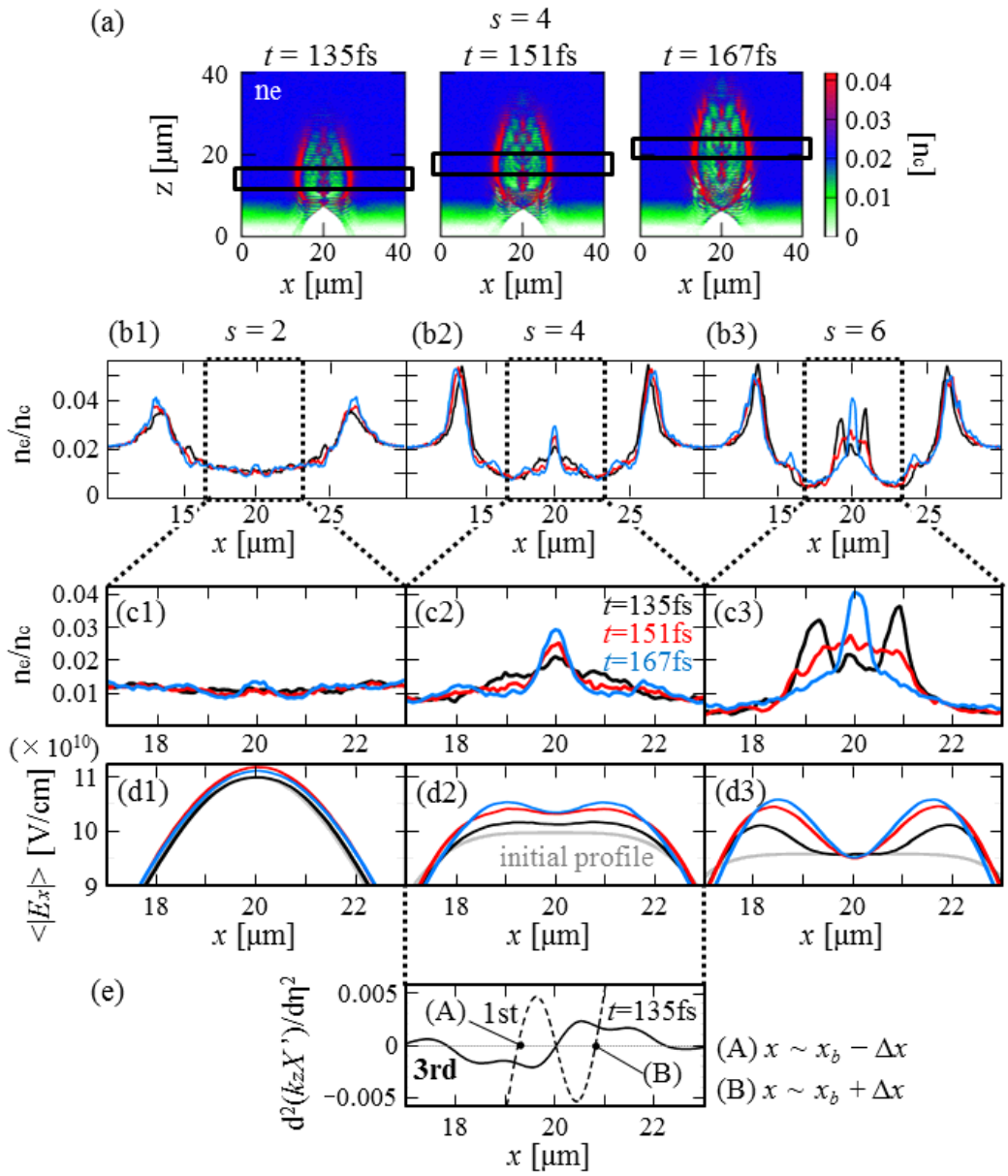

Figure 6.2: PIC simulation for the interaction between a plasma and laser beam with the Gaussian ($s = 2$) and super Gaussian ($s = 4$, 6) transverse beam profiles. (a) Electron density distribution in the x-z plane for $s = 4$. (b1)-(b3) Transverse electron density profiles for $s = 2$, 4 and 6. (c1)-(c3) Electron density and (d1)-(d3) electric field profiles in a limited region in (b1)-(b3). (e) The first and third order ponderomotive forces for the field profile given in (d2).

The structures of density and laser field in the cases of $s = 2$ Gaussian and $s = 6$ super Gaussian beams are shown in Figs. 6.2 (b1), (c1), (d1) and Figs. 6.2 (b3), (c3), (d3), respectively. It is found that the density hump becomes wider for $s = 6$ than that for $s = 4$ while almost disappears for $s = 2$, suggesting that the flatter the field profile is, the broader the hump becomes. Correspondingly, the field profile suffers from a significant change leading to a prominent follow structure for $s = 6$, whereas from little change essentially keeping the Gaussian profile for $s = 2$.

Here, we note that the time evolution of field amplitude profile is different from that in the case of vacuum for both $s = 4$ and 6. For $s = 6$ for instance, the field profile in vacuum once exhibits a hollow concave structure at the beam center and then shifts to a convex peak structure after $t = 167$ fs as is seen from Fig. 6.1. On the other hand, in the case with plasma shown in Fig. 6.2, the field profile at the beam center keeps a concave structure which is considered to be an effect from the electrons remaining at the beam center.

Such a delicate response of the laser field profile suggests that the flat-top structure has an unstable characteristic, and thus, the propagation dynamics and structure formation are determined by the delicate balance between ponderomotive force and Coulomb force, where the higher order nonlocal ponderomotive force is expected to play a crutial role.

Effect of the third order ponderomotive force in the modulated laser beam profiles in plasma

The first and third order ponderomotive forces, $d^2(k_x X')/d\eta^2$, obtained from Eq. (3.147) are shown in Fig. 6.2 (e) for the field profile given in Fig. 6.2 (d2) at t =135 fsec for $s = 4$. Besides the beam axis, two points (A) and (B) at which the field gradient and then the first order ponderomotive force vanish, i.e., $x \sim x_b \pm \Delta x$ where $x_b = 20\,\mu$m the beam axis and $\Delta x \sim 0.8\,\mu$m in this case, are found to appear. Namely, the higher order ponderomotive force plays an important role in regulating the interaction around $x_b - 1.5\Delta x < x < x_b + 1.5\Delta x$. Interestingly, the width $1.5\Delta x$ roughly corresponds to that of the density hump observed in Fig. 6.2 (c2). This relation is found to be fulfilled also in the case of $s = 6$ where $\Delta x \sim 1.6\,\mu$m is estimated from Figs. 6.2 (c3) and (d3).

These structure and dynamics are considered to result from plural physical processes such as the higher order ponderomotive force near the axis described by Eq. (3.147), the resultant density modulation, generation of the Coulomb field, and change of linear and nonlinear susceptibilities.

6.4 Conclusions

In this chapter, we carried out two-dimensional PIC simulations for the propagation of the fourth and sixth order super Gaussian laser beams in a plasma in order to examine the nonlocal ponderomotive theory presented in the previous chapters.

During the self-consistent interaction between laser field and plasma, the field amplitude is found to change its profile from the original flat top structure to that of a weak concave with a positive curvature. Such a structure modulation becomes more prominent in the case of flatter super Gaussian beam. At the peripheral of the

beam axis in the spontaneously-established field profile, we found a region in which the higher order ponderomotive force becomes dominant.

These structure and dynamics could be represented by a generalized NS equation system including the higher order nonlocal effect of the ponderomotive force, which will be studied in future work.

Part II

Numerical study on the interaction between high power laser and cluster medium

Chapter 7

Introduction

7.1 Laser-cluster interaction

The interaction between high power laser and matter has opened up various kinds of application such as high energy particle acceleration for both ions and electrons, generation of intense radiations (EUV, x-ray and gamma-ray), and neutron production [6]. Here, the state of material is a key ingredient which determines the characteristics of the interaction, and has to be chosen properly according to the purpose.

Among various mediums, cluster and cluster medium are widely interested. Clusters are few-body systems which show both underdense and overdense properties. Namely, a medium composed of multi clusters, which we refer to as cluster medium, has a solid density locally, whereas in average, it can have an intermediate density between solid and gas. Such a high degree of freedom of cluster medium is attributed to having many parameters that determine the internal structure of the medium, e.g., cluster size, packing fraction and spatial configuration of clusters. Clusters exhibits several prominent features that are essentially due to or existence of the surface of cluster and the large ratio of surface to volume. A cluster mode (slow mode) is one of the examples where the laser can propagate even when the average density of the clustered medium is higher than the critical density [29]. This propagation mode results from the surface polarization of the cluster. Neutron generation by nuclear fusion utilizing the Coulomb explosion of clusters has been intensively studied [9]. Recently, high energy ion acceleration has been realized in the interaction between such a cluster medium and high intensity laser [31]. These phenomena have so far been investigated using laser intensities up to around $10^{21}\mathrm{W/cm}^2$.

In the study in Part II, we investigate such interactions between laser and cluster medium extending the intensity higher than $10^{21}\mathrm{W/cm}^2$ up to $10^{24}\mathrm{W/cm}^2$ on the basis of numerical simulation using a fully-relativistic electromagnetic particle-in-cell (PIC) code (EPIC3D) [33, 34]. At these intensities, ions enter into the relativistic regime, so that ion acceleration by the cluster Coulomb explosion is incorporated with dynamics of ions that are relativistically accelerated by the laser piston mechanism. Such a new interaction dynamics will lead to high energy ion accelerations depending on the cluster size, packing flaction, species (Z), etc.

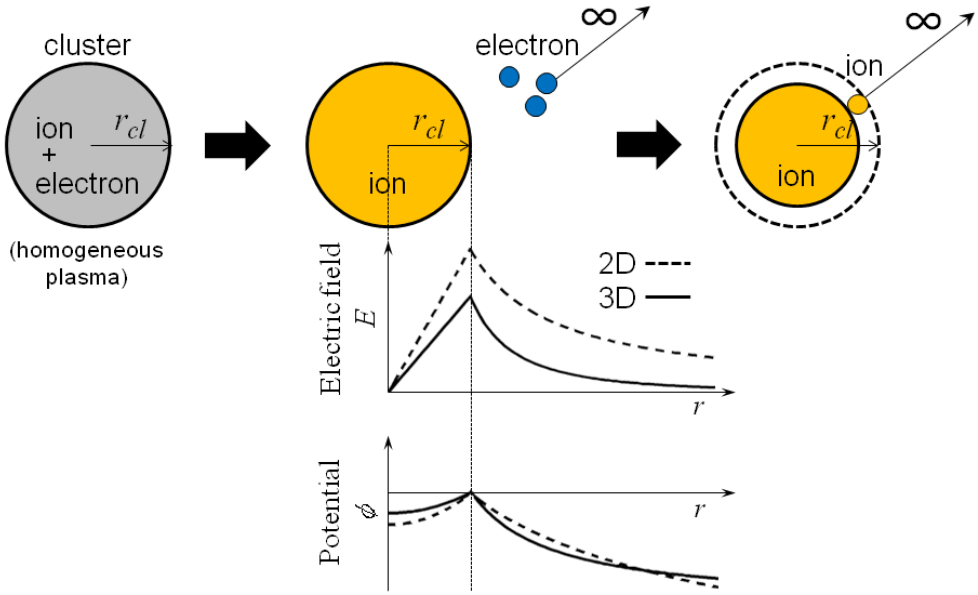

Figure 7.1: A model of cluster Coulomb explosion.

7.2 Cluster Coulomb explosion

When a cluster is irradiated by a laser light, the cluster gains energy from the laser and expands forming a cloud at the peripheral of the cluster core. The expansion of cluster is considered to be by a combination of hydrodynamic expansion and Coulomb explosion. In the laser-cluster interaction in high intensity regime in which the energy of electrons in the laser electric field is large enough in comparison to the Coulomb potential built up, the Coulomb explosion dominates the expansion dynamics.

Here, we introduce fundamental properties of the Coulomb explosion on the basis of a simple model discussed in Ref. [42]. We note that a self-similar solution for a cluster expansion is presented by Murakami and Basko which describes nonrelativistic expansion of a finite plasma mass into vacuum with a full account of charge separation effects [43]. In their paper, an analytical solution is obtained that represents both the hydrodynamic expansion of a quasineutral plasma and the Coulomb explosion of a bare ion sphere.

Besides such a detailed analytical solution, we here evaluate the energy of Coulomb explosion of a single cluster based on a simple model illustrated in Fig. 7.1. When the laser intensity is sufficiently high to satisfy that the skindepth c/ω_p is much larger than the cluster radius, the cluster irradiated by the laser is ionized as a whole, and electrons in the cluster are repelled from it. A single cluster exhibits its maximum Coulomb potential energy when all the electrons are expelled from the cluster to infinity while ions remain in the cluster. Such a situation can occur when the kinetic energy of electrons expelled by the laser field far exceeds the electrostatic potential caused by the charge separation. After that, the remained ions suffers from the Coulomb repulsion force that results in the Coulomb explosion.

Here, we assume that the cluster of radius r_{cl} is fully ionized and becomes a pure

ion plasma where ions are distributed uniformly with the density n_i and charge state Z. The kinetic energy of ions resulting from the Coulomb explosion corresponds to the Coulomb potential energy at their initial positions. The electric field caused by the fully ionized ions is given by

$$E(r) = \frac{4\pi}{3} eZn_i r \quad (0 \le r \le r_{cl}), \tag{7.1}$$

$$E(r) = \frac{4\pi}{3} eZn_i \frac{r_{cl}^3}{r^2} \quad (r > r_{cl}), \tag{7.2}$$

where r is the position from the center of the cluster and e is the elementary charge. The corresponding electrostatic potential is

$$\phi(r) = -\frac{2\pi}{3} eZn_i (r - r_{cl})^2 \quad (0 \le r \le r_{cl}), \tag{7.3}$$

$$\phi(r) = \frac{4\pi}{3} eZn_i r_{cl}^2 \left(\frac{r_{cl}}{r} - 1\right) \quad (r > r_{cl}), \tag{7.4}$$

where we assume $\phi(r_{cl}) = 0$. The ion initially located at $r = r_0 \le r_{cl}$ with kinetic energy $\epsilon_{\rm i}(r_0) = 0$ gains kinetic energy of $\epsilon_{\rm i}(\infty)$ that can be given by the energy conservation with the Coulomb potential as

$$\begin{aligned} \epsilon_{\rm i}(\infty) &= eZ(\phi(r_0) - \phi(\infty)) \\ &= \frac{2\pi}{3} e^2 Z^2 n_i \left(2r_{cl}^2 - (r_0 - r_{cl})^2\right), \end{aligned} \tag{7.5}$$

at $r = \infty$. Therefore, the maximum ion energy $\epsilon_{\rm imax}$ achieved by the Coulomb explosion is obtained by taking $r = r_{cl}$ as

$$\epsilon_{\rm imax} = \frac{4\pi}{3} e^2 Z^2 n_i r_{cl}^2. \tag{7.6}$$

On the other hand, in the 2D case, in which the present PIC simulation is performed, the electric field caused by the fully ionized ions is given by

$$E_{2D}(r) = 2\pi eZn_i r \quad (0 \le r \le r_{cl}), \tag{7.7}$$

$$E_{2D}(r) = 2\pi eZn_i \frac{r_{cl}^2}{r} \quad (r > r_{cl}). \tag{7.8}$$

The corresponding electrostatic potential is

$$\phi_{2D}(r) = -\pi eZn_i (r - r_{cl})^2 \quad (0 \le r \le r_{cl}), \tag{7.9}$$

$$\phi_{2D}(r) = -2\pi eZn_i r_{cl}^2 \ln\left(\frac{r}{r_{cl}}\right) \quad (r > r_{cl}). \tag{7.10}$$

Here, we notice that the potential energy in the 2D geometry exhibit a logarithmic divergence as $r \to \infty$. This is due to the rod structure of clusters that extend in the perpendicular z direction infinitely. Therefore, in evaluating the ion energy resulting from the Coulomb explosion, it should be noted that the 2D simulation model overestimates them compared with that of 3D.

Chapter 8

PIC simulation for laser-matter interaction in cluster medium

8.1 Simulation setup

In the previous chapter, we introduced the background of the study on laser-cluster interaction. Here, we investigate the interaction between high power laser and cluster medium in the intensity regime of 10^{21-24}W/cm^2 based on the two-dimensional PIC simulation.

In the numerical calculation, we employ the periodic and outgoing boundary conditions in x and y directions with the size of $L_x = 128$ and $L_y = 2048$ in normalized unit, which correspond to $l_x = 1.28$ μm and $l_y = 20.48$ μm, respectively. The mesh number in x and y directions are $N_x = 128$ and $N_y = 2048$. A laser pulse with the wavelength $\lambda_L = 820$ nm excited by the antenna located at $y = 0.02$ μm propagates in the y direction with linear p-polarization in the x direction. The laser field is uniform in the transverse direction while the Gaussian profile in time with the dulation $\tau = 40$ fs (FWHM) is assumed. Here, we consider five cases of laser amplitude, i.e., a_0 =50, 200, 400, 600 and 800, where laser intensity ranges from $I = 5.1 \times 10^{21}$W/cm^2 ($a_0 = 50$) to 1.3×10^{24}W/cm^2 ($a_0 = 800$). The corresponding transverse excursion lengths of electron and carbon ion with the charge state $Z = 6$, ξ_e and ξ_i, are found to range from $\xi_e = 6.5$ μm and $\xi_i = 0.3$ nm for $a_0 = 50$ to $\xi_e = 104$ μm and $\xi_i = 4.7$ nm for $a_0 = 800$.

In this study, we introduce three cluster targets consisting of the same mass, i.e. same packing fraction, but having different cluster radius as shown in Figs. 8.1 (A), (B) and (C). We also consider a solid thin film as shown in Fig. 8.1 (D) for comparison. Here, we model the cluster by a fully ionized uniform density plasma column occupying an area of radius r_{cl} =80, 160 and 320 nm for cases (A), (B) and (C), respectively, in the x-y plane. The species of the cluster is assumed to be a solid carbon ($Z = 6$) whose density is that of the diamond, i.e., $n_{cl}^{(i)} = 1.76 \times 10^{23}$ cm^{-3}. The electron density of the cluster satisfies $n_{cl}^{(e)} = Z n_{cl}^{(i)}$ and $n_{cl}^{(e)}/n_c = 637.4$, where n_c is the cutoff density defined by $n_c \equiv m_e \omega_L^2/(4\pi e^2)$. The skin depth of the cluster for fully ionized state is $\delta_e = 5.17$ nm. Such clusters are regularly distributed in the region $2.56 \leq y \leq 6.40$ μm. The packing fraction defined by $f = N_{cl}\pi r_{cl}^2/S$ is given by $f = 0.21$ for all the cases (A)-(C), where $S = 3.20 \times 3.84$ μm^2 is the area occupied and N_{cl} is the number of clusters in the area S. Then, the average density of electron

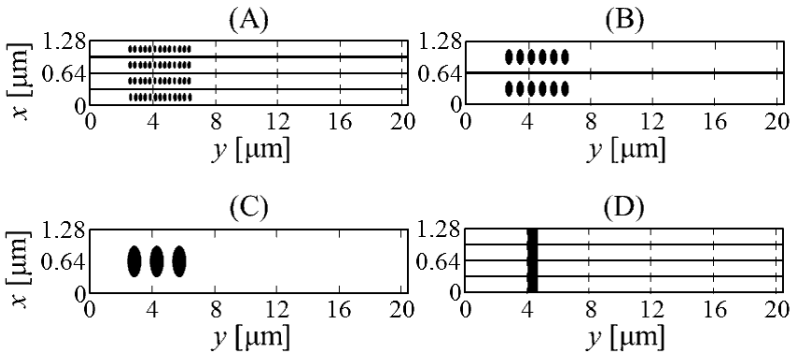

Figure 8.1: Initial plasma distributions in the simulation for cases (A) uniform low density plasma, (B) multi cluster medium with cluster radius $r_{cl} = 80$nm, (C) $r_{cl} = 160$nm, and (D) $r_{cl} = 320$nm, and (E) solid thin foil.

$n_{av}^{(e)}$ in the area S is given by $n_{av}^{(e)}/n_c = 130.4$ ($n_{av}^{(e)} = 2.16 \times 10^{23}$ cm^{-3}). Hence, the cluster medium is overdense in average if the relativistic effect is not taken into account. In case (D), i.e., the case of thin film, we also assume the same solid carbon plasma with $Z = 6$ that is uniformlly distributed in the region $4.09 \leq y \leq 4.87$ μm. Here, we set the film thickness $l_{film} = 785$ nm so that the total mass included in the medium is same as that in the cluster medium. The relative relation among the electron and ion excursion lengths, incident laser wavelength, film thickness, cluster radius, and skin depth is given by $\xi_e > \lambda_L > l_{film} > r_{cl} \gg \delta_e \sim \xi_i$ in all the situations considered in this study.

We here remind that, in Sec. 7.2, we have mentioned the difference of the cluster potential energy and the corresponding maximum ion energy achieved by the Coulomb explosion between 2D and 3D geomerties. Namely, we have seen that the 2D simulation model might overestimates the ion energy compared with that of 3D due to a logarithmic divergence of the potential energy in the 2D geometry. However, we note that the simplified 2D model simulation performed in this study is physically valuable because we here employ the p-polarized laser field, by which the interaction dynamics becomes essentially 2D.

8.2 Laser-matter interactions in multi cluster medium and solid thin film

First, we investigate the interactions for the cluster medium (B) and thin film (D) in the cases of two laser intensities, $a_0 = 200$ and 800. The time histories of electron and ion energies, field energy and total energy in the system, and also spatial profiles of electromagnetic field E_x and ion charge density normalized by en_c at $t = 80$ fsec are shown for the cluster medium (B) in the case of $a_0 = 200$ (Figs. 8.2 (B1) and (B2)) and of $a_0 = 800$ (Figs. 8.2 (B3) and (B4)), respectively. The corresponding figures for the thin film (D) are shown in Figs. 8.2 (D1) and (D2) for $a_0 = 200$ and in Figs. 8.2 (D3) and (D4) for $a_0 = 800$, respectively. The initial density distribution is also shown by the dotted line in Figs. 8.2 (B2) and (B4) where six clusters along the y-axis can be seen and in Figs. 8.2 (D2) and (D4) for the thin film. For comparison,

the time history of field energy in vacuum and the corresponding spatial profile of E_x at $t = 80$ fsec are shown for $a_0 = 200$ in Figs. 8.2 (I) and (II), where laser front emitted from antenna reaches to the right-hand side boundary and escape from the system at $t \sim 100$ fsec.

At first, we study cases of the thin film (D) and cluster medium (B) for $a_0 = 200$. In the case of thin film (D), after the laser hits the target, the electron energy increases initially and ion energy does subsequently as seen in Fig. 8.2 (D1). Then, the electron energy saturates and decreases while the ion energy keeps increasing gradually, suggesting that ions are accelerated by the target normal sheath acceleration (TNSA) at the rear surface. This feature can be seen in the ion density distribution in Fig. 8.2 (D2) at $t = 80$ fsec where the large amount of ions are pushed in the forward direction. As found from the decrease of the total energy at $t \sim 45$ fsec from the maximum value, approximately half of the incident laser energy is found to be reflected while partially transmitted due to the relativistic effect as seen in Fig. 8.2 (D2). Namely, the target becomes relativistically transparent with the quiver energy of $\gamma \sim \sqrt{1 + a_0^2/2} \sim 140$ by which the cutoff density increases from n_c to γn_c.

On the other hand, in the case of cluster medium (B), the dynamics is qualitatively similar whereas energy partition is found to be significantly different. Firstly, the energy absorption by electron and then the conversion to ion energy reach almost double, which is found from the fact that the decrease of the total energy from the maximum value at $t \sim 45$ fsec is small compared with that observed in Fig. 8.2 (D1). As seen in Fig. 8.2 (B2), the initial discrete cluster distributions are disintegrated except that of the most rear side. Here, more ions are found to be pushed not only in forward direction but also backward direction. This is due to the fact that the cluster Coulomb explosion takes place in both directions, while forward direction is stronger due to the radiation pressure force.

Next, we consider the same cases (D) and (B) but for $a_0 = 800$. The case of the thin film is shown in Fig. 8.2 (D3) and (D4). In this case, after the laser hits the target, electron and ion energies increase simultaneously as seen in Fig. 8.2 (D3). Interestingly, even after the electron energy saturates, ion energy keeps increasing to a certain level, which is balanced with the decrease of the laser field energy. Namely, it is found that the laser field energy is directly transferred to that of ions. As found in Fig. 8.2 (D4), this corresponds to the situation that the laser pulse pushes the whole thin film consisting of a bunch of ions, which is referred to as laser piston by radiation pressure. The Doppler shifted long wavelength reflected laser light can also be seen.

In the case of the cluster medium (B), the dynamics is qualitatively similar to those in Figs. 8.2 (D3) and (D4). Namely, initial cluster distribution is disintegrated and pushed forward by the radiation pressure. The ion energy in Fig. 8.2 (B3) is slightly smaller than that in case (D3) whereas the ion bunch is preceded compared with that observed in Fig. 8.2 (D4) at $t = 80$ fsec.

The ion energy distribution function at $t = 200$ fsec is shown in (D) in Fig. 8.3 (II). A quasi-monoenergetic component exhibiting a energy hump around $\epsilon_i = 8$ GeV can be seen. The maximum ion energy, which is approximately 15 GeV, is also indicated in (D) in Fig. 8.3 (I) together with other laser amplitudes including the

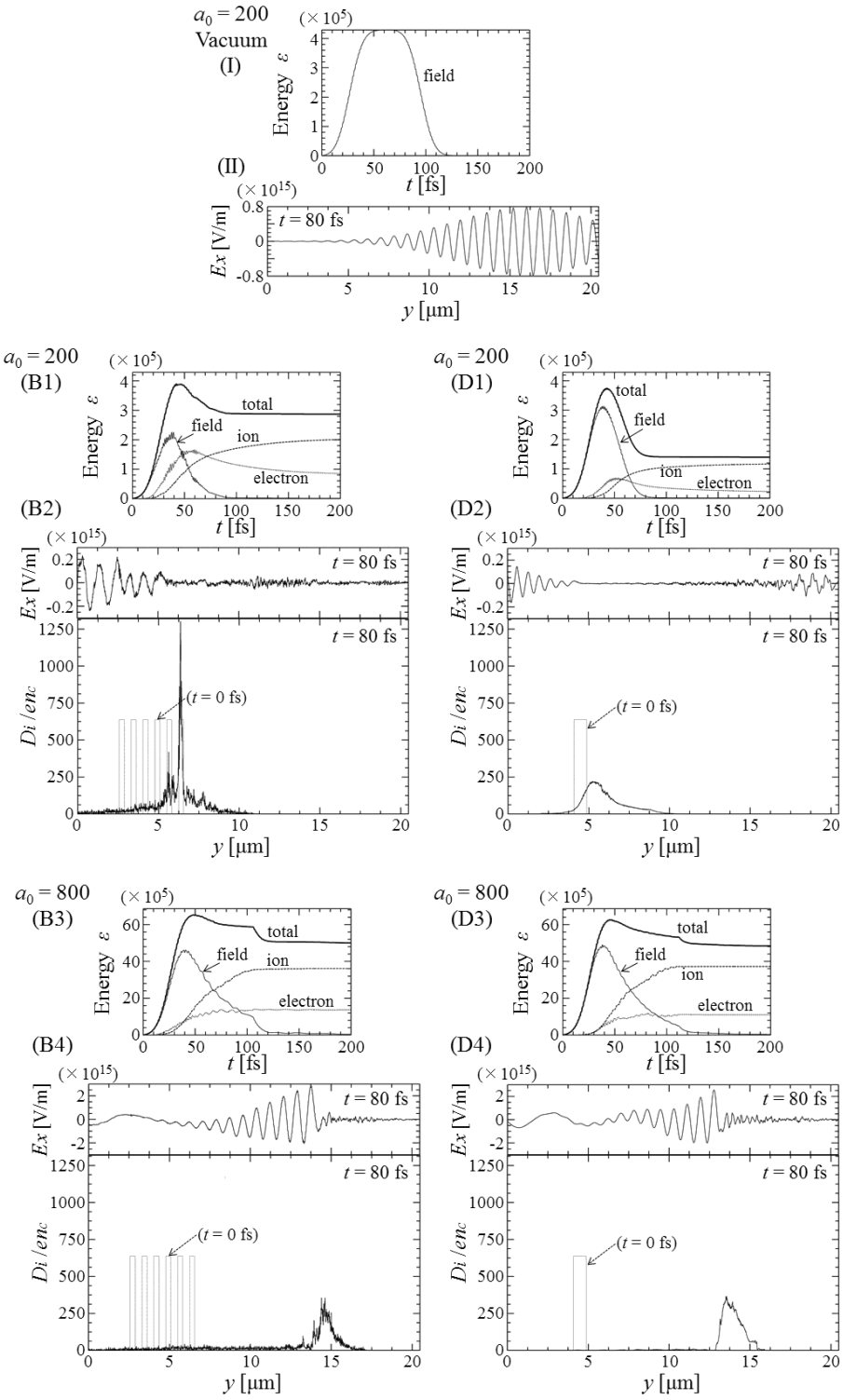

Figure 8.2: Time evolution of energies of electons, ions and field, and the total energy in the system for (B) $a_0 = 200$ and (C) $a_0 = 800$. For comparison, the energy evolution in the case of vacuum propagation for the same pulse used in (B) is shown in (I) and (II).

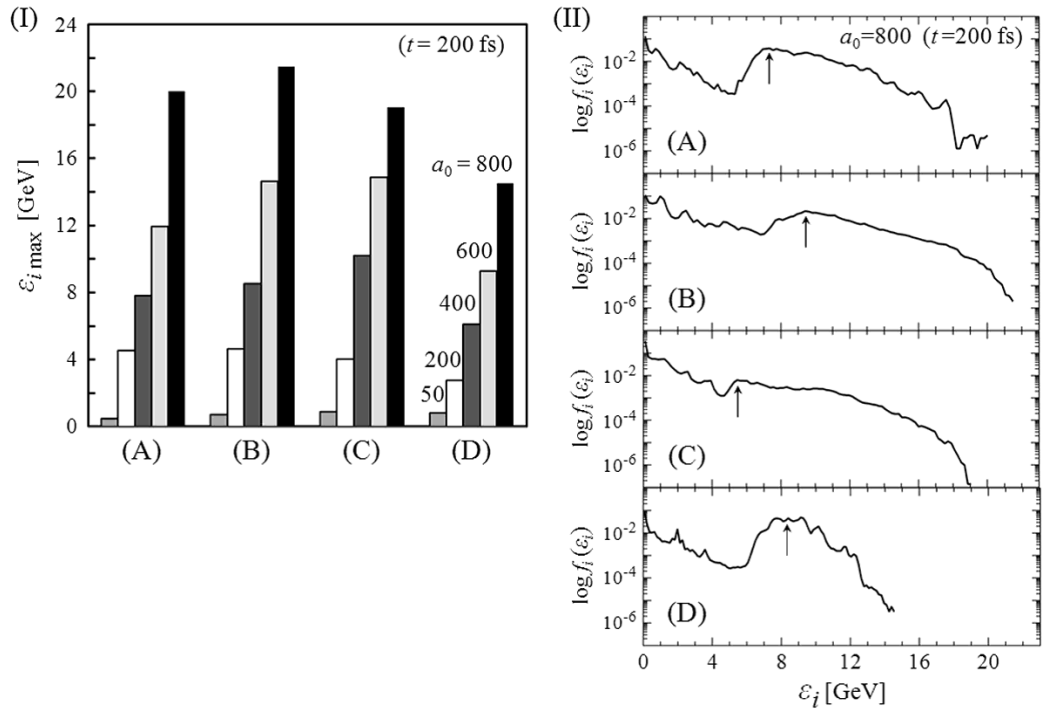

Figure 8.3: (I) Maximum ion energy for various media at $t = 200$ fs ($a_0 = 200, 800$). (II) Energy distribution of ions in each medium for $a_0 = 800$ at $t = 200$ fs.

case of $a_0 = 200$ which is around 3 GeV.

It is interesting to note in Fig. 8.3 (II) that in case (B), the maximum ion energy reaches to approximately 22 GeV which is significantly larger than that in case (D), while the quasi-monoenergetic component located around 10 GeV is slightly larger than case (D). This feature is also shown in (B) in Fig. 8.3 (I). This is found to result from the acceleration due to the Coulomb explosion of clusters which is added to that of the laser piston.

8.3 Dependence of ion energy on the internal structure of targets

Here, we summarize the ion energy distribution for $a_0 = 800$ and the maximum ion energy achieved in the interaction for different laser intensities including the case of (A) $r_{cl} = 80$ and (C) 320 nm in Fig. 8.1 in addition to those of $r_{cl} = 160$ nm and thin film. Note that the energy of the ion bunch due to the laser piston is estimated as (A) 7 GeV, (B) 9.5 GeV, (C) 6 GeV and (D) 8 GeV per ion which are, for nucleon, (A) 580 MeV/u, (B) 790 MeV/u, (C) 500 MeV/u and (D) 670 MeV/u, respectively. It is found that the maximum ion energy achieved in the cluster media (A), (B) and (C) leads to higher values than that in the solid thin film (D) for for $a_0 \geq 200$.

This tendency can be explained by the Coulomb explosion of clusters contained in the medium. Here, we estimate the effect from the Coulomb explosion on the basis of the simple model for a single cluster explosion shown in Fig. 7.1. In Sec. 7.1, we obtained the maximum ion energy achieved by the single cluster Coulomb explosion

as $\epsilon_{i\ \max} = 4\pi Z^2 e^2 n_i r_{cl}^2$ (Eq. (7.6)). Therefore, the values of $\epsilon_{i\ \max}$ for clusters with radius (A) 80 nm, (B) 160 nm and (C) 320 nm are obtained as 0.24 GeV, 0.98 GeV and 3.92 GeV per ion, respectively, in the 3D model. In Fig.8.3 (I), the increases of $\epsilon_{i\ \max}$ in the cluster mediums compared with the thin film are 5.0-8.0 GeV in the case of $a_0 = 800$, which are in the same order as the estimated maximum energy $\epsilon_{i\ \max}$ shown in the above. Thus, the large maximum ion energy achieved in the cluster media can be regarded as a result of the Coulomb explosion inside of the media. In other words, the higher internal free energy of the cluster media is used to accelerate the ions to higher energy.

Here, the above comparison of maximum ion energy between theory and simulation is based on the 3D model, whereas our simulation is carried out using the 2D calculation code. As is discussed in Sec. 7.1, in the 2D geometry, the potential energy exhibits a logarithmic divergence as $r \to \infty$ as shown in Eq. (7.10). Thus, it is expected that the ion maximum energy increases as the the system length in the rear side of the target is extended. For this reason, the value of the ion maximum energy $\epsilon_{i\ \max}$ obtained in the present 2D simulation cannot be simply compared with experiments. However, the increase of $\epsilon_{i\ \max}$ due to the clusters and its difference depending on the cluster radius, which are obtained using a fixed simulation system length, are considered to be valuable.

It is also interesting to note that the relation between the maximum ion energy and cluster radius is different depending on a_0. Namely, in the case of $a_0 = 200$, medium with smaller cluster radius, e.g. (A) and (B), exhibit larger $\epsilon_{i\ \max}$ than case (C). In contrast, in the case of a_0 =400 and 600, larger $\epsilon_{i\ \max}$ is achieved in the medium with larger cluster radius. Finally, in the case of $a_0 = 800$, the case (B) shows the largest $\epsilon_{i\ \max}$ compared with the other cases. The details will be studied in future work.

8.4 Conclusions

In this chapter, based on the two-dimensional PIC simulation, we studied the interaction between laser field in the regime of a_0 = 50-800 and targets consisting of same mass but having different internal structure, i.e., cluster media with different cluster radii and solid thin film.

Comparison of ion energies achieved in the interactions with different targets shows the effects of the Coulomb explosion of the clusters constituting the medium. The results indicate that the internal structure, which corresponds to the free energy of the target medium, is important in determining the interaction dynamics and the resulting ion accerelation.

In this study, we have not included the radiation damping effect, which will be important in discussing intense radiation emissions from cluster medium. The ion maximum energy shown here is obtained in an ideal one-dimensional situation where transverse expansions of laser field and target are not taken into account. These issues are devoted to future work.

Finally, it is interesting to note that in the interaction between laser fields and cluster mediums, even when the incident laser field is uniform in the transverse direction as is assumed in this chapter, such an uniform field profile is deformed

by the interaction with the nonuniform surface of the cluster medium, which will generate a fine scale pattern on the field amplitude. This corresponds to a generation of the ponderomotive force, where the higher order nonlocal effect derived in Part I of the present thesis is expected to be crucial. Namely, the laser propagation and channeling in the cluster medium will be determined by the balance relation among the ponderomotive force including the higher order nonlocal effects, Coulomb force due to the charge separation, and also pressure of the hot electrons from clusters. In addition, the polarization of the cluster surface inside of the medium will lead to an unique propagation dynamics different from the case of uniform plasma studied in Part I of this thesis [29].

To consider the role of ponderomotive force in the high intensity laser-cluster interaction, an problem is such that the ponderomotive theory becomes ambiguous as the expansion parameter ϵ tends to unity in the ultra high intensity regime where the particle excursion length is no longer small compared with the scale length of field amplitude variation. However, in the parameter regime in which the scale separation is well-satisfied, e.g. see Fig. 1.5, the interaction between laser and cluster medium can be an important example for the application of the nonlocal ponderomotive theory which we established in Part I.

Conclusion and appendix

Chapter 9

Concluding remarks

9.1 Summary

With the advent of laser technologies and innovative ideas for applications of high power short pulse lasers, requirements for precise control of laser-matter interaction is increasing in recent years. In this thesis, to achieve the fine scale control of laser-matter interaction and to understand the underlying physics, two parts of studies are presented.

In part I, we established a theory of the relativistic ponderomotive force that includes higher order nonlocal effect. Here, based on the noncanonical Lie perturbation method, we derived a new formula for the relativistic ponderomotive force that depends not only on the local field gradient but also on the curvature and its variation. Such higher-order derivative terms originate from nonlocal particle motion not simply expressed by the local field gradient as Fick's law. The formula is then accessible to the regime in which laser fields exhibit characteristic transverse structures such that higher derivatives of the field amplitude regulate the interaction. The higher-order terms are found to be subject to the symmetry of the field structure and also to a constraint that the ponderomotive force is a pressure force free from the sign of the particle charge. These terms are of importance in pursuing long time scale particle dynamics in high power lasers with complex field patterns that are spontaneously established within the medium during interaction and/or artificially designed for specific applications.

As an example, we have applied the formula to study particle motion in a flat-top super Gaussian laser beam. In this profile, since the local field gradient is diminished near the beam center, the higher derivatives dominate the dynamics. Comparison with the direct integration of the particle orbit demonstrates the validity of the derived formula with sufficient convergence of the expansion series up to $\mathscr{O}\left(\epsilon^3\right)$. This suggests that information along the excursion of the particle over a wider range than that only estimated by the local field gradient has to be taken into account. The result could be checked by measuring the amount of X-ray which may reflects the number of interacting particles [44]. As another example, we have also considered particle confinement in a hollow concave laser profile. In this case, the difference between the first- and third-order formulae is observed as a betatron frequency shift.

To demonstrate the advantage of the noncanonical phase space Lagrangian ap-

proach performed here, we have applied the averaging method directly to the particle equation of motion in deriving the higher-order terms. We found that the higher-order terms exhibit the same parametric dependence as Eq. (3.147) but the coefficients are different. As a result, the oscillation center trajectory derived by the averaging method does not agree with the direct integration of the particle orbit. This discrepancy is considered to be a direct consequence of the lack of Hamiltonian structure in the averaging method whereas it is kept rigorously in the present approach.

In the present study, we only consider the vacuum case, whereas various additional fields and their corresponding forces, e.g., self-induced electromagnetic fields and longitudinal and/or transverse plasma waves, are incorporated in plasmas. Such fields can be phenomenologically included in the present theoretical framework [38]. However, in plasmas, the laser field is suffered from the reaction from plasma particle dynamics, so that the interaction has to be determined self-consistently. We consider applying the idea of the nonlocal ponderomotive force to obtain the governing equation system that describes such a self-consistent interaction. To achieve it, it is necessary to derive the equations of motion keeping the electrostatic potential and also to derive the Maxwell equations whose coordinates are transformed to those in the noncanonical Lie perturbation analysis. Though derivation of the equation system is a future work, we can readily see that the equation system exhibits higher order spatial derivatives, i.e., the fourth order spatial derivatives, while the second order in the conventional NS equation. Therefore, we can expect that the generalized equation system describes the propagation of laser fields with delicate field patterns such that the first order field gradient vanishes. In the case of the super Gaussian shape discussed here, the related problem is whether such a shape can be sustained in plasma channels, in which the long time scale interaction between the self-focused laser beam and particles dominated by the ponderomotive force plays a key role [35]. The formula derived here thus provides a theoretical basis for exploring such a delicate nonlinear laser-plasma interaction.

In order to examine the nonlocal ponderomotive theory, we carried out two-dimensional (2D) particle-in-cell (PIC) simulations for the propagation of the fourth and sixth order super Gaussian laser beams in a plasma. It is found that the electron density exhibits a peaking near the axis as time goes on, while at the same time, the field amplitude changes the profile from the original flat top structure to that of a weak concave with a positive curvature. Such a structure modulation becomes more prominent in the case of flatter super Gaussian beam. Besides the beam axis, two points at which the field gradient and then the first order ponderomotive force vanish are found to appear. Namely, the higher order ponderomotive force plays an important role in regulating the interaction around these points. These structure and dynamics are considered to result from plural physical processes such as the higher order ponderomotive force near the axis described by Eq. (3.147), the resultant density modulation, generation of the Coulomb field, and change of linear and nonlinear susceptibilities.

In considering a fine scale control of high power laser-matter interaction, the state and structure of the target material are key ingredients to be chosen properly according to the purpose. In Part II of the thesis, we studied the effect from internal structure of target mediums on the laser-matter interaction based on the

PIC simulation. Here, we investigated the interaction between high power laser and targets consisting of same mass but having different internal structures, i.e., cluster mediums with different cluster radii and solid thin film, in the intensity regime of $10^{21-24}\mathrm{W/cm}^2$ ($a_0 = 50-800$) . Comparison of interaction dynamics and ion energy distribution among different targets show the effects of the cluster Coulomb explosion inside of the medium. The results indicate that the internal structure, which corresponds to the free energy of the target medium, is important in determining the interaction dynamics and the resulting ion acceleration.

We also discussed that, even when the incident laser field is uniform, a fine scale pattern will be generated on the field amplitude by the interaction with the nonuniform surface of the cluster medium. This corresponds to a generation of the ponderomotive force, where the higher order nonlocal effect derived in Part I is expected to be crucial.

In summary, through the study in Part I and II, we have explored a theory which can be a basis in considering fine scale control of high power laser-matter interaction. As the key ingredients determining the interaction, we focused on the incident laser beam profile and the corresponding ponderomotive force in Part I and the internal structure of target mediums in Part II, respectively. These studies are expected to contribute to the development of mathematical and numerical methodologies for the analyses of nonlinear laser-plasma interactions. The results obtained in this thesis can give basic understandings for delicate control of laser-matter interaction which will be of special importance in developing various applications using high power lasers.

9.2 Future works

Several issues are remained as future work. Some topics are summarized as follows:

(1) In the Lie perturbation analysis, we used a paraxial approximation for the laser field in vacuum, while the modification to the field in satisfying the Maxwell equations is also an important ingredient to be discussed.

(2) In the case where the field exhibits more gentle and/or fine-scale structures including asymmetry, i.e., $a_x = a_0 \sum_{s\geq 5} f_s \exp\left[-\left(x/w_s\right)^s\right]$, which can be achieved even in present experiments, we may need to evaluate nonlocal effects of higher order than $\mathscr{O}\left(\epsilon^3\right)$, e.g., the next is $\mathscr{O}\left(\epsilon^5\right)$, to determine the particle dynamics correctly.

(3) To further improve the nonlocal ponderomotive theory, to generalize the nonlinear Schrödinger equation system in order to describe the self-consistent laser-plasma interaction is an important issue.

(4) In describing higher order nonlocal effects, an empirical integral representation using a modulated kernel should also be an interesting subject for future work.

(5) In the numerical study on laser-cluster interaction, we have not included the radiation damping effect, which will be important in discussing intense radiation emissions from cluster medium. The ion maximum energy shown here is obtained in an ideal one-dimensional situation where transverse expansions of laser field and target are not taken into account. These issues are devoted to future work.

Appendix A

Derivation of the higher-order ponderomotive force by using the averaging method

In Part I, we have derived the higher order ponderomotive force on the basis of the noncanonical Lie perturbation theory, in which one considers purturbation expansion based on the phase space Lagrangian so that the Hamilton structure is maintained rigorously. On the other hand, we showed in the introduction Sec. 1.3 that more direct approach, i.e., the averaging method, is applicable to derive the first order ponderomotive force. Different from the Hamiltonian mechanics, in the averaging method, the scale separation and perturbation expansion are applied directly to the equation of motion. As a result, in the averaging method, the equation of motion in higher orders does not generally maintain the Hamiltonian structure. From this fact, we can expect that the equations of motion derived by the averaging method and Hamiltonian-based perturbation theory are different in higher orders.

In this Appendix, we obtain the higher-order ponderomotive force by using the averaging method starting from the equation of motion of a charged particle in electromagnetic field.

A.1 Variable transformation from time t to phase η

The equations of motion of a charged particle in electromagnetic field is given by

$$\frac{d\mathbf{x}}{dt} = \mathbf{v} = \frac{\mathbf{p}}{\gamma m}, \tag{A.1}$$

$$\frac{d\mathbf{p}}{dt} = e\left(\mathbf{E} + \frac{\mathbf{v}}{c} \times \mathbf{B}\right) = mc\left[-\frac{\partial \mathbf{a}}{\partial t} + \mathbf{v} \times (\nabla \times \mathbf{a})\right]. \tag{A.2}$$

Here, $\mathbf{a}$ is the normalized vector potential and the scalar potential ϕ is assumed to be zero, i.e., $\phi = 0$. The total derivative can be separated to partial derivatives as

$$\frac{d}{dt} = \frac{\partial}{\partial t} + \frac{d\mathbf{x}}{dt} \cdot \frac{\partial}{\partial \mathbf{x}} = \frac{\partial}{\partial t} + \mathbf{v} \cdot \nabla. \tag{A.3}$$

Here, we assume a scalar function f that has a explcit variable dependence on $\alpha(t, \mathbf{x})$ and $\mathbf{x}$, i.e., $f = f(\alpha, \mathbf{x})$, where $\mathbf{x}$ has the dependence $\mathbf{x} = \mathbf{x}(\alpha)$. Then, the total time derivative operates on f as

$$\frac{df(\alpha, \mathbf{x})}{dt} = \left[\left(\frac{\partial}{\partial t} + \mathbf{v} \cdot \nabla\right) \alpha(t, \mathbf{x})\right] \frac{df(\alpha, \mathbf{x})}{d\alpha}, \tag{A.4}$$

where $\mathbf{v} = d\mathbf{x}/dt$ and

$$\frac{df(\alpha, \mathbf{x})}{d\alpha} = \frac{\partial f}{\partial \alpha}\bigg|_{\mathbf{x}} + \frac{d\mathbf{x}}{d\alpha} \cdot \nabla f\big|_{\alpha}. \tag{A.5}$$

Here, we consider the case $\alpha = \omega t - kz \equiv \eta(t, z)$. The total time derivative of η is calculated as

$$\left(\frac{\partial}{\partial t} + \mathbf{v} \cdot \nabla\right) \eta(t, z) = \omega - v_z k = \frac{\omega}{\gamma mc}(\gamma mc - p_z). \tag{A.6}$$

The quantity $\gamma mc - p_z$ appearing in the RHS is a constant given by $p_z - \gamma mc = -\zeta_0 mc$ when we assume a vector potential $\mathbf{a}$ without z component. Then, followed from the relation Eq (A.5), the total time derivative of $f = f(\eta(t, z), \mathbf{x})$ is written in terms of η derivative as

$$\frac{df(\eta, \mathbf{x})}{dt} = \frac{\omega}{\gamma}\zeta_0 \frac{df(\eta, \mathbf{x})}{d\eta}, \tag{A.7}$$

which corresponds to the change of the variables from (t, z) to (η, z). Then, the total time derivatives of $\mathbf{p}(\eta)$ and $\mathbf{x}(\eta)$ in the LHS of the equations of motion Eqs. (A.1) and (A.2) are translated into the total η-derivative as

$$\frac{d\mathbf{x}}{d\eta} = \frac{\gamma}{\omega\zeta_0}\frac{\mathbf{p}}{\gamma m} = \frac{\mathbf{p}}{m\omega\zeta_0}, \tag{A.8}$$

$$\frac{d\mathbf{p}}{d\eta} = \frac{\gamma mc}{\omega\zeta_0}\left[-\frac{\partial \mathbf{a}}{\partial t} + \mathbf{v} \times (\nabla \times \mathbf{a})_t\right]. \tag{A.9}$$

Here, subscript t after the operator ∇ indicates that the spatial derivative is taken while the time t, not η, is fixed; therefore, the RHS is not yet transformed to the notation (η, z).

We further rewrite the RHS of Eq.(A.9). By using the relations

$$-\frac{\partial \mathbf{a}}{\partial t} = -\frac{d\mathbf{a}}{dt} + (\mathbf{v} \cdot \nabla)_t \mathbf{a}, \tag{A.10}$$

$$\mathbf{v} \times (\nabla \times \mathbf{a})_t = \left(\overleftrightarrow{\nabla \mathbf{a}}\right)_t \cdot \mathbf{v} - (\mathbf{v} \cdot \nabla)_t \mathbf{a}, \tag{A.11}$$

Eq. (A.9) is written as

$$\frac{d\mathbf{p}}{d\eta} = \frac{\gamma mc}{\omega\zeta_0}\left[-\frac{d\mathbf{a}}{dt} + (\mathbf{v}\cdot\nabla)_t\,\mathbf{a} + \mathbf{v}\times(\nabla\times\mathbf{a})_t\right] = \frac{\gamma mc}{\omega\zeta_0}\left[-\frac{d\mathbf{a}}{dt} + \left(\overleftrightarrow{\nabla}\mathbf{a}\right)_t\cdot\mathbf{v}\right]. \tag{A.12}$$

Using Eq. (A.7), we obtain

$$\begin{aligned}\frac{d\mathbf{p}}{d\eta} &= -mc\left(\frac{\partial\mathbf{a}}{\partial\eta} + \frac{1}{m\omega\zeta_0}(\mathbf{p}\cdot\nabla)_\eta\,\mathbf{a}\right) + \frac{c}{\omega\zeta_0}\left[(\gamma m\mathbf{v}\cdot\nabla)_t\,\mathbf{a} + \gamma m\mathbf{v}\times(\nabla\times\mathbf{a})_t\right] \\ &= -mc\left(\frac{\partial\mathbf{a}}{\partial\eta} + \frac{1}{m\omega\zeta_0}(\mathbf{p}\cdot\nabla)_\eta\,\mathbf{a}\right) + \frac{mc}{m\omega\zeta_0}\left[(\mathbf{p}\cdot\nabla)_t\,\mathbf{a} + \mathbf{p}\times(\nabla\times\mathbf{a})_t\right].\end{aligned} \tag{A.13}$$

The last term on the RHS of Eq. (A.13) needs careful treatment: The z derivative is performed with fixed time t, thus, it operates both on z in $\eta(t,z)$ and *bare* z of $\mathbf{a} = \mathbf{a}\left[\eta(t,z),\mathbf{x}\right]$. Namely, the general relation is given by

$$\nabla\Big|_t f\left[\alpha(t,\mathbf{x}),\mathbf{x}\right] = \left((\nabla\alpha)_t\,\frac{\partial}{\partial\alpha}\Big|_{\mathbf{x}} + \nabla\Big|_\alpha\right) f(\alpha,\mathbf{x}). \tag{A.14}$$

For $f = a_i$ ($a_i = x,y,z$) and $\alpha(t,\mathbf{x}) = \eta(t,z)$, the relation is given as

$$\frac{\partial}{\partial x}\Big|_t \mathbf{a}(\eta,\mathbf{x}) = \frac{\partial}{\partial x}\Big|_\eta \mathbf{a}(\eta,\mathbf{x}), \tag{A.15}$$

$$\frac{\partial}{\partial y}\Big|_t \mathbf{a}(\eta,\mathbf{x}) = \frac{\partial}{\partial y}\Big|_\eta \mathbf{a}(\eta,\mathbf{x}), \tag{A.16}$$

$$\frac{\partial}{\partial z}\Big|_t \mathbf{a}(\eta,\mathbf{x}) = \left(-k\frac{\partial}{\partial\eta}\Big|_z + \frac{\partial}{\partial z}\Big|_\eta\right)\mathbf{a}(\eta,\mathbf{x}). \tag{A.17}$$

Then, Eq. (A.13) becomes

$$\begin{aligned}\frac{d\mathbf{p}}{d\eta} &= -mc\left(\frac{\partial\mathbf{a}}{\partial\eta} + \frac{1}{m\omega\zeta_0}(\mathbf{p}\cdot\nabla)_\eta\,\mathbf{a}\right) + \frac{mc}{m\omega\zeta_0}\left[(\mathbf{p}\cdot\nabla)_\eta\,\mathbf{a} + \mathbf{p}\times(\nabla\times\mathbf{a})_\eta\right] \\ &\quad - mck\left(\mathbf{p}\cdot\frac{\partial\mathbf{a}}{\partial\eta}\Big|_{\mathbf{x}}\right)\hat{\mathbf{e}}_z \\ &= mc\left[-\frac{\partial\mathbf{a}}{\partial\eta} + \frac{1}{m\omega\zeta_0}\left(\mathbf{p}\times(\nabla\times\mathbf{a})_\eta - k\left(\mathbf{p}\cdot\frac{\partial\mathbf{a}}{\partial\eta}\Big|_{\mathbf{x}}\right)\hat{\mathbf{e}}_z\right)\right].\end{aligned} \tag{A.18}$$

Together with Eq. (A.8), the equation of motion with variables $(\eta,\mathbf{x})$ is obtained as

$$\frac{d\mathbf{x}}{d\eta} = \frac{\mathbf{p}}{m\omega\zeta_0}, \tag{A.19}$$

$$\frac{d\mathbf{p}}{d\eta} = mc\left[-\frac{\partial\mathbf{a}}{\partial\eta}\Big|_{\mathbf{x}} + \frac{1}{m\omega\zeta_0}\left(\mathbf{p}\times(\nabla\times\mathbf{a})_\eta - k\left(\mathbf{p}\cdot\frac{\partial\mathbf{a}}{\partial\eta}\Big|_{\mathbf{x}}\right)\hat{\mathbf{e}}_z\right)\right]. \tag{A.20}$$

By using the energy equation

$$\frac{d}{dt}\gamma mc^2 = -mc\mathbf{v}\cdot\left.\frac{\partial \mathbf{a}}{\partial t}\right|_{\mathbf{x}}, \tag{A.21}$$

and assuming that $\mathbf{a}$ does not depend on z explicitly and also $a_z = 0$, Eq. (A.20) is reduced to

$$\frac{d\mathbf{p}_\perp}{d\eta} = mc\left[-\left.\frac{\partial \mathbf{a}_\perp}{\partial \eta}\right|_{\mathbf{x}} + \frac{1}{m\omega\zeta_0}\left(\mathbf{p}\times(\nabla\times\mathbf{a})_\eta\right)_\perp\right], \tag{A.22}$$

$$\frac{d}{d\eta}\left(p_z - \gamma mc\right) = 0. \tag{A.23}$$

When we additionally assume

$$\mathbf{a} = a(x,\eta)\hat{\mathbf{e}}_x \ \text{ or } \ \mathbf{a} = a(y,\eta)\hat{\mathbf{e}}_y \ \text{ or } \ \partial_x a_y - \partial_y a_x = 0,$$

which is satisfied in the Lie perturbation analysis in Part I, the last term on the RHS of Eq. (A.22) becomes zero, and then the equation of motion is obtained as

$$\frac{d\mathbf{x}}{d\eta} = \frac{\mathbf{p}}{m\omega\zeta_0}, \tag{A.24}$$

$$\frac{d\mathbf{p}_\perp}{d\eta} = -mc\left.\frac{\partial \mathbf{a}}{\partial \eta}\right|_{\mathbf{x}}, \tag{A.25}$$

$$\frac{d}{d\eta}\left(p_z - \gamma mc\right) = 0. \tag{A.26}$$

A.2 Scale separation

Based on the Eq. (A.25), we consider the scale separation

$$\mathbf{p} = \langle\mathbf{p}\rangle + [\mathbf{p}]_{os.} = \mathbf{p}_s + \mathbf{p}_f, \tag{A.27}$$

which we introduced in Sec. 1.3.1. Namely, the angle bracket denotes taking average over one cycle of η and the bracket $[\ \ ]_{os.}$ denotes taking oscillatory part. The subscripts s and f represent slowly and fastly varying parts, respectively.

Here, we define the variable dependence as follows:

$$\mathbf{x} = \mathbf{x}(\eta), \tag{A.28}$$

$$\mathbf{p} = \mathbf{p}(\mathbf{x}(\eta),\eta), \tag{A.29}$$

$$\mathbf{a} = \mathbf{a}(\mathbf{x}(\eta),\eta). \tag{A.30}$$

We also note that partial derivatives are now defined as

$$\frac{\partial}{\partial \eta} = \frac{\partial}{\partial \eta}\bigg|_{\mathbf{x}} \quad \text{and} \quad \nabla = \nabla\big|_{\eta}. \tag{A.31}$$

By using the scale separation Eq. (A.27), the equation of motion Eq. (A.25) is written as

$$\frac{\partial \left(\mathbf{p}_{s\perp} + \mathbf{p}_{f\perp}\right)}{\partial \eta} + \frac{\mathbf{p}_s \cdot \nabla \mathbf{p}_{s\perp}}{m\omega\zeta_0} + \frac{\mathbf{p}_s \cdot \nabla \mathbf{p}_{f\perp}}{m\omega\zeta_0} + \frac{\mathbf{p}_f \cdot \nabla \mathbf{p}_{s\perp}}{m\omega\zeta_0} + \frac{\mathbf{p}_f \cdot \nabla \mathbf{p}_{f\perp}}{m\omega\zeta_0} = -mc\frac{\partial \mathbf{a}}{\partial \eta}. \tag{A.32}$$

Taking the average over η, Eq. (A.32) leads to the slow scale equation,

$$\frac{\partial \mathbf{p}_{s\perp}}{\partial \eta} + \frac{\mathbf{p}_s \cdot \nabla \mathbf{p}_{s\perp}}{m\omega\zeta_0} + \frac{\langle \mathbf{p}_f \cdot \nabla \mathbf{p}_{f\perp} \rangle}{m\omega\zeta_0} = \mathbf{0}. \tag{A.33}$$

Then, subtracting Eq. (A.33) from Eq. (A.32), we obtain the fast scale equation as

$$\frac{\partial \mathbf{p}_{f\perp}}{\partial \eta} + \frac{\mathbf{p}_s \cdot \nabla \mathbf{p}_{f\perp}}{m\omega\zeta_0} + \frac{\mathbf{p}_f \cdot \nabla \mathbf{p}_{s\perp}}{m\omega\zeta_0} + \frac{\left[\mathbf{p}_f \cdot \nabla \mathbf{p}_{f\perp}\right]_{os.}}{m\omega\zeta_0} = -mc\frac{\partial \mathbf{a}}{\partial \eta}. \tag{A.34}$$

A.3 Perturbation analysis up to the third order

Here, we consider perturbation expansion based on the expansion parameter ϵ that is defined by Eq. (1.46) in Sec. 1.3.1 as

$$l\,\nabla f_s\left(\mathbf{x}, \eta\right) \sim \epsilon \quad \text{and} \quad l\,\nabla f_f\left(\mathbf{x}, \eta\right) \sim \epsilon, \tag{A.35}$$

which indicate that both slow and fast components vary gently in space.

A.3.1 Zeroth order equation of motion

The zeroth order component of Eqs. (A.33) and (A.34) are given as

$$\frac{\partial \mathbf{p}_{s\perp}^{(0)}}{\partial \eta} = \mathbf{0}, \tag{A.36}$$

$$\frac{\partial \mathbf{p}_{f\perp}^{(0)}}{\partial \eta} = -mc\frac{\partial \mathbf{a}}{\partial \eta}, \tag{A.37}$$

The RHS of Eq. (A.36) can be approximated to the total derivative of η, i.e.,

$$\frac{d\mathbf{p}_{s\perp}^{(0)}}{d\eta} = \mathbf{0} + \mathscr{O}\left(\epsilon\right), \tag{A.38}$$

which corresponds to the zeroth order slow scale equation of motion. The solution for $\mathbf{p}_{s\perp}$ in the zeroth order is then found to be

$$\mathbf{p}_{s\perp}^{(0)}(\mathbf{x},\eta) = \mathbf{0}, \tag{A.39}$$

where we assumed an initial condition $\mathbf{p}_0 = 0$ at $\eta = 0$. From Eq. (A.37), the solution for $\mathbf{p}_{f\perp}$ in the zeroth order is derived as

$$\mathbf{p}_{f\perp}^{(0)}(\mathbf{x},\eta) = -mc\mathbf{a}(\mathbf{x},\eta). \tag{A.40}$$

A.3.2 First order equation of motion

The first order component of Eqs. (A.33) and (A.34) are given as

$$\frac{\partial \mathbf{p}_{s\perp}^{(1)}}{\partial\eta} + \frac{\mathbf{p}_s^{(0)}\cdot\nabla\mathbf{p}_{s\perp}^{(0)}}{m\omega\zeta_0} + \frac{\left\langle \mathbf{p}_f^{(0)}\cdot\nabla\mathbf{p}_{f\perp}^{(0)}\right\rangle}{m\omega\zeta_0} = \mathbf{0}, \tag{A.41}$$

$$\frac{\partial \mathbf{p}_{f\perp}^{(1)}}{\partial\eta} + \frac{\mathbf{p}_s^{(0)}\cdot\nabla\mathbf{p}_{f\perp}^{(0)}}{m\omega\zeta_0} + \frac{\mathbf{p}_f^{(0)}\cdot\nabla\mathbf{p}_{s\perp}^{(0)}}{m\omega\zeta_0} + \frac{\left[\mathbf{p}_f^{(0)}\cdot\nabla\mathbf{p}_{f\perp}^{(0)}\right]_{os.}}{m\omega\zeta_0} = \mathbf{0}. \tag{A.42}$$

By using the solution Eq. (A.39), the above equations are reduced to

$$\frac{\partial \mathbf{p}_{s\perp}^{(1)}}{\partial\eta} + \frac{\left\langle \mathbf{p}_f^{(0)}\cdot\nabla\mathbf{p}_{f\perp}^{(0)}\right\rangle}{m\omega\zeta_0} = \mathbf{0}, \tag{A.43}$$

$$\frac{\partial \mathbf{p}_{f\perp}^{(1)}}{\partial\eta} + \frac{\left[\mathbf{p}_f^{(0)}\cdot\nabla\mathbf{p}_{f\perp}^{(0)}\right]_{os.}}{m\omega\zeta_0} = \mathbf{0}. \tag{A.44}$$

Substituting the solution Eq. (A.40), Eq. (A.43) becomes

$$\frac{\partial \mathbf{p}_{s\perp}^{(1)}}{\partial\eta} = -\frac{mc^2}{\omega\zeta_0}\left\langle(\mathbf{a}\cdot\nabla)\,\mathbf{a}\right\rangle. \tag{A.45}$$

The RHS of Eq. (A.45) can be approximated to the total derivative of η. Therefore, from Eqs. (A.36) and (A.45), we obtain the slow scale equation of motion up to the first order as

$$\frac{d\mathbf{p}_{s\perp}}{d\eta} = -\frac{mc^2}{\omega\zeta_0}\left\langle(\mathbf{a}\cdot\nabla)\,\mathbf{a}\right\rangle + \mathscr{O}\left(\epsilon^2\right). \tag{A.46}$$

This equation corresponds to the ponderomotive formula of order ϵ, which is consistent with that obtained by the Lie perturbation analysis Eq. (3.119). The solution

for $\mathbf{p}_{s\perp}$ up to the first order is obtained from Eq. (A.45) as

$$\mathbf{p}_{s\perp}(\mathbf{x},\eta) = -\frac{mc^2}{\omega\zeta_0}\langle \mathbf{a}(\mathbf{x},\eta)\cdot\nabla\mathbf{a}(\mathbf{x},\eta)\rangle\,\eta + \mathscr{O}\left(\epsilon^2\right). \tag{A.47}$$

For the fast component, by substituting the solution Eq. (A.40) into Eq. (A.44), we have

$$\frac{\partial\mathbf{p}_{f\perp}^{(1)}}{\partial\eta} = -\frac{mc^2}{\omega\zeta_0}\left[(\mathbf{a}\cdot\nabla)\,\mathbf{a}\right]_{os.}, \tag{A.48}$$

from which the solution for $\mathbf{p}_{f\perp}$ in the first order can be obtained as

$$\mathbf{p}_{f\perp}^{(1)}(\mathbf{x},\eta) = -\frac{mc^2}{\omega\zeta_0}\int\partial\eta\left[\mathbf{a}(\mathbf{x},\eta)\cdot\nabla\mathbf{a}(\mathbf{x},\eta)\right]_{os.}, \tag{A.49}$$

where we use the notation $\int\partial\eta$ to denote the integration that corresponds to the partial derivative $\partial/\partial\eta$.

A.3.3 Second order equation of motion

The second order component of Eqs. (A.33) and (A.34) are given as

$$\frac{\partial\mathbf{p}_{s\perp}^{(2)}}{\partial\eta} + \frac{\mathbf{p}_s^{(0)}\cdot\nabla\mathbf{p}_{s\perp}^{(1)}}{m\omega\zeta_0} + \frac{\mathbf{p}_s^{(1)}\cdot\nabla\mathbf{p}_{s\perp}^{(0)}}{m\omega\zeta_0} + \frac{\left\langle\mathbf{p}_f^{(0)}\cdot\nabla\mathbf{p}_{f\perp}^{(1)}\right\rangle}{m\omega\zeta_0} + \frac{\left\langle\mathbf{p}_f^{(1)}\cdot\nabla\mathbf{p}_{f\perp}^{(0)}\right\rangle}{m\omega\zeta_0} = \mathbf{0}, \tag{A.50}$$

$$\begin{aligned}\frac{\partial\mathbf{p}_{f\perp}^{(2)}}{\partial\eta} &+ \frac{\mathbf{p}_s^{(0)}\cdot\nabla\mathbf{p}_{f\perp}^{(1)}}{m\omega\zeta_0} + \frac{\mathbf{p}_s^{(1)}\cdot\nabla\mathbf{p}_{f\perp}^{(0)}}{m\omega\zeta_0} + \frac{\mathbf{p}_f^{(0)}\cdot\nabla\mathbf{p}_{s\perp}^{(1)}}{m\omega\zeta_0} + \frac{\mathbf{p}_f^{(1)}\cdot\nabla\mathbf{p}_{s\perp}^{(0)}}{m\omega\zeta_0} \\ &+ \frac{\left[\mathbf{p}_f^{(0)}\cdot\nabla\mathbf{p}_{f\perp}^{(1)}\right]_{os.}}{m\omega\zeta_0} + \frac{\left[\mathbf{p}_f^{(1)}\cdot\nabla\mathbf{p}_{f\perp}^{(0)}\right]_{os.}}{m\omega\zeta_0} = \mathbf{0}.\end{aligned} \tag{A.51}$$

By using the solution Eq. (A.39), the above equations are reduced to

$$\frac{\partial\mathbf{p}_{s\perp}^{(2)}}{\partial\eta} = -\frac{\left\langle\mathbf{p}_f^{(0)}\cdot\nabla\mathbf{p}_{f\perp}^{(1)}\right\rangle}{m\omega\zeta_0} - \frac{\left\langle\mathbf{p}_f^{(1)}\cdot\nabla\mathbf{p}_{f\perp}^{(0)}\right\rangle}{m\omega\zeta_0}, \tag{A.52}$$

$$\frac{\partial\mathbf{p}_{f\perp}^{(2)}}{\partial\eta} = -\frac{\mathbf{p}_s^{(1)}\cdot\nabla\mathbf{p}_{f\perp}^{(0)}}{m\omega\zeta_0} - \frac{\mathbf{p}_f^{(0)}\cdot\nabla\mathbf{p}_{s\perp}^{(1)}}{m\omega\zeta_0} - \frac{\left[\mathbf{p}_f^{(0)}\cdot\nabla\mathbf{p}_{f\perp}^{(1)}\right]_{os.}}{m\omega\zeta_0} - \frac{\left[\mathbf{p}_f^{(1)}\cdot\nabla\mathbf{p}_{f\perp}^{(0)}\right]_{os.}}{m\omega\zeta_0}. \tag{A.53}$$

Substituting the solution $\mathbf{p}_{f\perp}^{(0)}$ and $\mathbf{p}_{f\perp}^{(1)}$, which are respectively given by Eqs. (A.40) and (A.49), Eq. (A.52) becomes

$$\frac{\partial \mathbf{p}_{s\perp}^{(2)}}{\partial \eta} = -\frac{mc^2}{\omega^2\zeta_0^2}\left\langle\left[\left(\int \partial\eta\left[(\mathbf{a}\cdot\nabla)\,\mathbf{a}\right]_{os.}\right)\cdot\nabla\right]\mathbf{a}\right\rangle - \frac{mc^2}{\omega^2\zeta_0^2}\left\langle(\mathbf{a}\cdot\nabla)\left(\int \partial\eta\left[(\mathbf{a}\cdot\nabla)\,\mathbf{a}\right]_{os.}\right)\right\rangle. \tag{A.54}$$

The LHS of Eq. (A.54) can be approximated to the total derivative of η in the second order. Therefore, from Eqs. (A.36), (A.45) and (A.54), we obtain the slow scale equation of motion up to the second order as

$$\frac{d\mathbf{p}_{s\perp}}{d\eta} = -\frac{mc^2}{\omega\zeta_0}\langle(\mathbf{a}\cdot\nabla)\,\mathbf{a}\rangle - \frac{mc^2}{\omega^2\zeta_0^2}\left\langle\left[\left(\int \partial\eta\left[(\mathbf{a}\cdot\nabla)\,\mathbf{a}\right]_{os.}\right)\cdot\nabla\right]\mathbf{a}\right\rangle - \frac{mc^2}{\omega^2\zeta_0^2}\left\langle(\mathbf{a}\cdot\nabla)\left(\int \partial\eta\left[(\mathbf{a}\cdot\nabla)\,\mathbf{a}\right]_{os.}\right)\right\rangle + \mathscr{O}\left(\epsilon^3\right). \tag{A.55}$$

The solution for $\mathbf{p}_{s\perp}^{(2)}$ can be obtained by integrating Eq. (A.54). Here, the integrants in the second and third terms on the RHS of Eq. (A.55) have the dependence $\mathbf{a}^3$. Noting that the cube of phase functions, such as the sine and cosine functions, has no secular term, one can find that the $\mathbf{a}^3$ terms become zero after averaging in this order. Hence, the slow scale equation of motion up to the second order is

$$\frac{d\mathbf{p}_{s\perp}}{d\eta} = -\frac{mc^2}{\omega\zeta_0}\langle(\mathbf{a}\cdot\nabla)\,\mathbf{a}\rangle + \mathscr{O}\left(\epsilon^3\right). \tag{A.56}$$

For the fast component, substituting the solution Eqs. (A.40), (A.47) and (A.49), we obtain each term on the RHS of Eq. (A.53) as follows:

$$-\frac{\mathbf{p}_s^{(1)}\cdot\nabla\mathbf{p}_{f\perp}^{(0)}}{m\omega\zeta_0} = -\frac{mc^3}{\omega\zeta_0}\left(\langle(\mathbf{a}\cdot\nabla)\,\mathbf{a}\rangle\,\eta\cdot\nabla\right)\mathbf{a}, \tag{A.57}$$

$$-\frac{\mathbf{p}_f^{(0)}\cdot\nabla\mathbf{p}_{s\perp}^{(1)}}{m\omega\zeta_0} = -\frac{mc^3}{\omega\zeta_0}(\mathbf{a}\cdot\nabla)\langle(\mathbf{a}\cdot\nabla)\,\mathbf{a}\rangle\,\eta = -\frac{mc^3}{\omega\zeta_0}\mathbf{a}\left[\left\langle(\nabla\mathbf{a})^2\right\rangle\eta + \mathbf{a}\left(\nabla^2\mathbf{a}\right)\eta\right], \tag{A.58}$$

$$-\frac{\left[\mathbf{p}_f^{(0)}\cdot\nabla\mathbf{p}_{f\perp}^{(1)}\right]_{os.}}{m\omega\zeta_0} = -\frac{mc^3}{\omega\zeta_0}\left[(\mathbf{a}\cdot\nabla)\int\partial\eta\left[(\mathbf{a}\cdot\nabla)\,\mathbf{a}\right]_{os.}\right]_{os.} = -\frac{mc^3}{\omega\zeta_0}\left[\mathbf{a}\int\partial\eta\left[(\nabla\mathbf{a})^2 + \mathbf{a}\left(\nabla^2\mathbf{a}\right)\right]_{os.}\right]_{os.}, \tag{A.59}$$

$$-\frac{\left[\mathbf{p}_f^{(1)}\cdot\nabla\mathbf{p}_{f\perp}^{(0)}\right]_{os.}}{m\omega\zeta_0} = -\frac{mc^3}{\omega\zeta_0}\left[\left(\int\partial\eta\left[(\mathbf{a}\cdot\nabla)\,\mathbf{a}\right]_{os.}\cdot\nabla\right)\mathbf{a}\right]_{os.}. \tag{A.60}$$

Then, the solution for $\mathbf{p}_{f\perp}^{(2)}$ is found to be

$$\begin{aligned}\mathbf{p}_{f\perp}^{(2)}(\mathbf{x},\eta) = &-\frac{mc^3}{\omega\zeta_0}\int\partial\eta\left(\left[\langle(\mathbf{a}\cdot\nabla)\,\mathbf{a}\rangle\,\eta\cdot\nabla\right]\mathbf{a}\right)\\ &-\frac{mc^3}{\omega\zeta_0}\int\partial\eta\left(\mathbf{a}\left[\left\langle(\nabla\mathbf{a})^2\right\rangle\eta+\mathbf{a}\left(\nabla^2\mathbf{a}\right)\eta\right]\right)\\ &-\frac{mc^3}{\omega\zeta_0}\int\partial\eta\left[\mathbf{a}\int\partial\eta\left[(\nabla\mathbf{a})^2+\mathbf{a}\left(\nabla^2\mathbf{a}\right)\right]_{os.}\right]_{os.}\\ &-\frac{mc^3}{\omega\zeta_0}\int\partial\eta\left[\left(\int\partial\eta\left[(\mathbf{a}\cdot\nabla)\,\mathbf{a}\right]_{os.}\cdot\nabla\right)\mathbf{a}\right]_{os.}.\end{aligned}\tag{A.61}$$

A.3.4 Third order equation of motion

The second order component of Eqs. (A.33) is given as

$$\begin{aligned}&\frac{\partial\mathbf{p}_{s\perp}^{(3)}}{\partial\eta}+\frac{\mathbf{p}_s^{(0)}\cdot\nabla\mathbf{p}_{s\perp}^{(2)}}{m\omega\zeta_0}+\frac{\mathbf{p}_s^{(1)}\cdot\nabla\mathbf{p}_{s\perp}^{(1)}}{m\omega\zeta_0}+\frac{\mathbf{p}_s^{(2)}\cdot\nabla\mathbf{p}_{s\perp}^{(0)}}{m\omega\zeta_0}\\ &\quad+\frac{\left\langle\mathbf{p}_f^{(0)}\cdot\nabla\mathbf{p}_{f\perp}^{(2)}\right\rangle}{m\omega\zeta_0}+\frac{\left\langle\mathbf{p}_f^{(1)}\cdot\nabla\mathbf{p}_{f\perp}^{(1)}\right\rangle}{m\omega\zeta_0}+\frac{\left\langle\mathbf{p}_f^{(2)}\cdot\nabla\mathbf{p}_{f\perp}^{(0)}\right\rangle}{m\omega\zeta_0}=\mathbf{0}.\end{aligned}\tag{A.62}$$

By using the solution Eq. (A.39), the above equation is reduced to

$$\frac{\partial\mathbf{p}_{s\perp}^{(3)}}{\partial\eta}+\frac{\mathbf{p}_s^{(1)}\cdot\nabla\mathbf{p}_{s\perp}^{(1)}}{m\omega\zeta_0}=-\frac{\left\langle\mathbf{p}_f^{(0)}\cdot\nabla\mathbf{p}_{f\perp}^{(2)}\right\rangle}{m\omega\zeta_0}-\frac{\left\langle\mathbf{p}_f^{(1)}\cdot\nabla\mathbf{p}_{f\perp}^{(1)}\right\rangle}{m\omega\zeta_0}-\frac{\left\langle\mathbf{p}_f^{(2)}\cdot\nabla\mathbf{p}_{f\perp}^{(0)}\right\rangle}{m\omega\zeta_0}.\tag{A.63}$$

Substituting the solution Eqs. (A.40), (A.49) and (A.61), each term on the RHS of Eq. (A.63) becomes

$$-\frac{\left\langle\mathbf{p}_f^{(0)}\cdot\nabla\mathbf{p}_{f\perp}^{(2)}\right\rangle}{m\omega\zeta_0}=\frac{c}{\omega^2\zeta_0^2}\left\langle(\mathbf{a}\cdot\nabla)\,(\text{A.61})\right\rangle,\tag{A.64}$$

$$\begin{aligned}-\frac{\left\langle\mathbf{p}_f^{(1)}\cdot\nabla\mathbf{p}_{f\perp}^{(1)}\right\rangle}{m\omega\zeta_0}&=-\frac{mc^4}{\omega^3\zeta_0^3}\left\langle\left(\int\partial\eta\left[(\mathbf{a}\cdot\nabla)\,\mathbf{a}\right]_{os.}\cdot\nabla\right)\int\partial\eta\left[(\mathbf{a}\cdot\nabla)\,\mathbf{a}\right]_{os.}\right\rangle\\ &=-\frac{mc^4}{\omega^3\zeta_0^3}\left\langle\int\partial\eta\left[(\mathbf{a}\cdot\nabla)\,\mathbf{a}\right]_{os.}\int\partial\eta\left[(\nabla\mathbf{a})^2+\mathbf{a}\left(\nabla^2\mathbf{a}\right)\right]_{os.}\right\rangle,\end{aligned}\tag{A.65}$$

$$-\frac{\left\langle\mathbf{p}_f^{(2)}\cdot\nabla\mathbf{p}_{f\perp}^{(0)}\right\rangle}{m\omega\zeta_0}=\frac{c}{\omega^2\zeta_0^2}\left\langle((\text{A.61})\cdot\nabla)\,\mathbf{a}\right\rangle,\tag{A.66}$$

where (A.61) on the RHS of Eqs. (A.64) and (A.66) indicates the RHS of Eq. (A.61).

Together with Eq. (A.55), we obtain the slow scale equation of motion up to the third order as

$$\frac{\partial \mathbf{p}_{s\perp}^{(0+1+2+3)}}{\partial \eta} + \frac{\mathbf{p}_s^{(1)} \cdot \nabla \mathbf{p}_{s\perp}^{(1)}}{m\omega\zeta_0} = (\text{A.55}) + (\text{A.64}) + (\text{A.65}) + (\text{A.66}) + \mathscr{O}\left(\epsilon^4\right). \quad \text{(A.67)}$$

This equation denotes the ponderomotive force up to the third order with respect to ϵ.

Hereafter, we assume the laser field given by

$$\mathbf{a}\left(\mathbf{x}, \eta\right) = a\left(x\right) \sin\eta \; \hat{\mathbf{e}}_x, \quad \text{(A.68)}$$

which is same as that assumed in the Lie perturbation analysis in Chap. 3. By substituting Eq. (A.68) to the RHS of Eq. (A.67), we obtain

$$\begin{aligned}
&\left(\frac{\partial}{\partial\eta} + \frac{\mathbf{p}_s \cdot \nabla}{m\omega\zeta_0}\right) \mathbf{p}_{s\perp} \\
&\quad = -\epsilon \frac{mc^2}{2\omega\zeta_0} a(x) \frac{\partial a(x)}{\partial x} \hat{\mathbf{e}}_x \\
&\qquad - \frac{\epsilon^3}{16} \frac{mc^4}{\omega^3\zeta_0^3} a(x) \left[\frac{43}{2} a(x) \frac{\partial a(x)}{\partial x} \frac{\partial^2 a(x)}{\partial x^2} + 3a^2(x) \frac{\partial^3 a(x)}{\partial x^3} + \frac{25}{2} \left(\frac{\partial a(x)}{\partial x}\right)^3\right] \hat{\mathbf{e}}_x \\
&\qquad + \mathscr{O}\left(\epsilon^4\right). \quad \text{(A.69)}
\end{aligned}$$

Using the notation

$$L^{-1}\left(x\right) \equiv \frac{1}{a(x)} \frac{\partial a(x)}{\partial x}, \quad \text{(A.70)}$$

$$R^{-1}\left(x\right) \equiv \frac{1}{a(x)} \frac{\partial^2 a(x)}{\partial x^2}, \quad \text{(A.71)}$$

$$T^{-1}\left(x\right) \equiv \frac{1}{a(x)} \frac{\partial^3 a(x)}{\partial x^3}, \quad \text{(A.72)}$$

$$\quad \text{(A.73)}$$

Eq. (A.69) can be written as

$$\begin{aligned}
\left(\frac{\partial}{\partial\eta} + \frac{\mathbf{p}_s \cdot \nabla}{m\omega\zeta_0}\right) \mathbf{p}_{s\perp} = &-\epsilon \frac{mca(x)}{2} \frac{l}{L}\bigg|_x \hat{\mathbf{e}}_x \\
&- \epsilon^3 \frac{mca(x)}{16} \left[\frac{43}{2} \frac{l}{L} \frac{l^2}{R}\bigg|_x + 3\frac{l^3}{T}\bigg|_x + \frac{25}{2} \frac{l^3}{L^3}\bigg|_x\right] \hat{\mathbf{e}}_x + \mathscr{O}\left(\epsilon^4\right). \quad \text{(A.74)}
\end{aligned}$$

A.4 Oscillation center description

In the above equation Eq. (A.74), the field amplitude a and also the excursion length l is written in terms of x, which generally includes oscillatory component. Hence, we cannot obtain the averaged motion, i.e., the motion of the oscillation center of the particle, by solving only Eqs. (A.74) and (A.1). Namely, to obtain the trajectory $\mathbf{p}(\eta)$ and $\mathbf{x}(\eta)$, one needs to additionally solve the oscillatory motion in order to evaluate x appears in the RHS of Eq. (A.74). This is different from the ponderomotive formula obtained in the Lie perturbation analysis, which is expressed in terms of the oscillation center variable X. Therefore, in the next step, we rewrite Eqs. (A.74) and (A.1) to those expressed in terms of oscillation center variables $\overline{x}$ and $\overline{\mathbf{p}}$ where overline indicates the average over η.

For this purpose, we consider the Taylor expansion of $\mathbf{a}(x)$ around $\overline{x}$ where

$$\overline{x} = x - \left(\tilde{x}^{(0)} + \tilde{x}^{(1)} + \tilde{x}^{(2)} + \cdots\right), \tag{A.75}$$

as

$$a(x) = a(\overline{x}) + \left.\frac{\partial a}{\partial x}\right|_{\overline{x}} \left(\tilde{x}^{(0)} + \tilde{x}^{(1)} + \tilde{x}^{(2)} + \cdots\right) + \frac{1}{2!}\left.\frac{\partial^2 a}{\partial x^2}\right|_{\overline{x}} \left(\tilde{x}^{(0)} + \tilde{x}^{(1)} + \tilde{x}^{(2)} + \cdots\right)^2 + \cdots. \tag{A.76}$$

Since we are deriving the ponderomotive force up to the third order ϵ^3, and the force in Eq. (A.74) has only the first and smaller order terms of ϵ, we need to consider the Taylor expansion Eq. (A.76) only up to the second order ϵ^2, i.e.,

$$a(x) = a(\overline{x}) + \left.\frac{\partial a}{\partial x}\right|_{\overline{x}} \left(\tilde{x}^{(0)} + \tilde{x}^{(1)}\right) + \frac{1}{2!}\left.\frac{\partial^2 a}{\partial x^2}\right|_{\overline{x}} \tilde{x}^{(0)2} + \mathscr{O}\left(\epsilon^3\right). \tag{A.77}$$

Here, $\tilde{x}^{(0)}$ and $\tilde{x}^{(1)}$ are obtained by Eqs. (A.40) and (A.49) as

$$\tilde{x}^{(0)} = l(\overline{x}) \cos\eta, \tag{A.78}$$

$$\tilde{x}^{(1)} = \frac{l(\overline{x})}{8}\left.\frac{l}{L}\right|_{\overline{x}} \cos 2\eta. \tag{A.79}$$

Then, the expansion Eq. (A.77) yields to

$$a(x) = a(\overline{x}) + \left.\frac{\partial a}{\partial x}\right|_{\overline{x}} l(\overline{x}) \cos\eta + \left.\frac{\partial a}{\partial x}\right|_{\overline{x}} \frac{l(\overline{x})}{8}\left.\frac{l}{L}\right|_{\overline{x}} \cos 2\eta + \frac{1}{2!}\left.\frac{\partial^2 a}{\partial x^2}\right|_{\overline{x}} l^2(\overline{x}) + \mathscr{O}\left(\epsilon^3\right). \tag{A.80}$$

Then, in taking average in Eqs. (A.46) and (A.55), we now take into account not only explicit but also implicit dependences on η, i.e. $\mathbf{a}(\mathbf{x}(\eta), \eta)$. By considering the implicit dependence, the additional secular terms appear due to the coupling with the explicit $\cos 2\eta$ in the RHS of Eq. (A.46) or the first term on the RHS in Eq. (A.55), and $\cos\eta$ on the second and third terms in Eq. (A.55). Namely, they

are expanded as

$$\begin{aligned}\langle(\mathbf{a}\cdot\nabla)\,\mathbf{a}\rangle &= \left\langle a\left(\overline{x}\right)\frac{\partial a}{\partial x}\bigg|_{\overline{x}}\frac{1}{2}\left(1-\cos 2\eta\right)\right\rangle + \left\langle\left(\frac{\partial a}{\partial x}\bigg|_{\overline{x}}\frac{l\left(\overline{x}\right)}{8}\frac{l}{L}\bigg|_{\overline{x}}\cos 2\eta\right)\frac{\partial a}{\partial x}\bigg|_{\overline{x}}\frac{1}{2}\left(1-\cos 2\eta\right)\right\rangle \\ &\quad+\left\langle\left(\frac{1}{2!}\frac{\partial^2 a}{\partial x^2}\bigg|_{\overline{x}}l^2\left(\overline{x}\right)\frac{1}{2}\left(1+\cos 2\eta\right)\right)\frac{\partial a}{\partial x}\bigg|_{\overline{x}}\frac{1}{2}\left(1-\cos 2\eta\right)\right\rangle \\ &\quad+\left\langle\left(\frac{\partial a}{\partial x}\bigg|_{\overline{x}}l\left(\overline{x}\right)\cos\eta\right)\left(\frac{\partial^2 a}{\partial x^2}\bigg|_{\overline{x}}l\left(\overline{x}\right)\cos\eta\right)\frac{1}{2}\left(1-\cos 2\eta\right)\right\rangle \\ &= \frac{k_z^2\zeta_0^2}{2}l\left(\overline{x}\right)\frac{l}{L}\bigg|_{\overline{x}} - \frac{k_z^2\zeta_0^2}{32}l\left(\overline{x}\right)\frac{l^3}{L^3}\bigg|_{\overline{x}} + \frac{3}{16}k_z^2\zeta_0^2 l\left(\overline{x}\right)\frac{l}{L}\bigg|_{\overline{x}}\frac{l^2}{R}\bigg|_{\overline{x}}, \end{aligned} \tag{A.81}$$

$$\begin{aligned}&\left\langle\left[\left(\int\partial\eta\left[\left(\mathbf{a}\cdot\nabla\right)\mathbf{a}\right]_{os.}\right)\cdot\nabla\right]\mathbf{a}\right\rangle \\ &= \left\langle a\left(x\right)\left(\frac{\partial a}{\partial x}\bigg|_{x}\right)^2\sin\eta\int\partial\eta\left[\frac{1}{2}\left(1-\cos 2\eta\right)\right]_{os.}\right\rangle \\ &= -\frac{k_z^3\zeta_0^3}{16}l\left(\overline{x}\right)\left(\frac{l^3}{L^3}\bigg|_{\overline{x}}+2\frac{l}{L}\bigg|_{\overline{x}}\frac{l^2}{R}\bigg|_{\overline{x}}\right),\end{aligned} \tag{A.82}$$

$$\begin{aligned}&\left\langle\left(\mathbf{a}\cdot\nabla\right)\left(\int\partial\eta\left[\left(\mathbf{a}\cdot\nabla\right)\mathbf{a}\right]_{os.}\right)\right\rangle \\ &= \left\langle\left[a\left(x\right)\left(\frac{\partial a}{\partial x}\bigg|_{x}\right)^2+a^2\left(x\right)\frac{\partial^2 a}{\partial x^2}\bigg|_{x}\right]\sin\eta\int\partial\eta\left[\frac{1}{2}\left(1-\cos 2\eta\right)\right]_{os.}\right\rangle \\ &= -\frac{k_z^3\zeta_0^3}{16}l\left(\overline{x}\right)\left(\frac{l^3}{L^3}\bigg|_{\overline{x}}+4\frac{l}{L}\bigg|_{\overline{x}}\frac{l^2}{R}\bigg|_{\overline{x}}+\frac{l^3}{T}\bigg|_{\overline{x}}\right).\end{aligned} \tag{A.83}$$

Using Eqs. (A.81), (A.82) and (A.83), we express Eq. (A.67) by the oscillation center variables as

$$\begin{aligned}\left(\frac{\partial}{\partial\eta}+\frac{\overline{\mathbf{p}}\cdot\nabla}{m\omega\zeta_0}\right)\overline{\mathbf{p}}_{\perp} &= -\epsilon\frac{mca(\overline{x})}{2}\frac{l}{L}\bigg|_{\overline{x}}\hat{\mathbf{e}}_x \\ &\quad-\epsilon^3\frac{mca(\overline{x})}{16}\left[\frac{37}{2}\frac{l}{L}\frac{l^2}{R}\bigg|_{\overline{x}}+2\frac{l^3}{T}\bigg|_{\overline{x}}+10\frac{l^3}{L^3}\bigg|_{\overline{x}}\right]\hat{\mathbf{e}}_x+\mathscr{O}\left(\epsilon^4\right).\end{aligned} \tag{A.84}$$

This equation corresponds to the ponderomotive formula up to the third order which is described by the oscllation center variables. Therefore, one can obtain the oscillation center trajectory by integrating Eq. (A.84) together with the slow scale relation between $\mathbf{p}$ and $\mathbf{x}$, i.e.,

$$\frac{d\overline{\mathbf{x}}}{d\eta}=\frac{\overline{\mathbf{p}}}{m\omega\zeta_0} \tag{A.85}$$

One can see that Eq. (A.84) possesses the same dependence on the field structure consisting of terms proportional to l^3/LR, l^3/T and l^3/L^3 with same signs as those derived by the Lie perturbation method, however, the coefficients of each terms are different.

Appendix B

Degree of freedom of the coordinate and gauge transformations

B.1 Removal of oscillations using the degree of freedom of the coordinate transformation

In Sec. 3.2.2, we have noted that the undesirable oscillation in the oscillation center equation of motion can be removed both by the gauge transformation and by using the degree of freedom of the coordinate transformation, i.e., taking $\delta_z = -1$ in the definition of the coordinate transformation Eq. (3.74). For reference, we here show the definition of the coordinate transformation Eqs. (3.72)-(3.77):

$$x\left(X,\eta\right) = X + \delta_x \tilde{x}^{(0)} = X + \delta_x \sigma l(X)\cos\eta, \tag{B.1}$$
$$y\left(Y\right) = Y, \tag{B.2}$$
$$z\left(Z,X,\eta\right) = Z + \delta_z \tilde{z}^{(0)} = Z - \delta_z \frac{k_z l^2(X)}{8}\sin 2\eta, \tag{B.3}$$
$$p_x\left(X,P_x,\eta\right) = P_x + \delta_x \tilde{p}_x^{(0)} = P_x - \delta_x \sigma mca_x(X)\sin\eta, \tag{B.4}$$
$$p_y\left(P_y\right) = P_y, \tag{B.5}$$
$$p_\eta\left(p_\eta\right) = p_\eta, \tag{B.6}$$

In this appendix, we derive the equations of motion up to the third order of ϵ by the same Lie perturbation procedure performed in Sec. 3.2, without using the gauge transformation described in Sec. 3.2.3, and instead using $\delta_z = -1$. Here, we start from the coordinates Z^μ given in Eq. (3.71), i.e., $Z^\mu = (\eta; X, Y, Z, P_x, P_y, p_\eta)$, and the corresponding covariant vector Γ_μ in Eqs. (3.103)-(3.80). Here we assume $\delta_x = 1$ and rewrite the zeroth order 1-form Eq. (3.107):

$$\Gamma_0^{(0)} = \frac{m^2c^2 + P_x^2 + p_\eta^2}{2p_\eta k_z} - (1+\alpha)\, P_x l(X)\sigma \sin\eta + \alpha^2 \frac{p_\eta k_z l^2(X)}{4} - \frac{p_\eta k_z l^2(X)}{4}\left(\delta_z + \alpha^2\right)\cos 2\eta, \tag{B.7}$$

$$\Gamma_6^{(0)} = 0, \tag{B.8}$$

and $\Gamma_1^{(0)} = P_x$, $\Gamma_2^{(0)} = P_y$, $\Gamma_3^{(0)} = p_\eta$ and $\Gamma_4^{(0)} = \Gamma_5^{(0)} = \Gamma_6^{(0)} = 0$. In this case, the resultant equations of motion in the X and Z directions are obtained as

$$\frac{dX}{d\eta} = \frac{P_x}{mc\zeta_0 k_z}, \tag{B.9}$$

$$\frac{dP_x}{d\eta} = -\epsilon\frac{mca_x}{2}\frac{l}{L} + \epsilon\frac{mca_x}{2}\frac{l}{L}\left(\delta_z + 1\right)\cos 2\eta, \tag{B.10}$$

$$\frac{dZ}{d\eta} = \frac{1-\zeta_0^2}{2\zeta_0^2 k_z} + \frac{k_z l^2}{4} + \frac{1}{2k_z}\left(\frac{P_x}{mc\zeta_0}\right)^2 - \frac{P_x}{mc\zeta_0}\sigma l \sin\eta + \frac{k_z l^2}{4}\left(\delta_z - 1\right)\cos 2\eta, \tag{B.11}$$

which are the same as Eqs. (3.94)-(3.96) with $\delta_x = 1$. For comparison, we remind that when the preparatory gauge transformation defined by Eq. (3.99) is employed, the zeroth order 1-form and the resultant equations of motion in the X and Z directions are given by Eq. (3.107) and Eqs. (3.118)-(3.120), respectively. We here rewrite them remaining δ_z:

$$\Gamma_0^{(0)}\Big|_S = \frac{m^2c^2 + P_x^2 + p_\eta^2}{2p_\eta k_z} - (1+\alpha)\, P_x l(X)\sigma \sin\eta + \alpha^2 \frac{p_\eta k_z l^2(X)}{4}, \tag{B.12}$$

$$\Gamma_6^{(0)}\Big|_S = \frac{k_z l^2}{8}\left(\delta_z - \alpha^2\right)\sin 2\eta, \tag{B.13}$$

and $\Gamma_1^{(0)}\big|_S = P_x$, $\Gamma_2^{(0)}\big|_S = P_y$, $\Gamma_3^{(0)}\big|_S = p_\eta$ and $\Gamma_4^{(0)}\big|_S = \Gamma_5^{(0)}\big|_S = \Gamma_6^{(0)}\big|_S = 0$ are the zeroth order components of the covariant vector, and the equations of motion in the X and Z directions are given by

$$\left.\frac{dX}{d\eta}\right|_S = \frac{P_x}{mc\zeta_0 k_z}, \tag{B.14}$$

$$\left.\frac{dP_x}{d\eta}\right|_S = -\epsilon\frac{mca_x}{2}\frac{l}{L}, \tag{B.15}$$

$$\left.\frac{dZ}{d\eta}\right|_S = \frac{1-\zeta_0^2}{2\zeta_0^2 k_z} + \frac{k_z l^2}{4} + \frac{1}{2k_z}\left(\frac{P_x}{mc\zeta_0}\right)^2 - \frac{P_x}{mc\zeta_0}\sigma l \sin\eta + \frac{k_z l^2}{4}\left(\delta_z - 1\right)\cos 2\eta, \tag{B.16}$$

We herein use the subscript $|_S$ for the 1-form and the resulting equation of motion in which the gauge transformation Eq. (3.99) is applied, in order to avoid confusing

with those without the gauge transformation Eqs. (B.9)-(B.11). Here we fix $\delta_z = -1$ in Eqs. (B.9)-(B.11) and $\delta_z = 1$ in Eqs. (B.14)-(B.16) that lead to

$$\frac{dX}{d\eta} = \frac{P_x}{mc\zeta_0 k_z}, \tag{B.17}$$

$$\frac{dP_x}{d\eta} = -\epsilon\frac{mca_x}{2}\frac{l}{L}, \tag{B.18}$$

$$\frac{dZ}{d\eta} = \frac{1-\zeta_0^2}{2\zeta_0^2 k_z} + \frac{k_z l^2}{4} + \frac{1}{2k_z}\left(\frac{P_x}{mc\zeta_0}\right)^2 - \frac{P_x}{mc\zeta_0}\sigma l\sin\eta - \frac{k_z l^2}{2}\cos 2\eta, \tag{B.19}$$

and

$$\left.\frac{dX}{d\eta}\right|_S = \frac{P_x}{mc\zeta_0 k_z}, \tag{B.20}$$

$$\left.\frac{dP_x}{d\eta}\right|_S = -\epsilon\frac{mca_x}{2}\frac{l}{L}, \tag{B.21}$$

$$\left.\frac{dZ}{d\eta}\right|_S = \frac{1-\zeta_0^2}{2\zeta_0^2 k_z} + \frac{k_z l^2}{4} + \frac{1}{2k_z}\left(\frac{P_x}{mc\zeta_0}\right)^2 - \frac{P_x}{mc\zeta_0}\sigma l\sin\eta. \tag{B.22}$$

From Eqs. (B.18) and (B.21), one can see that both procedures, i.e., the coordinate transformation with $\delta_z = -1$ and the gauge transformation Eq. (3.99), successfully remove the oscillation from the X direction. However, comparing Eq. (B.19) and Eq. (B.22), we find that an additional oscillatory term proportional to $\cos 2\eta$ appears in the case employing $\delta_z = -1$, i.e., the last term on the RHS of Eq. (B.19). This oscillation is twice the zeroth order figure-eight oscillation in the z direction (See the figure-eight motion obtained in Eq. (3.67)). The appearance of such a term is consistent with the fact that Eq. (B.19) is derived on the basis of the non-oscillation center coordinates where the sign of oscillation is reversed as $\delta_z = -1$.

Hereafter, we proceed the Lie perturbation analysis up to the third order of ϵ using the 1-form without the gauge transformation considered in Sec. 3.2.2. In the following analysis, we remain δ_z not being fixed to -1 in order to see its role explicitly. Finally, a comparison between the equations of motion derived in this appendix and those obtained in Sec. 3.2 is disscussed.

B.2 Lie perturbation analysis in the non-oscillation center coordinates

First-order analysis

The first-order component of the covariant vector Γ_μ is given by

$$\Gamma_\mu^{(1)} = \Bigg(-\frac{p_\eta k_z l^2}{4}\alpha\sigma\frac{l}{L}\left(\cos\eta - \cos 3\eta\right); \\ \frac{p_\eta k_z l}{2}\frac{l}{L}\left(\alpha - \frac{\delta_z}{2}\right)\sin 2\eta + P_x\sigma\frac{l}{L}\cos\eta, 0, 0, 0, 0, 0\Bigg) = C_\mu^{(1)}, \tag{B.23}$$

from which Γ'_0 in the Lie-transformed coordinates is obtained as

$$\Gamma_0'^{(1)} = \overline{C_\mu^{(1)} \left(V^{(0)\mu}\right)^{(0)}} = 0, \tag{B.24}$$

Hence, the first order 1-form $\Gamma_\mu'^{(1)} dZ'$ is independent of δ_z, and the equation of motion up to the first order of ϵ is same as that of the zeroth order.

The first order oscillatory terms are obtained from the first-order Lie generator, which is given by

$$g^{(1)1} = -\frac{1}{4}\left(1+\frac{\delta_z}{2}\right) l \frac{l}{L} \cos 2\eta, \tag{B.25}$$

$$g^{(1)3} = -\frac{k_z l^2}{4}\sigma \frac{l}{L}\left(1+\frac{\delta_z}{2}\right)\left(\sin\eta - \frac{1}{3}\sin 3\eta\right), \tag{B.26}$$

$$g^{(1)4} = \frac{mca_x}{2}\frac{l}{L}\left(1+\frac{\delta_z}{2}\right)\sin 2\eta, \tag{B.27}$$

and $g^{(1)2} = g^{(1)5} = g^{(1)6} = 0$ where we have substituted the solution $p_\eta = -mc\zeta_0$ and $\alpha\,(= p_\eta/mc\zeta_0) = -1$. The components $g^{(1)1}$, $g^{(1)3}$ and $g^{(1)4}$ are found to depend on δ_z, which indicates that the choice of δ_z affects the first order oscillation of X, Z and P_x after the backward Lie transformation $\mathscr{G}_{\rm b}^\mu(\cdot) = \mathscr{I}^\mu(\cdot) - \epsilon g^{(1)\mu}(\cdot)$.

Here, we consider the relation between Eqs. (B.27) and (B.10). By solving the equation of motion (B.10) assuming a_x and l/L are constant, we can obtain an approximated solution for the oscillatory part of P'_x as

$$\left[P'_x\right]_{\rm os.} = \epsilon\frac{mca_x}{4}\frac{l}{L}\left(\delta_z+1\right)\sin 2\eta, \tag{B.28}$$

which indicates that $\delta_z = 1$ adds the oscillation $\epsilon mca_x l L^{-1}\sin(2\eta)/2$ to the solution for $\delta_z = -1$. This solution is transformed backwardly as

$$P_x = P'_x - \frac{mca_x}{2}\frac{l}{L}\left(1+\frac{\delta_z}{2}\right)\sin 2\eta. \tag{B.29}$$

In the above backward transformation, $\delta_z = -1$ adds $\epsilon mca_x l L^{-1}\sin(2\eta)/2$ to the solution for $\delta_z = 1$. As a consequense, the same first-order oscillation in the original coordinate P_x is obtained after the backward transformation regardless of $\delta_z = \pm 1$.

Second-order analysis

The second-order component of the covariant vector Γ_μ is independent of δ_z and is given by

$$\begin{aligned}\Gamma_\mu^{(2)} = \Bigg(& -\frac{p_\eta}{16}k_z l^2 \alpha \frac{l^2}{R}\left(1-\cos 4\eta\right) \\ & ; \frac{p_\eta k_z l}{8}\alpha\sigma\left(\frac{l^2}{R}+2\frac{l^2}{L^2}\right)\left(\sin 3\eta + \sin\eta\right), 0, 0, 0, 0, 0\Bigg).\end{aligned} \tag{B.30}$$

Here, note that as can be seen from Eqs. (3.103) and (3.104), the components smaller than order ϵ^2 have no dependence on δ_z. Γ_0'' in the Lie-transformed coordinates is calculated from

$$\Gamma_0''^{(2)} = \overline{D_\mu^{(2)} \left(V^{(0)\mu}\right)^{(0)}}, \tag{B.31}$$

which finally leads to the 1-form up to the second-order in the Lie-transformed coordinates:

$$Z''^{\mu} = \left(\eta; X'', Y'', Z'', P_x'', P_y'', p_\eta''\right) \tag{B.32}$$

$$\begin{aligned}
\Gamma_\mu'' = \Bigg(& \frac{m^2c^2 + P_x''^2 + P_y''^2 + p_\eta''^2}{2p_\eta'' k_z} - (1+\alpha) P_x'' \sigma l \sin\eta + \frac{p_\eta'' k_z l^2}{4} \left[\alpha^2 - \left(\delta_z + \alpha^2\right)\cos 2\eta\right] \\
& + \epsilon^2 \frac{l}{16} p_\eta'' k_z l \Bigg[- \left(2\alpha^3 + (1-\delta_z)\alpha^2 - 2\delta_z\alpha - \delta_z\right)\frac{l^2}{R} \\
& \qquad - \left(4\alpha^3 + \left(-\frac{3}{2}\delta_z + 4\right)\alpha^2 - 4\delta_z\alpha - 2\delta_z + \frac{\delta_z^2}{4}\right)\frac{l^2}{L^2}\Bigg] \\
& + \epsilon^2 \frac{P_x''^2}{p_\eta'' k_z}\left[\frac{1}{2}(1+\alpha)\frac{l^2}{R} - \left(\alpha + \frac{1}{4}\right)\frac{l^2}{L^2}\right] \\
& ; P_x'', P_y'', p_\eta'', 0, 0, 0 \Bigg),
\end{aligned} \tag{B.33}$$

As in Sec. 3.2, by using the solution $p_\eta'' = -mc\zeta_0 \Leftrightarrow 1 + \alpha = 0$, we obtain the equations of motion in the X direction as

$$\frac{dX''}{d\eta} = \frac{P_x''}{mc\zeta_0 k_z}\left(1 + \epsilon^2 \frac{3}{2}\frac{l^2}{L^2}\right), \tag{B.34}$$

$$\begin{aligned}
\frac{dP_x''}{d\eta} = & -\frac{mca_x}{2}\left[\epsilon\frac{l}{L} + \frac{\epsilon^3}{8}\left(\mathrm{A}_1\frac{l}{L}\frac{l^2}{R} + \frac{l^3}{T} + \mathrm{A}_2\frac{l^3}{L^3}\right)\right] \\
& + \epsilon\frac{mca_x}{2}\frac{l}{L}(1+\delta_z)\cos 2\eta,
\end{aligned} \tag{B.35}$$

where

$$\mathrm{A}_1 = -\delta_z - \frac{\delta_z^2}{2} + 3, \tag{B.36}$$

$$\mathrm{A}_2 = -\delta_z - \frac{\delta_z^2}{2}. \tag{B.37}$$

Here, we neglected the term proportional to $P_x''^2 L^{-1} R^{-1} \sim \epsilon^5$ as in Sec. 3.2. We have $(\mathrm{A}_1, \mathrm{A}_2) = (3/2, -3/2)$ for $\delta_z = 1$ and $(\mathrm{A}_1, \mathrm{A}_2) = (7/2, 1/2)$ for $\delta_z = -1$. The equation of motion for Z'' is obtained from (B.33) and using the solution $p_\eta'' = -mc\zeta_0$

as

$$\frac{dZ''}{d\eta} = \frac{1-\zeta_0^2}{2\zeta_0^2 k_z} + \frac{k_z l^2}{4} + \frac{1}{2k_z}\left(\frac{P_x''}{mc\zeta_0}\right)^2 - \delta_{p_x}\frac{P_x''}{mc\zeta_0}\sigma l\sin\eta + \frac{k_z l^2}{4}(\delta_z - 1)\cos 2\eta - \epsilon^2\frac{k_z l^2}{16}\left[-3\frac{l^2}{R} + \frac{l^2}{L^2}\left(-4 + \frac{\delta_z}{2} - \frac{\delta_z^2}{4}\right)\right]. \tag{B.38}$$

First, we discuss the equations of motion in the X'' direction, i.e., Eqs. (B.34) and (B.35), for cases $\delta_z = 1$ and -1. In the case of $\delta_z = 1$, which corresponds to the usual oscillation center coordinate, Eq. (B.35) becomes

$$\frac{dP_x''}{d\eta} = -\frac{mca_x}{2}\left[\epsilon\frac{l}{L} + \frac{\epsilon^3}{8}\left(\frac{3}{2}\frac{l}{L}\frac{l^2}{R} + \frac{l^3}{T} - \frac{3}{2}\frac{l^3}{L^3}\right)\right] + \epsilon mca_x\frac{l}{L}\cos 2\eta, \tag{B.39}$$

while in the case of $\delta_z = -1$, it becomes

$$\frac{dP_x''}{d\eta} = -\frac{mca_x}{2}\left[\epsilon\frac{l}{L} + \frac{\epsilon^3}{8}\left(\frac{7}{2}\frac{l}{L}\frac{l^2}{R} + \frac{l^3}{T} + \frac{1}{2}\frac{l^3}{L^3}\right)\right]. \tag{B.40}$$

Equations (B.39) and (B.40) exhibit two different points; one is the coefficients of the third order terms, and another is the oscillatory term appearing only in Eq. (B.39). The latter indicates that the coordinate transformation with $\delta_z = -1$ successfully removes the 1st-order oscillatory term originating from the 0th-order 1-form. To consider the difference in the coefficients of the secular terms, we compare them with the secular term obtained in Sec. 3.2, in which a preparatory gauge transformation is employed. The equation of motion derived in Sec. 3.2 is given by Eq. (3.145), i.e.,

$$\frac{dP_x''}{d\eta} = -\frac{mca_x}{2}\left[\epsilon\frac{l}{L} + \frac{\epsilon^3}{8}\left(\frac{7}{2}\frac{l}{L}\frac{l^2}{R} + \frac{l^3}{T} + \frac{1}{2}\frac{l^3}{L^3}\right)\right]. \tag{B.41}$$

From Eqs. (B.39)-(B.41), it is found that the secular terms are same in Eqs. (B.40) and (B.41), whereas different in Eq. (B.39). This result can be considered as follows. In Eq. (B.39), a first-order oscillatory term is remained, which generates an oscillation in the X'' direction in the order of ϵ. Here, notice that the first-order oscillatory term includes a_x, l and L^{-1} that are evaluated at X''. Therefore, when the oscillating X'' is substituted in a_x, l and L^{-1}, it may generates the higher order secular terms. For this reason, we can conclude that the third order term in Eq. (B.39) does not represent the secular force completely. This result indicates the importance of elliminating the oscillatory terms completely from the equation of motion.

Next, we discuss the equation of motion in the Z'' direction, i.e., Eqs. (B.38), for cases $\delta_z = 1$ and -1. In the case of $\delta_z = 1$, which corresponds to the oscillation

center coordinate, Eq. (B.38) becomes

$$\frac{dZ''}{d\eta} = \frac{1-\zeta_0^2}{2\zeta_0^2 k_z} + \frac{k_z l^2}{4} + \frac{1}{2k_z}\left(\frac{P_x''}{mc\zeta_0}\right)^2 - \frac{P_x''}{mc\zeta_0}\sigma l \sin\eta + \epsilon^2 \frac{k_z l^2}{16}\left(3\frac{l^2}{R} + \frac{15}{4}\frac{l^2}{L^2}\right), \tag{B.42}$$

while in the case of $\delta_z = -1$, it becomes

$$\frac{dZ''}{d\eta} = \frac{1-\zeta_0^2}{2\zeta_0^2 k_z} + \frac{k_z l^2}{4} + \frac{1}{2k_z}\left(\frac{P_x''}{mc\zeta_0}\right)^2 - \frac{P_x''}{mc\zeta_0}\sigma l \sin\eta - \frac{k_z l^2}{2}\cos 2\eta + \epsilon^2 \frac{k_z l^2}{16}\left(3\frac{l^2}{R} + \frac{19}{4}\frac{l^2}{L^2}\right). \tag{B.43}$$

Here, we again see the zeroth order figure-eight oscillation proportional to $\cos 2\eta$ in the fifth term of Eq. (B.43), which is consistent with the fact that Eq. (B.43) is derived on the basis of the non-oscillation center coordinates with $\delta_z = -1$. In addition, we find that the coefficient of the last term in Eqs. (B.42) and (B.43) is different. The difference is considered to originate from the oscillatory term in the X'' direction in Eq. (B.39), as same as the discussion for Eqs. (B.39) and (B.40) in the previous paragraph. Namely, the difference of coefficient suggests that the first-order oscillation of P_x'' and X'' couples in the fourth fifth term on the RHS of Eq. (B.42).

Appendix C

Equations of motion in a laser field with a small longitudinal component

C.1 Vector potential with the longitudinal z-component

In the Lie perturbation analysis presented in Chap. 3, we assumed a laser field given by $\mathbf{a} = a_x(x)\sin\eta\,\hat{\mathbf{e}}_x$. However, electromagnetic fields with non-uniform amplitude profiles in vacuum must have extra components of the vector potential in satisfying the Maxwell equations. For instance, when the gradient of the field amplitude is assumed to be $\mathscr{O}(\epsilon)$ as in the present study, the z-component of the vector potential a_z in the first order of ϵ appears as the solution for the Maxwell equations [45, 46]. In this appendix, we investigate how the inclusion of ϵa_z affects the formulation of the higher-order ponderomotive force.

In Sec. 1.3.2 in the introduction, we derived the wave equation in vacuum in the form

$$\left(\frac{\partial^2}{\partial x^2}+\frac{\partial^2}{\partial y^2}+\frac{\partial^2}{\partial z^2}\right)a_i = 2ik_z\frac{\partial}{\partial z}a_i, \tag{C.1}$$

i.e., Eq. (E.13),where $a_i(i=x,y,z)$ is the amplitude part of the normalized vector potential. Here, the Coulomb gauge $\nabla\cdot\mathbf{a}=0$ is employed, which is expressed in the coordinates $(\eta=\omega t-k_z z,x,y,z)$ as

$$\nabla\cdot\mathbf{a}+k_z\frac{\partial}{\partial\eta}\hat{\mathbf{e}}_z\cdot\mathbf{a}=0. \tag{C.2}$$

When the field amplitude is x-dependent, i.e. $a_x=a_x(x)$, as assumed in the present study, Eqs. (C.1) and (C.2) lead to

$$\frac{\partial^2 \mathbf{a}}{\partial x^2} = 0, \tag{C.3}$$

$$\frac{\partial}{\partial x}\hat{\mathbf{e}}_x \cdot \mathbf{a} - k_z \frac{\partial}{\partial \eta}\hat{\mathbf{e}}_z \cdot \mathbf{a} = 0. \tag{C.4}$$

Because the spatial derivative of the field amplitude is clasified to $\mathscr{O}(\epsilon)$, Eqs. (C.3) and (C.4) can be satisfied up to the first order of ϵ when the amplitude in the z direction a_z is assumed to be $\mathscr{O}(\epsilon)$.

Therefore, here we assume the laser field as

$$\mathbf{a} = a_x(x)\sin\eta\,\hat{\mathbf{e}}_x + \epsilon a_z \cos\eta\,\hat{\mathbf{e}}_z, \tag{C.5}$$

where a_z is a finite constant amplitude in the order of ϵ. In the following, we investigate how the inclusion of ϵa_z affects the nonlocal ponderomotive force.

C.2 Fundamental one-form with a_z component

In the case where the laser field is assumed to be Eq. (C.5), the covariant vector that corresponds to the coordinates given by Eq. (3.54) has an ϵa_z term in the $\mu = 3$ component as

$$\gamma_\mu = \Bigg(\frac{1}{2p_\eta k_z}\left(m^2c^2 + p_x^2 + p_y^2 + p_\eta^2\right); \\ p_x + mc\sigma a_x(x)\sin\eta, p_y, p_\eta + \epsilon mc\sigma a_z\cos\eta, 0, 0, 0\Bigg). \tag{C.6}$$

After transforming the coordinates to those of the oscillation center given by Eq. (3.71), i.e., $Z^\mu = (\eta; X, Y, Z, P_x, P_y, p_\eta)$, and using the gauge transformation given by the gauge function Eq. (3.99), Eq. (C.6) is transformed to the new one Λ_μ as

$$\gamma_\mu \mapsto \Lambda_\mu = \Gamma_\mu + \Gamma_{\mathrm{add}.\mu}, \tag{C.7}$$

where Γ_μ is given by Eqs. (3.103)-(3.106) and the additional term $\Gamma_{\mathrm{add}.\mu}$ is given by

$$\Gamma_{\mathrm{add}.0} = -\epsilon\frac{k_z l^2}{4}\frac{mc}{2}a_z\sigma\left(\cos 3\eta + \cos\eta\right), \tag{C.8}$$

$$\Gamma_{\mathrm{add}.1} = -\epsilon^2\frac{k_z l}{8}mca_z\sigma\frac{l}{L}\left(\sin 3\eta + \sin\eta\right), \tag{C.9}$$

$$\Gamma_{\mathrm{add}.3} = \epsilon mc\sigma a_z\cos\eta, \tag{C.10}$$

$$\Gamma_{\mathrm{add}.i} = 0 \quad (i = 2, 4, 5, 6). \tag{C.11}$$

Here, we see that since the amplitude a_z is assumed to be $\mathscr{O}(\epsilon)$, the inclusion of a_z does not affect the zeroth order 1-form and the resulting equation of motion.

C.3 Effect of the a_z component to the higher order secular motion

The first-order component of the covariant vector Λ_μ includes a_z in the $\mu = 0$ and $\mu = 3$ components as

$$\Lambda_\mu^{(1)} = \Bigg(-\frac{p_\eta k_z l^2}{4}\alpha\sigma\frac{l}{L}\left(\cos\eta - \cos 3\eta\right) - \epsilon\frac{k_z l^2}{8}mca_z\sigma\left(\cos\eta + \cos 3\eta\right); \\ \frac{p_\eta k_z l}{2}\frac{l}{L}\left(\alpha + \frac{\alpha^2}{2}\right)\sin 2\eta + P_x\sigma\frac{l}{L}\cos\eta, 0, \epsilon mc\sigma a_z\cos\eta, 0, 0, 0\Bigg) = C_\mu^{(1)}. \tag{C.12}$$

By the first order Lie transformation $Z^\mu \mapsto Z'^\mu = \exp\left(\epsilon\mathscr{L}^{(1)}\right)Z^\mu$, the covariant vector is transformed to Λ'_μ. Here, its first order component, $\Lambda_\mu'^{(1)}$, which is derived from the relation $\Lambda_\mu'^{(1)} = \left(\overline{\left(C_\mu^{(1)}V^{(0)\mu}\right)^{(0)}}; \mathbf{0}\right)$, is found to be zero even in the case we include the field component a_z. This indicates that the inclusion of a_z has no influence on the oscillation center motion which is derived from the 1-form up to the first order of ϵ.

Therefore, at first we find $dp'_\eta/d\eta = 0$, which leads to the solution $p'_\eta = const.$ Here, we define $p'_\eta \equiv -mc\zeta'_0$ with a constant ζ'_0 which is determined by the initial condition for p'_η. Then, by substituting the above solution for p'_η, we obtain the equations of motion up to the first order of ϵ in the X' and Z' directions as

$$\frac{dX'}{d\eta} = \frac{P'_x}{mc\zeta'_0 k_z} + \sigma l\left(1 - \frac{\zeta_0}{\zeta'_0}\right)\sin\eta, \tag{C.13}$$

$$\frac{dP'_x}{d\eta} = -\epsilon\frac{\zeta_0}{\zeta'_0}\frac{mca_x}{2}\frac{l}{L} - \epsilon P'_x\sigma\frac{l}{L}\left(1 - \frac{\zeta_0}{\zeta'_0}\right)\sin\eta, \tag{C.14}$$

$$\frac{dZ'}{d\eta} = \frac{1 - \zeta_0'^2}{2\zeta_0'^2 k_z} + \frac{k_z l^2}{4}\frac{\zeta_0^2}{\zeta_0'^2} - \frac{P'_x}{mc\zeta'_0}\sigma l\frac{\zeta_0}{\zeta'_0}\sin\eta + \frac{k_z l^2}{4}\left(1 - \frac{\zeta_0^2}{\zeta_0'^2}\right)\cos 2\eta, \tag{C.15}$$

Note that in the case without the a_z component, $\zeta'_0 = \zeta_0$ is satisfied, and the above equations become equivalent to Eqs. (3.118)-(3.120). However, in the present case with a_z, $\zeta'_0 \neq \zeta_0$ is found, which means that the initial condition for p_η in the original coordinates Z^μ is different from that for p'_η in the Lie transformed coordinates Z'^μ. This can be seen from the first order Lie generator as follows.

In the case with a_z component, the first order gauge function and Lie generator include oscillatory terms that depend on a_z. Namely, the first-order gauge function $S^{(1)}$ is obtained by the relation

$$\frac{\partial S^{(1)}}{\partial\eta} = -\left[C_\mu^{(1)}\left(V^{(0)\mu}\right)\right]_{\text{os.}}, \tag{C.16}$$

and then, the $i = 6$ component of the first-order Lie generator is obtained as

$$g^{(1)6} = \epsilon mc\sigma a_z \cos\eta, \tag{C.17}$$

From Eq. (C.17), we find the initial value of $g^{(1)6}$ as $g^{(1)6}(\eta = 0) = \epsilon mc\sigma a_z$. Hence, we obtain the relationship between initial conditions in the coordinates Z^μ and Z'^μ as

$$p_\eta(\eta = 0) = p'_\eta(\eta = 0) - g^{(1)6}(\eta = 0), \tag{C.18}$$

$$\Leftrightarrow\ p'_\eta(\eta = 0) = -mc\zeta_0 + \epsilon mc\sigma a_z. \tag{C.19}$$

In this case, the equations of motion up to the first order, Eqs. (C.13)-(C.15), suffer from a modification originated from the inclusion of a_z. Namely, the relation $\zeta'_0 = \zeta_0 - \epsilon\sigma a_z$ leads to

$$\frac{dX'}{d\eta} = \frac{P'_x}{mc\zeta_0 k_z}\left(1 + \epsilon\sigma\frac{a_z}{\zeta_0}\right) - \epsilon\frac{a_z}{\zeta_0} l\sin\eta, \tag{C.20}$$

$$\frac{dP'_x}{d\eta} = -\epsilon\frac{mca_x}{2}\frac{l}{L}, \tag{C.21}$$

$$\frac{dZ'}{d\eta} = \frac{1-\zeta_0^2}{2\zeta_0^2 k_z} + \frac{k_z l^2}{4}\left(1 + 2\epsilon\sigma\frac{a_z}{\zeta_0}\right) - \frac{P'_x}{mc\zeta_0}\sigma l\sin\eta + \epsilon\sigma\frac{a_z}{\zeta_0}\frac{k_z l^2}{2}\cos 2\eta, \tag{C.22}$$

where we used the expansion $\zeta_0'^{-1} = \zeta_0^{-1}\left(1 + \epsilon\sigma a_z/\zeta_0\right) + \mathscr{O}\left(\epsilon^2\right)$ and neglected ϵ^2 order terms. Note that the equation of motion in the Y direction is also affected by a_z as

$$\frac{dY'}{d\eta} = \frac{P'_y}{mc\zeta_0 k_z}\left(1 + \epsilon\sigma\frac{a_z}{\zeta_0}\right), \tag{C.23}$$

$$\frac{dP'_y}{d\eta} = 0. \tag{C.24}$$

From Eqs. (C.20) and (C.21), we see that the secular motion in the X' direction is affected by the inclusion of a_z in the second order by the coupling $\epsilon^2 a_z l/L$.

In summary, it is found that the 1-form up to the first order, which is obtained from Eqs. (C.12), has the same form as that in the case without including ϵa_z. Consequently, the equations of motion derived from the 1-form up to the first order are not affected by the inclusion of ϵa_z. However, since the initial condition for p_η and p'_η are different, the equations of motion after substituting the solution p'_η have terms related to a_z in the first order of ϵ as shown in Eqs. (C.20)-(C.24).

Here, note that the correction terms from a_z have σ dependence, that is different from the usual characteristic of the ponderomotive force, i.e., the force does not depend on the charge of particles since it is a pressure force. From this feature, we

can expect that the modulation from a_z denotes not an additional ponderomotive force (light pressure) on the particle, but a modulation related to the coordinate transformation to a different X' in comparison to the case without the a_z component and the corresponding Lorentz transformation of the physical quantities.

For instance, assuming positively charged particles ($\sigma > 0$), we see from Eq. (C.20) that the ponderomotive force is found to be larger than the case without a_z component. Note here that for positive charges $\sigma > 0$, the relation ζ_0' $(= \zeta_0 - \epsilon\sigma a_z) < \zeta_0$ is found. Then, from the definition of ζ_0, i.e., $p_{z0}/mc = \gamma_0 - \zeta_0$, one can see that the above decrease of ζ_0 corresponds to the increase of the initial momentum in the positive z direction, p_{z0}. Therefore, we recognize that the X' frame with a_z component is moving in the negative z direction in comparison to the X' frame without a_z component. Then, the modulation of the secular term in the X' direction that is proportional to $\epsilon^2 a_z l/L$ is considered to be the effect associated with the change of the transverse E_x field in the moving frame.

In the third order ϵ^3, a term proportional to $\epsilon^3 a_z l^2/R$ is considered, however, is expected to disappear due to the symmetric nature of curvature. The other is a term proportional to $\epsilon^3 a_z l^2/L^2$, which essentially denotes a local effect. Thus, the a_z component is expected not to affect the qualitative characteristics of the nonlocal ponderomotive force derived in Chap. 3.

Appendix D

Ponderomotive potential up to ϵ^3

In Sec. 3.4.3, we have mentioned that the third order ponderomotive force derived by the Lie perturbation method cannot be expressed as a potential force that is proportional to the gradient of a scalar potential. In this appendix, we verify the above fact.

The equation of motion in the X'' direction up to the third order of ϵ, which represents the nonlocal ponderomotive force up to ϵ^3, is given by Eq. (3.147), i.e.,

$$\frac{d^2X''}{d\eta^2} = -\epsilon\frac{l}{2}\frac{l}{L} - \epsilon^3\frac{l}{16}\left(\frac{7}{2}\frac{l}{L}\frac{l^2}{R} + \frac{l^3}{T} + \frac{25}{2}\frac{l^3}{L^3}\right). \tag{D.1}$$

As is noted in Sec. 3.4.3, the first order ponderomotive force, i.e., the first term on the RHS of Eq. (D.1), can be expressed in the potential form as

$$\frac{d^2X''^{(1)}}{d\eta^2} = -\nabla\phi_p^{(1)}; \quad \phi_p^{(1)} = \frac{1}{4}l^2, \tag{D.2}$$

where $\nabla = \partial/\partial X''$.

Next, we consider to express the third order term on the RHS of Eq. (D.1) also in the scalar potential form $\nabla\phi_p$. Here, we write down all the candidates for ϕ_p that has the dimension of $l^4\nabla^2$ so that the dimension of $\nabla\phi_p$ becomes $l^4\nabla^3$, which is same as the dimension of the third order term on the RHS of Eq. (D.1). Then, considering a superposition of the candidate terms, we seek the possibility of obtaining the third order ponderomotive potential ϕ_p.

First, we find that the possible scalar can be cathegolized into the following three groups **A**-**C**:

Group A: Those equivalent to

$$\nabla\left(l^2\left(\nabla l\right)\left(\nabla l\right)\right) = 2l\left(\nabla l\right)^3 + 2l^2\left(\nabla^2 l\right)\left(\nabla l\right) = 2l\left(\frac{l^3}{L^3} + \frac{l}{L}\frac{l^2}{R}\right), \tag{D.3}$$

i.e.,

$$\nabla\left(l\left(\nabla l\right)\left(\nabla l^2\right)\right) = 2\nabla\left(l^2\left(\nabla l\right)\left(\nabla l\right)\right), \tag{D.4}$$

$$\nabla\left(\left(\nabla l^2\right)\left(\nabla l^2\right)\right) = 4\nabla\left(l^2\left(\nabla l\right)\left(\nabla l\right)\right), \tag{D.5}$$

$$\nabla\left(\left(\nabla l\right)\left(\nabla l^3\right)\right) = 3\nabla\left(l^2\left(\nabla l\right)\left(\nabla l\right)\right), \tag{D.6}$$

Group B:

$$\nabla\left(l^3\left(\nabla^2 l\right)\right) = 3l^2\left(\nabla l\right)\left(\nabla^2 l\right) + l^3\nabla^3 l = l\left(3\frac{l}{L}\frac{l^2}{R} + \frac{l^3}{T}\right), \tag{D.7}$$

Group C:

$$\nabla\left(l^2\left(\nabla^2 l^2\right)\right) = 2l\left(\nabla l\right)\left(\nabla^2 l^2\right) + l^2\nabla^3 l^2 = 2l\left(2\frac{l^3}{L^3} + 5\frac{l}{L}\frac{l^2}{R} + \frac{l^3}{T}\right). \tag{D.8}$$

Note that the other possible derivative operations,

$$\nabla\left(l\left(\nabla^2 l^3\right)\right) = \left(\nabla l\right)\left(\nabla^2 l^3\right) + l\nabla^3 l^2 = 3l\left(4\frac{l^3}{L^3} + 7\frac{l}{L}\frac{l^2}{R} + \frac{l^3}{T}\right), \tag{D.9}$$

and

$$\nabla\left(\left(\nabla^2 l^4\right)\right) = 8l\left(3\frac{l^3}{L^3} + 9\frac{l}{L}\frac{l^2}{R} + 2\frac{l^3}{T}\right), \tag{D.10}$$

can be constructed from groups **A** and **B** as

$$\frac{1}{8}(\text{Eq. (D.10)}) = \frac{3}{2}(\text{Eq. (D.3)}) + 2(\text{Eq. (D.7)}), \tag{D.11}$$

and from groups **B** and **C** as

$$\frac{1}{3}(\text{Eq. (D.9)}) = (\text{Eq. (D.8)}) - (\text{Eq. (D.7)}), \tag{D.12}$$

respectively. Combining the independent bases **A**-**C**, we construct the second term on the RHS of Eq. (D.1) which consists of terms for L^{-3}, $R^{-1}L^{-1}$ and T^{-1} with the ratio $25:7:2$. Namely, we consider the following equation with coefficients A, B and C to be determined:

$$\begin{aligned} A\left(L^{-3} + L^{-1}R^{-1}\right) + B\left(3L^{-1}R^{-1} + T^{-1}\right) + C\left(2L^{-3} + 5L^{-1}R^{-1} + T^{-1}\right) \\ = 25L^{-3} + 7L^{-1}R^{-1} + 2T^{-1}. \end{aligned} \tag{D.13}$$

By comparing coefficients of $L^{-3}, L^{-1}R^{-1}$ and T^{-1}, we have a system of equations given by

$$\begin{pmatrix} 1 & 0 & 2 \\ 1 & 3 & 5 \\ 0 & 1 & 1 \end{pmatrix}\begin{pmatrix} A \\ B \\ C \end{pmatrix} = \begin{pmatrix} 25 \\ 7 \\ 2 \end{pmatrix}. \tag{D.14}$$

The augmented matrix is simplified to

$$\begin{pmatrix} 1 & 0 & 2 & 1 \\ 0 & 1 & 1 & 2 \\ 0 & 0 & 0 & 1 \end{pmatrix}, \tag{D.15}$$

whose rank is 3 whereas that of the coefficient matrix is 2. Therefore, we conclude that the solution for A, B and C that satisfies Eq. (D.14) does not exist except $(A, B, C) = (0, 0, 0)$.

The above result indicates that there exists no scalar potential ϕ_p that can represent the third order ponderomotive force as the potential form as $d^2X''/d\eta^2 = -\nabla\phi_p$.

Appendix E

Laser beam propagation in vacuum

E.1 Laser beam propagation in the Hermite-Gaussian mode

In the introduction, we discussed the laser beam propagation in plasmas. In this appendix, we consider the laser beam propagation in vacuum.

We start from the wave equation for the vector potential,

$$\frac{1}{c^2}\frac{\partial^2 \mathbf{a}}{\partial t^2} - \nabla^2 \mathbf{a} = \frac{4\pi e}{m_e c}\mathbf{J}, \tag{E.1}$$

and the Poisson equation for the scalar potential,

$$-\nabla^2 \phi = \frac{4\pi e}{m_e c^2}\rho. \tag{E.2}$$

which are derived in Sec. 1.3.2.

In the case of vacuum, the laser vector potential satisfies the wave equation Eq. (E.1) with $\mathbf{J} = \mathbf{0}$, i.e.,

$$\frac{1}{c^2}\frac{\partial^2 \mathbf{a}}{\partial t^2} - \nabla^2 \mathbf{a} = \mathbf{0}. \tag{E.3}$$

A laser beam is assumed to be linearly polarized and propagate in the z direction, while its amplitude is non-uniform transversely and also longitudinally. We here employ the paraxial approximation assuming that the wave vector of the electromagnetic field lies in a narrow cone with a small opening angle:

$$\frac{|\mathbf{k}_\perp|}{k_z} \ll 1, \tag{E.4}$$

Here, we note that the plane wave solution for the Maxwell equation, in which

$|\mathbf{k}_\perp| = 0$ is satisfied, has a spatially uniform amplitude as

$$\mathbf{a} = \mathbf{a}_0 e^{i\omega t - ik_z z}, \tag{E.5}$$

where $\mathbf{a}_0$ is constant. From this fact, we can expect that the paraxial field satisfying Eq. (E.4) has a gentle amplitude variation. In expressing such a gentle amplitude variation in the z (or time t) direction, we note the fact that the envelope propagates rapidly with the group velocity $v_g = d\omega/dk$, which is equivalent to c in vacuum. Therefore, we here introduce coordinates that moves in the z direction with velocity v_g. Namely, we define a new coordinate variable $\tau = t - \frac{v_g}{c^2} z$ and transform coordinates as

$$(t, z) \mapsto (\tau, z)\,. \tag{E.6}$$

In this coordinate, the gently-varying field amplitude may be a function of x, y and z. Hence, we assume an electric field given by

$$a_x = f\,(x, y, z)\, e^{i\omega\tau}, \tag{E.7}$$
$$a_y = 0, \tag{E.8}$$
$$a_z = g\,(x, y, z)\, e^{i\omega\tau}, \tag{E.9}$$

where spatial derivative of the amplitude are small compared with the wavelength, i.e.,

$$k_z^{-1}\nabla f \ll 1, \quad k_z^{-1}\nabla g \ll 1. \tag{E.10}$$

In the coordinate (τ, x, y, z), derivatives in the wave equations Eq. (E.3) becomes

$$\frac{\partial^2}{\partial t^2} = \frac{\partial^2}{\partial \tau^2}, \tag{E.11}$$
$$\begin{aligned}\frac{\partial^2}{\partial z^2} &= \frac{\partial}{\partial z}\left(\frac{\partial}{\partial z} - \frac{v_g}{c^2}\frac{\partial}{\partial \tau}\right) \\ &= \frac{\partial^2}{\partial z^2} - 2\frac{v_g}{c^2}\frac{\partial^2}{\partial \tau \partial z} + \frac{v_g^2}{c^4}\frac{\partial^2}{\partial \tau^2}.\end{aligned} \tag{E.12}$$

By using these relations, the wave equation Eq. (E.3) leads to the equation for the envelope f given by

$$\frac{\partial^2 f}{\partial x^2} + \frac{\partial^2 f}{\partial y^2} + \frac{\partial^2 f}{\partial z^2} = 2ik_z \frac{\partial f}{\partial z}. \tag{E.13}$$

The same relation is obtained for the envelope g, and the relation between f and g

are derived from the Poisson equation Eq. (E.2) as

$$\frac{\partial f}{\partial x} = ik_z g - \frac{\partial g}{\partial z}. \tag{E.14}$$

To analize Eq. (E.3), we here define a smallness parameter $\epsilon \ll 1$ by the ratio between spatial derivatives of the field amplitude and the wavelength as

$$k_z^{-1}\frac{\partial f}{\partial x} \sim k_z^{-1}\frac{\partial f}{\partial y} \sim \epsilon. \tag{E.15}$$

Then, the order of each term in Eq. (E.13) can be expressed as

$$\left(\epsilon^2 \frac{1}{k_z^2}\frac{\partial^2}{\partial x^2} + \epsilon^2 \frac{1}{k_z^2}\frac{\partial^2}{\partial y^2} + \frac{1}{k_z^2}\frac{\partial^2}{\partial z^2} - 2\frac{i}{k_z}\frac{\partial}{\partial z}\right) f = 0. \tag{E.16}$$

From Eq. (E.16), we can see that the last term on the LHS needs to be the order of ϵ^2, i.e.,

$$k_z^{-1}\frac{\partial f}{\partial z} \sim \epsilon^2. \tag{E.17}$$

Under this assumption, we neglect the third term on the LHS of Eq. (E.16), which is $\mathscr{O}\left(\epsilon^4\right)$, and then we obtain the Helmholtz equation for the paraxial field:

$$\frac{\partial^2 f}{\partial x^2} + \frac{\partial^2 f}{\partial y^2} = 2ik_z \frac{\partial f}{\partial z}. \tag{E.18}$$

Here, we find a solution for Eq. (E.18) in the form

$$f(x,y,z) = X(\xi)\, Y(\eta)\, Z(z) \exp\left[-\frac{x^2+y^2}{F(z)}\right], \tag{E.19}$$

where $\xi = x/G(z)$ and $\eta = y/G(z)$. In this case, Eq. (E.18) becomes

$$\begin{aligned}&\frac{1}{X}\left(\frac{X''}{G^2} - \frac{4\xi X'}{F} + \frac{2ik_z \xi G' X'}{G}\right) + \frac{1}{Y}\left(\frac{Y''}{G^2} - \frac{4\eta Y'}{F} + \frac{2ik_z \eta G' Y'}{G}\right) \\ &- \frac{4}{F} - \frac{2ik_z Z'}{Z} + \frac{2\left(\xi^2+\eta^2\right)G^2}{F^2}\left(2 - ik_z F'\right) = 0.\end{aligned} \tag{E.20}$$

Here, since F, X and Y must be a function only of z, ξ and η, respectively, terms on the LHS of Eq. (E.20) yield to

$$2 - ik_z F' = 0, \tag{E.21}$$

and requirements such that

$$X'' - 2\xi X' \left(\frac{2G^2}{F} - ik_z GG' \right), \tag{E.22}$$

must be a function of ξ and

$$Y'' - 2\eta Y' \left(\frac{2G^2}{F} - ik_z GG' \right), \tag{E.23}$$

must be a function of η. The above two requirements are satisfied by

$$\frac{2G^2}{F} - ik_z GG' = C_1 = \text{const.} \tag{E.24}$$

Here, we choose $C_1 = 1$ without loss of generality. From Eqs. (E.21) and (E.24), the relation

$$-\frac{2F'G^2}{F^3} + \frac{2GG'}{F^2} = -\frac{F'}{F^2}, \tag{E.25}$$

is obtained, which can be solved as

$$G^2 = F + C_2 F^2, \tag{E.26}$$

where C_2 is a constant of integration.

On the other hand, Eq. (E.21) can be satisfied by

$$F = \frac{2}{ik_z}(z - z_0) + w_0^2, \tag{E.27}$$

where w_0 is the beam waist size at $z = z_0$.

Finally, by substituting Eqs. (E.21) and (E.24) to Eq. (E.20), we obtain

$$\left(X'' - 2\xi X'\right)\frac{1}{X} + \left(Y'' - 2\eta Y'\right)\frac{1}{Y} - \left(\frac{4}{F} + \frac{2ik_z Z'}{Z}\right) G^2 = 0. \tag{E.28}$$

Separation of variables leads to

$$X'' - 2\xi X' + 2nX = 0, \tag{E.29}$$

$$Y'' - 2\eta Y' + 2mY = 0, \tag{E.30}$$

$$-\left(\frac{4}{F} + 2ik_z \frac{Z'}{Z}\right) G^2 = 2(m+n), \tag{E.31}$$

where we choose constants in the separation by m and n. The solutions for Eqs. (E.29) and (E.30) are khown to be the Hermite polynomial, and therefore, we obtain

$$X = H_m(\xi), \quad Y = H_n(\eta). \tag{E.32}$$

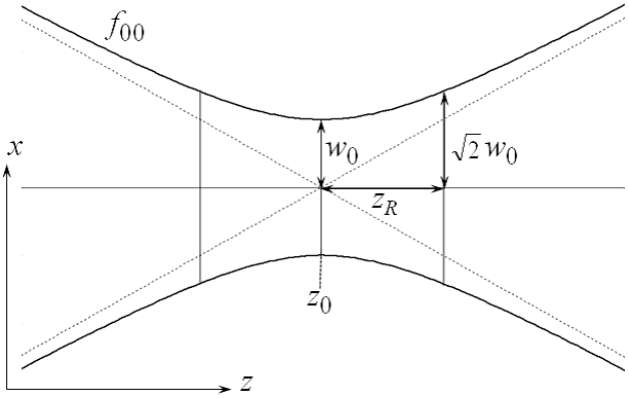

Figure E.1: The lowest order mode of the Hermite Gaussian beam profile in the x-z plane.

The fundamental properties of the Hermite polynomial are given in the next section (Sec. E.2). On the other hand, the solution for Z is obtained from Eq. (E.31) as

$$Z = C_3 F^{-\frac{m+n+2}{2}} \left(1 + C_2\right)^{\frac{m+n}{2}}, \tag{E.33}$$

where C_3 is a constant of integration. Thus, the general solution for Eq. (E.20) is given by

$$f = \sum_{n=0}^{\infty} \sum_{m=0}^{\infty} f_{mn}, \tag{E.34}$$

where

$$f_{mn} = \frac{C_3}{F} \left(\frac{1 + C_2 F}{F}\right)^{\frac{m+n}{2}} H_m\left(\frac{x}{\sqrt{F + C_2 F^2}}\right) H_n\left(\frac{y}{\sqrt{F + C_2 F^2}}\right) \exp\left[-\frac{x^2 + y^2}{F}\right], \tag{E.35}$$

Here, $F = F\left(z\right)$ is given by Eq. (E.27). When we choose $C_2 = 0$, Eq. (E.35) reduces to

$$f_{mn} = \frac{C_3}{F^{\frac{m+n+2}{2}}} H_m\left(\frac{x}{\sqrt{F}}\right) H_n\left(\frac{y}{\sqrt{F}}\right) \exp\left[-\frac{x^2 + y^2}{F}\right], \tag{E.36}$$

which is referred to as the Hermite-Gaussian mode with the mode number of (m, n). The lowest order mode f_{00} is referred to as the fundamental Gaussian mode which is given using the relation $H_0\left(x\right) = 1$ and introducing the Rayleigh length $z_R = k_z w_0^2/2$ as

$$f_{00}(x,y,z) = \frac{1}{w_0\sqrt{1+z^2/z_R^2}} \exp\left[-\frac{x^2+y^2}{w_0^2\left(1+z^2/z_R^2\right)}\right] \times \exp\left[i\left(k_z z + \frac{z}{z_R}\frac{x^2+y^2}{w_0^2\left(1+z^2/z_R^2\right)} - \arctan\left(\frac{z}{z_R}\right)\right)\right], \quad \text{(E.37)}$$

where $C_3 = w_0^2$ is defined to satisfy $f_{00}(0,0,z_0) = 1$. The last term in the phase component, $-\arctan(z/z_R)$, is referred to as Gouy phase. In Fig. E.1, we show f_{00} in the x-z plane.

E.2 Hermite polynomial

Here, we show the fundamental properties of the Hermite polynomial used in expressing the transverse laser beam profile as in Eq. (E.36). The Hermite polynomial $H_n(\xi)$ is defined as the coefficient of the Taylor expansion of $\exp\left(-t^2+2\xi t\right)$ in t as

$$e^{-t^2+2\xi t} = e^{\xi^2} e^{-(t-\xi)^2} \equiv \sum_{n=0}^{\infty} \frac{1}{n!} H_n(\xi)\, t^n. \quad \text{(E.38)}$$

The Hermite polynomial satisfies the following equation for a function $u(\xi)$:

$$\left(\frac{d^2}{d\xi^2} - 2\xi\frac{d}{d\xi} + 2n\right) u_n(\xi) = 0. \quad \text{(E.39)}$$

Namely, the solution of this equation becomes $u_n(\xi) = A_n H_n(\xi)$ with an integral coeficient A_n. One can see that Eq. (E.39) is equivalent to the one-dimensional Schödinger equation

$$\left(-\frac{\hbar^2}{2m}\frac{d^2}{dx^2} + V(x)\right)\phi(x) = E\phi(x), \quad \text{(E.40)}$$

with a pendular potential

$$V(x) = \frac{k}{2}x^2, \quad \text{(E.41)}$$

by using the relations

$$\omega = \sqrt{\frac{k}{m}}, \quad \text{(E.42)}$$

$$\xi = \sqrt{\frac{m\omega}{\hbar}}x, \quad \text{(E.43)}$$

$$\phi(\xi) = u(\xi)\, e^{-\xi^2/2}, \quad \text{(E.44)}$$

$$E = \frac{\hbar\omega}{2}(2n+1) \quad (n = 0,1,2,\cdots). \quad \text{(E.45)}$$

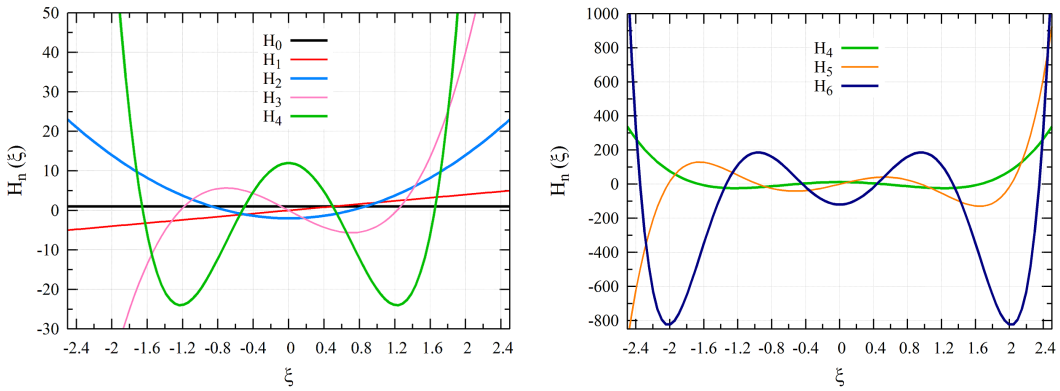

Figure E.2: Hermite polynomial $H_n(\xi)$ for $n = 0, \cdots, 4$ (left) and $n = 4, \cdots, 6$ (right).

The Hermite polynomial satisfies the orthogonal relationship

$$\int_{-\infty}^{\infty} H_m(\xi) H_n(\xi) e^{-\xi^2} d\xi = 2^n \sqrt{\pi} n! \delta_{mn}. \tag{E.46}$$

The normalize condition for the wave function $\phi(\xi)$, i.e.,

$$\int_{-\infty}^{\infty} |\phi_n(\xi)|^2 d\xi = |A_n|^2 2^n \sqrt{\pi} n! \equiv 1, \tag{E.47}$$

determines the coefficient A_n as

$$A_n = \frac{1}{\left(2^n \sqrt{\pi} n!\right)^{1/2}}. \tag{E.48}$$

The series of the Hermite polynomial can be obtained by

$$H_0(\xi) = 1, \tag{E.49}$$

$$H_{n+1}(\xi) = e^{\xi^2/2} \left(\xi - \frac{d}{d\xi}\right) e^{-\xi^2/2} H_n(\xi) \quad (n \geq 1), \tag{E.50}$$

as

$$H_1(\xi) = 2\xi, \tag{E.51}$$

$$H_2(\xi) = 4\xi^2 - 2, \tag{E.52}$$

$$H_3(\xi) = 8\xi^3 - 12\xi, \tag{E.53}$$

$$H_4(\xi) = 16\xi^4 - 48\xi^2 + 12, \tag{E.54}$$

$$H_5(\xi) = 32\xi^5 - 160\xi^3 + 120\xi, \tag{E.55}$$

$$H_6(\xi) = 64\xi^6 - 480\xi^4 + 720\xi^2 - 120, \tag{E.56}$$

$$\cdots, \tag{E.57}$$

or, directly from the following formula:

$$H_n(\xi) = (-1)^n e^{\xi^2} \frac{d}{d\xi} e^{-\xi^2}. \tag{E.58}$$

From Eqs. (E.51)-(E.56), one can easily see that the Hermite functions with odd and even polynomials are odd and even functions, respectively. The Hermite functions $H_n(\xi)$ $(n = 0, \cdots, 6)$ are shown in Fig. E.2.

Appendix F

Covergence of maximum ion energy

In Sec. 8.3 in Part II, we showed the ion energy distribution and ion maximum energy obtained by the PIC simulation for targets (A)-(D), which are given in Fig. 8.1. Based on the obtained energy distribution, we also evaluated the maximum ion energy for each cases. In the numerical calculations, we used 42.7 super particles per mesh for electrons in the cases of cluster medium (A)-(C), i.e. $N_{\rm spe} = 42.7$/mesh, and $N_{\rm spe} = 64.1$/mesh in the case of thin film (D). In this appendix, we show the convergence of calculations by changing the super particle numbers.

Fig. F.1 shows the ion energy distributions for $a_0 = 800$, which are obtained by the same conditions in Sec. 8.3 except the super particle numbers. Namely, in Sec. 8.3, particle numbers shown by the blue lines ($N_{\rm spe} = 42.7$/mesh) for cases (A)-(C) and that shown by the brown line ($N_{\rm spe} = 64.1$/mesh) for case (D) are utilized.

From these figures, we see that in the case of thin film (D), although the energy humps around 8 GeV are almost same for all the calculations, the maximum value varies significantly among cases using different $N_{\rm spe}$. In contrast, the maximum energies in cases (A)-(C) show almost the same values for different $N_{\rm spe}$. For this reason, in the simulation in Sec. 8.3, we have used a larger super particle number per mesh for case (D). Here, it is found that the difference of the maximum energy between different $N_{\rm spe}$ is smaller in the case using larger cluster size.

We also confirmed that in the case of $a_0 = 200$, the difference of ion distribution and also the maxmum ion energy among calculations using different $N_{\rm spe}$ are small compared with the case of $a_0 = 800$.

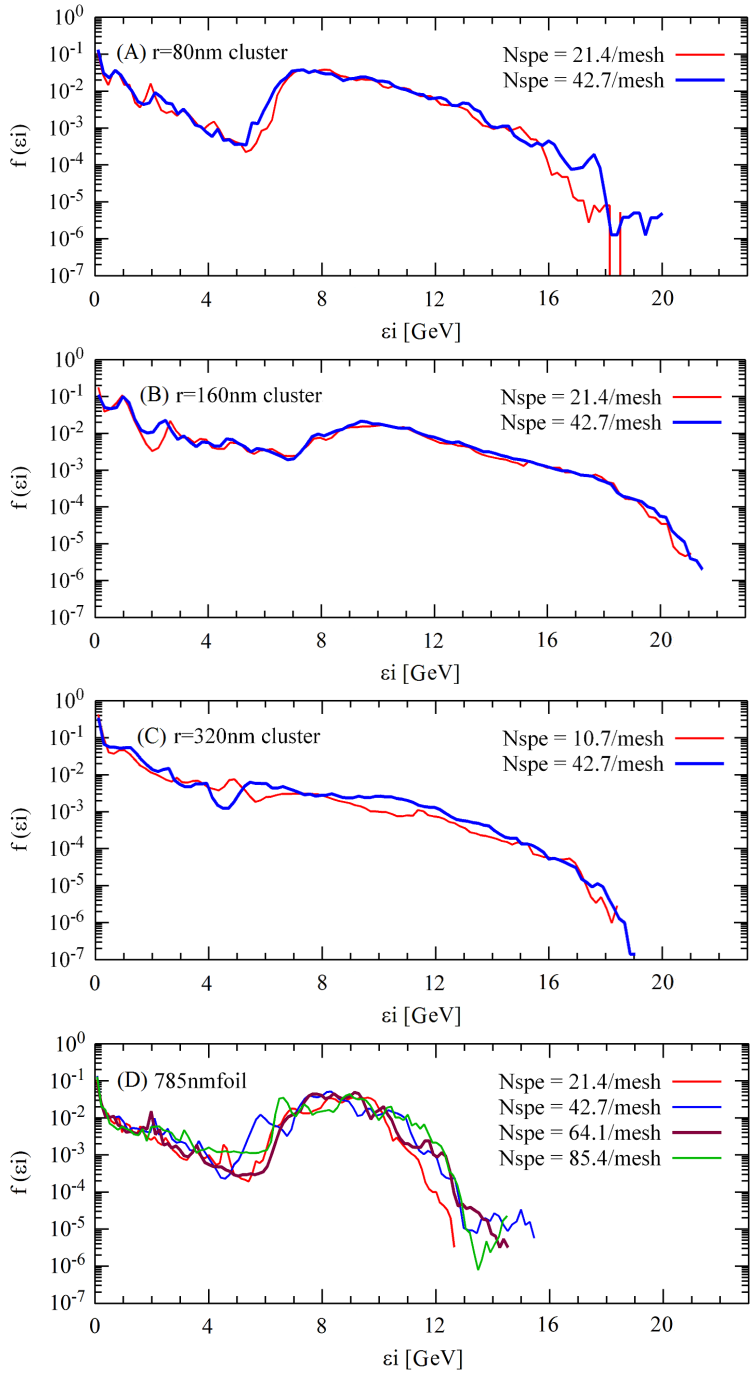

Figure F.1: Convergence of ion energy distributions in the case of $a_0 = 800$ for PIC simuilations performed in Sec. 8.3 in Part II.

Appendix G

List of Scientific Conributions

Published papers in academic journals

(Author underlined)

Peer-reviewed papers

- Natsumi Iwata and Yasuaki Kishimoto, "Higher-order nonlocal effects of a relativistic ponderomotive force in high-intensity laser fields", Physical Review Letters **112**, 035002 (2014).
- Natsumi Iwata and Yasuaki Kishimoto, "On the nonlocal properties of relativistic ponderomotive force", Physics of Plasmas **20**, 083107 (2013).
- Natsumi Iwata and Yasuaki Kishimoto, "Nonlocal Ponderomotive Force in a Super Gaussian Laser Beam and the Conditions for Long Time Scale Interaction", Plasma and Fusion Research **8**, 1201160 (2013).
- Natsumi Iwata and Yasuaki Kishimoto, "Relativistic Ponderomotive Force Including Higher Order Nonlocal Effects in High Intensity Laser Fields", Plasma and Fusion Research **8**, 1201094 (2013).
- Natsumi Iwata, Kenji Imadera and Yasuaki Kishimoto, "Analysis of Relativistic Particle Orbit in a Transversely Focused High-Power Laser Field by Using the Noncanonical Lie Perturbation Method", Plasma and Fusion Research **5**, 028 (2010).

Conference proceedings (with review)

- Natsumi Iwata, Yasuaki Kishimoto and Kenji Imadera, "Nonlocal properties of ponderomotive force in strongly nonuniform high intensity laser fields", Proceedings of the Seventh International Conference on Inertial Fusion Sciences and Applications (IFSA 2011), Edited by P. Mora, K. A. Tanaka and E. Moses, EPJ Web of Conferences **59**, 05015 (2013).
- Natsumi Iwata, Yasuaki Kishimoto and Kenji Imadera, "Theoretical Study of Particle Motion under High Intensity Laser-Plasma Interaction Aiming

for High Energy Density Science", Proceedings of the 3rd G-COE International Symposium, Zero-Caron Energy Kyoto 2011, Edited by T. Yao, Springer (2012) pp.185-191.

- Natsumi Iwata, Yasuaki Kishimoto and Kenji Imadera, "Analysis of relativistic ponderomotive force and higher-order particle motion in a non-uniform laser field using the noncanonical Lie perturbation method", Plasma and Fusion Research **6** Special Issue 1, Papers from the 20th International Toki Conference, 2404105 (2011).

Non-reviewed papers

- Natsumi Iwata, Yasuaki Kishimoto and Kenji Imadera, " Noncanonical Lie perturbation analysis for the relativistic ponderomotive force ", Proceedings of International Conference on Physics in Intense Fields (PIF2010), KEK Proceedings 2010-13 (2011), Edited by K. Itakura et al., pp.153-155.

- Natsumi Iwata, Yasuaki Kishimoto and Kenji Imadera, " Nonlocal Properties of the Ponderomotive Force in High Intensity Laser Fields - An Approach Based on the Noncanonical Lie Perturbation Theory- ", Proceedings of the 3rd International Symposium " Laser-Driven Relativistic Plasmas Applied to Science, Energy, Industry, and Medicine "(LDRP-2011), Edited by S. V. Bulanov et al., AIP Conference Proceedings 1465 (2012) pp. 113-117.

Submitted conference proceedings (with review)

- Natsumi Iwata, Yasuaki Kishimoto, Ryutaro Matsui and Yuji Fukuda, "Laser-matter interaction in cluster medium in the radiation dominated regime", submitted to Proceedings of the Eighth International Conference on Inertial Fusion Sciences and Applications (IFSA 2013), (Submitted 18 September 2013).

Presentations at academic conferences

(The speaker is underlined)

Presentations at international conferences

- Natsumi Iwata, Kenji Imadera, Yasuaki Kishimoto and J. Q. Li, " Relativistic particle orbit analysis in high intensity short pulse laser fields using noncanonical perturbation method ", Third International Meeting on Physics and Modeling of Mulch-scale Interaction in Plasmas, Clock Tower Centennial Hall, Kyoto University, Kyoto, Japan, March 9 - 10, 2010 (Poster No. 7, without review).

- Natsumi Iwata, Kenji Imadera and Yasuaki Kishimoto, " Relativistic particle orbit analysis in a transversely focused high power laser field by using noncanonical Lie perturbation method ", The 2nd International Symposium, Kyoto University Global COE Program, Kihada Hall, Obaku Plaza, Kyoto University Uji Campus, Kyoto, Japan, August 19 - 20, 2010 (Poster No. 60, with review).

- Natsumi Iwata, Yasuaki Kishimoto and Kenji Imadera, " Noncanonical Lie perturbation analysis for the relativistic ponderomotive force ", International Conference on Physics in Intense Fields (PIF2010), High Energy Accelerator Research Organization, KEK, 1-1 Oho, Tsukuba, Ibaraki 305-0801 Japan, November 24 - 26, 2010 (Poster No. 10, without review).

- Natsumi Iwata, Yasuaki Kishimoto and Kenji Imadera, " Analysis of relativistic ponderomotive force and higher-order particle motion in a non-uniform laser field using the noncanonical Lie perturbation method ", International Toki Conference (ITC-20), Ceratopia Toki, Toki-City, Gifu, Japan, December 7 - 10, 2010 (Poster No. P2-59, with review).

- Natsumi Iwata, Yasuaki Kishimoto and Kenji Imadera, " Nonlocal Properties of the Ponderomotive Force in High Intensity Laser Fields ?An Approach Based on the Noncanonical Lie Perturbation Theory- ", The 3rd International Symposium of Laser-Driven Relativistic Plasmas Applied to Science, Industry and Medicine (LDRP-2011), Kansai Photon Science Institute, Kizugawa, Kyoto, Japan, May 30 - June 2, 2011 (Oral, June 1, without review).

- Natsumi Iwata, Yasuaki Kishimoto and Kenji Imadera, " Theoretical Study of Particle Motion under High Intensity Laser-Plasma Interaction Aiming for High Energy Density Science ", The 3rd G-COE International Symposium (Specially Jointed with BK21 Program at Ajou University) " ZERO CARBON ENERGY 2011 ", Paldal-Hall (Rooms 108 and 110), Ajou University, Suwon, Korea, August 18-19, 2011 (Poster No. P-5(MPES), August 19, without review)

- Natsumi Iwata, Yasuaki Kishimoto and Kenji Imadera, " Nonlocal properties of the ponderomotive force in tightly focused high intensity laser fields ", The Seventh International Conference on Inertial Fusion Sciences and Applications (IFSA 2011), Palais des Congres de Bordeaux-Lac, France, September 12-16, 2011 (Poster No. P.Mo_76 at Poster session P+Q, September 12, with review)

- Natsumi Iwata, Yasuaki Kishimoto and Kenji Imadera, " Higher order nonlocal effects of relativistic ponderomotive force in high power lasers ", 54th Annual Meeting of the APS Division of Plasma Physics (APS-DPP 2012), Rhode Island Convention Center, Providence, Rhode Island, USA, October 29 - November 2, 2012 (Oral No. NO5.00008, Session No.5, October 31, with review)

- Natsumi Iwata and Yasuaki Kishimoto, " On the higher order nonlocal effect of relativistic ponderomotive force in high intensity lasers ", The 12th Asia Pacific Physics Conference (APPC12), International Conference Hall, Makuhari Messe, Chiba Japan, July 14-19, 2013 (Poster No. D3-PMo-06 at Session D-3, July 12, with review)

- Natsumi Iwata, Feng Wu, Yuji Fukuda and Yasuaki Kishimoto " Laser-matter interaction in cluster medium in the radiation dominated regime: Particle acceleration and radiation ", The Eighth International Conference on Inertial Fusion Sciences and Applications (IFSA 2013), Nara Prefectural New Public

Hall, Nara, Japan, September 8-13, 2013 (Oral No. O.Tu_B7 at session P1, September 10, with review)

Presentations at domestic conferences

- 岩田 夏弥, 岸本 泰明, 今寺 賢志, “ 非正準 Lie 摂動論による高強度極短パルスレーザー場中での相対論的粒子運動の解析 ”, 日本地球惑星科学連合 2010 年大会　物理・天文・地球惑星合同プラズマ科学シンポジウム, 幕張メッセ国際会議場, 2010 年 5 月 23 - 28 日 (Poster No. P-EM031-P02, 5 月 23 日，査読有)
- 岩田 夏弥, “ Noncanonical Lie Perturbation Analysis of Relativistic Ponderomotive Force and Higher-Order Particle Motion in a High Intensity Laser Field ”, 第１６回数値トカマク実験 (NEXT) 研究会, 京都テルサ, 2011 年 3 月 14 - 15 日 (Poster No. 13, 3 月 15 日，査読無)
- 岩田 夏弥, 岸本 泰明, 今寺 賢志, “ 非正準 Lie 摂動論による非一様レーザー場中での相対論的粒子運動の解析 ”, 日本物理学会 第 66 回年次大会, 新潟大学 五十嵐キャンパス, 2011 年 3 月 25- 28 日 (Oral No. 28aGAB-8, 3 月 28 日，査読無)
- 岩田 夏弥, 岸本 泰明, 今寺 賢志, “ Theoretical study of nonlocal effect of the ponderomotive force in high intensity laser fields using the noncanonical Lie perturbation theory (非正準 Lie 摂動論を用いた高強度レーザー場中での動重力の非局所効果に関する理論研究) ”, Plasma Conference 2011 (PLASMA2011)/ プラズマ・核融合学会第 28 回年会/ 応用物理学会第 29 回プラズマプロセシング研究会 /日本物理学会（領域 2）2011 年秋季大会，石川県金沢市 石川県立音楽堂，2011 年 11 月 22-25 日 (Oral No. 22C04, 11 月 22 日，査読無)
- 岩田 夏弥, 岸本 泰明, 今寺 賢志, “ 強集束高強度レーザー場中での相対論的粒子運動と非局所動重力 ”, 日本物理学会 第 67 回年次大会, 兵庫県西宮市 関西学院大学 西宮上ケ原キャンパス, 2012 年 3 月 24- 27 日 (Oral No. 27aYE-5, 3 月 27 日，査読無)
- 岩田 夏弥, 岸本 泰明, 今寺 賢志, “ 非正準 Lie 摂動論で導いた高次非局所効果を含む相対論的動重力の表式の特性と平均化法との相異 ”, 日本物理学会 2012 年秋季大会, 神奈川県横浜市　横浜国立大学, 2012 年 9 月 18- 21 日 (Oral No. 19aFJ-3, 9 月 19 日，査読無)
- 岩田 夏弥, 岸本 泰明, “ Higher order nonlocal effects of the relativistic ponderomotive force in high power lasers ”, 第 13 回光量子科学研究シンポジウム (The 13th Symposium on Advanced Photon Research), 京都府木津川市 日本原子力研究開発機構 関西光科学研究所, 2012 年 11 月 15-16 日 (Poster No. APR-13-25, 11 月 15 日，査読無)
- 岩田 夏弥, 岸本 泰明, “ 非正準 Lie 摂動論で導いた非局所動重力と荷電粒子の相互作用許容エミッタンス ”, レーザープラズマ科学のための最先端シミュレーションコードの共同開発・共用に関する研究会, 大阪府吹田市 大阪大学レーザーエネルギー学研究センター, 2013 年 1 月 7-8 日 (口頭, 1 月 8 日，査読無)
- 岩田 夏弥, 岸本 泰明, “ 高強度レーザービーム中での粒子ダイナミクスにおける相対論的動重力の高次非局所効果 ”, 日本物理学会 第 68 回年次大会, 広島県東広島市 広島大学 東広島キャンパス, 2013 年 3 月 26-29 日 (Oral No. 26aBC-9, 3 月 26 日，査読無)

Awards

(Author underlined)

- 日本物理学会領域 2 学生優秀発表賞, 岩田 夏弥, “ 強集束高強度レーザー場中での相対論的粒子運動と非局所動重力 ”, 日本物理学会 第 67 回年次大会, 兵庫県 西宮市 関西学院大学 西宮上ケ原キャンパス, 2012 年 3 月 24- 27 日 (講演：Oral No. 27aYE-5, 3 月 27 日).
- Best Poster Award, Natsumi Iwata, “ Theoretical study of high intensity laser-matter interaction including higher-order nonlocal effects ”, 2011 Annual Report Meeting of Kyoto University G-COE of Energy Science, ”Zero-Carbon Energy Kyoto 2011”, January 30, 2012, Kihada Hall, Obaku Plaza, Kyoto University Uji Campus, Uji, Kyoto, Japan.
- Best Poster Award, Jorge Gomez-Paredes, Rakesh M. Das, Shota Higashikura, Natsumi Iwata, RyoKoda, Yasunori Nakai, Kenji Nishioka, Haruki Seto, H.N. Zhang and Kazuchika Yamauchi, “ Accomplishing Japan ’s CO2 emission reduction targets in the absence of nuclear power ”, 2012 Annual Report Meeting of Kyoto University G-COE, ”Energy Science in the Age of Global Warming”, January 16, 2013, Clock Tower Centennial Hall, Kyoto University, Kyoto, Japan.

Fellowship

Japan Society for the Promotion of Science (JSPS) research fellow (日本学術振興会 特別研究員（DC2)）, No. 24-7688, April 2012 - March 2014.

Bibliography

[1] V. Yanovsky, V. Chvykov, G. Kalinchenko, P. Rousseau, T. Planchon, T. Matsuoka, A. Maksimchuk, J. Nees, G. Cheriaux, G. Mourou and K. Krushelnick, Opt. Express **16**, 2109 (2008).

[2] T. H. Maiman, Nature **187**, 493 (1960).

[3] F. J. McClung and R. W. Hellwarth, J. Appl. Phys. **33**, 828 (1962).

[4] M. DiDomenico Jr., J. E. Geusic, H. M. Marcos and R. G. Smith, Appl. Phys. Lett. **8**, 180 (1966).

[5] D, Strickland and G. Mourou, Opt. Commun. **56**, 219 (1985).

[6] G. A. Mourou, T. Tajima and S. V. Bulanov, Rev. Mod. Phys. **78**, 309 (2006).

[7] H. Hamster, A. Sullivan, S. Gordon, W. White and R. W. Falcone, Phys. Rev. Lett. **71**, 2725 (1993).

[8] T. Nakamura, J. Koga, T. Zh. Esirkepov, M. Kando, G. Korn and S. Bulanov, Phys. Rev. Lett. **108**, 195001 (2012).

[9] T. Ditmire et al., Nature **398**, 489 (1999).

[10] T. Tajima and J. M. Dawson, Phys. Rev. Lett. **43**, 267 (1979).

[11] R. Kodama et al., Nature **412**, 798 (2001).

[12] A. Zhidkov, J. Koga, A. Sasaki and M. Uesaka, Phys. Rev. Lett. **88**, 185002 (2002).

[13] K. Nakashima and H. Takabe, Phys. Plasmas **9**, 1505 (2002).

[14] S. V. Bulanov, T. Zh. Esirkepov, D. Habs, F. Pegoraro, and T. Tajima, Eur. Phys. J. D **55**, 483 (2009).

[15] E. S. Sarachik and G. T. Schappert, Phys. Rev. D **1**, 2738 (1970).

[16] K. Mima and K. Nishikawa, *Handbook of Plasma Physics* Vol. 2 (Elsevier Science Publishers B.V., Amsterdam, 1984) Chap. 6.5.

[17] J. C. Maxwell, *A Treatise on Electricity and Magnetism* (Oxford University Press, Oxford, 1871).

[18] C. M. Bender and S. A. Orszag, *Advances Mahtematical Methods for Scientists and Engineers I, Asymptotic Methods and Perturbation Theory* (Springer, New York, 2010) Chap. 11.

[19] L. M. Gorbunov, Usp. Fiz. Nauk. **109**, 631 (1973).

[20] P. Gibbon, *Short Pulse Laser Interactions with Matter* (Imperial College Press, London, 2005) Chap. 3.

[21] D. Bauer, P. Mulser and W. H. Steeb, Phys. Rev. Lett. **75**, 4622 (1995).

[22] E. A. Startsev and C. J. McKinstrie, Phys. Rev. E **55**, 7527 (1997).

[23] P. K. Shukla, N. N. Rao, M. Y. Yu and N. L. Tsintsadze, Phys. Rep. **138**, 1 (1986).

[24] L. N. Tsintsadze, T. Tajima, K, Nishikawa, J. Koga, K. Nakagawa and Y. Kishimoto, Phys. Scr. T**84**, 94 (2000).

[25] T. Esirkepov, M. Borghesi, S. V. Bulanov, G. Mourou and T. Tajima, Phys. Rev. Lett. **92**, 175003 (2004).

[26] S. S. Bulanov *et al.*, Phys. Rev. E **78**, 026412 (2008).

[27] C. Kittel and H. Kroemer, *Thermal Physics* (W. H. Freeman and Company, San Francisco, 1980) Chap. 14.

[28] J. R. Cary and R. G. Littlejohn, Ann. Phys. **151**, 1 (1983).

[29] T. Tajima, Y. Kishimoto, and M. C. Downer, Phys. Plasmas **6**, 3759 (1999).

[30] Y. Kishimoto, T. Masaki and T. Tajima, Phys. Plasmas **9**, 589 (2002).

[31] Y. Fukuda et al., Phys. Rev. Lett. **103**, 165002 (2009).

[32] T. Tajima, Scientific Advisory Committee: Report on the ELI Science (2009).

[33] Y. Kishimoto and T. Masaki, J. Plasma Phys. **72**, 971 (2006).

[34] T. Masaki and Y. Kishimoto, Plasma Fusion Res. **81**, 643 (2005).

[35] A. V. Arefiev, B. N. Breizman, M. Schollmeier and V. N. Khudik, Phys. Rev. Lett. **108**, 145004 (2012).

[36] T. S. Hahm, Phys. Fluids **31**, 2670 (1988).

[37] A. J. Brizard and T. S. Hahm, Rev. Mod. Phys. **79**, 421 (2007).

[38] Y. Kishimoto, S. Tokuda and K. Sakamoto, Phys. Plasmas **2**, 1316 (1995).

[39] K. Imadera and Y. Kishimoto, Plasma Fusion Res. **6**, 1201004 (2011).

[40] B. Quesnel and P. Mora, Phys. Rev. E **58**, 3719 (1998).

[41] N. L. Tsintsadze, K. Mima, L. N. Tsintsadze and K. Nishikawa, Phys. of Plasmas, **9**, 4270 (2002).

[42] K. Nishihara, H. Amitani, M. Murakami, S. V. Bulanov and T. Zh. Esirkepov, Nucl. Instrum. Methods Phys. Res. A **464**, 98 (2001).

[43] M. Murakami and M. M. Basko, Phys. Plasmas **13**, 012105 (2006).

[44] Y. Ueshima, Y. Kishimoto, A. Sasaki and T. Tajima, Laser and Particle Beams **17**, 45 (1999).

[45] L. W. Davis, Phys. Rev. A **19**, 1177 (1979).

[46] M. O. Scully and M. S. Zubairy, Phys. Rev. A **44**, 2656 (1991).